

(NASA-CR-143881) ANALYSIS AND TRADE-OFF  
STUDIES OF LARGE LIGHTWEIGHT MIRROR  
STRUCTURES (Draper (Charles Stark) Lab.,  
Inc.) 150 p HC \$5.75 CSCL 20K

N75-26417

G3/39 Unclass  
27311

**R-873**

**ANALYSIS AND TRADE-OFF STUDIES OF  
LARGE LIGHTWEIGHT MIRROR STRUCTURES**

by

**Keto Soosaar  
Roland Grin  
Francois Ayer**

**April 1975**

**This report covers research conducted between  
September 1972 and December 1973**



**The Charles Stark Draper Laboratory, Inc.**  
Cambridge, Massachusetts 02139

R-873

ANALYSIS AND TRADE-OFF STUDIES OF  
LARGE LIGHTWEIGHT MIRROR STRUCTURES

by


Keto Soosaar  
Roland Grin  
Francois Ayer

April 1975

This report covers research conducted  
between September 1972 and December 1973

Approved:

  
N. Sears

  
W. Denhard

The Charles Stark Draper Laboratory, Inc.  
Cambridge, Massachusetts 02139

## ACKNOWLEDGEMENT

The assistance of Mr. James Joyce in the equivalent back-plate studies is gratefully acknowledged. Many thanks go to Mr. David Nasman, and Mr. Steven Anagnostis for preparation of the figures.

This report was prepared under Project 55-52100 sponsored by Marshall Space Flight Center of the National Aeronautics and Space Administration through Contract NAS8-29187. The guidance and advice of Dr. William Clarke, Mr. Duane Counter, Mr. Gwyn Faile and Mr. Charles Jones who at various times acted as the interface is most gratefully acknowledged.

The publication of this report does not constitute approval by the National Aeronautics and Space Administration of the findings or conclusions contained herein. It is published only for the exchange and stimulation of ideas.

Analysis and Trade-Off Studies of  
Large Lightweight Mirror Studies

by

Keto Soosaar  
Roland Grin  
and  
Francois Ayer

ABSTRACT

While the methodology of analysis of large lightweight mirror structures has been developed to a high degree of feasibility, the costs of analysis are still extremely high. The work reported herein constitutes an attempt to minimize this cost by the development of simpler, less costly modelling techniques, and an evaluation of price that then must be paid in for accuracy. A "Phase A" candidate CERVIT mirror, hexagonally lightweighted, is first analyzed under various loadings using as complete a procedure as possible. Then successive simplifications are introduced and compared to the original analysis. A model which is a reasonable compromise between accuracy and cost is found and is used for making trade-off studies of the various structural parameters of the lightweighted mirror. An additional chapter reports a brief look into the possibility of a scaled-down mirror for technology studies. Conclusions and recommendations complete the report.

## TABLE OF CONTENTS

Chapter		Page
1	INTRODUCTION.....	1-1
2	ANALYSIS OF 120" MIRROR.....	2-1
2.1	Description of Mirror.....	2-1
2.2	Methods of Mirror Structural Modelling.....	2-3
2.3	Descriptions of Mirror Models Used...	2-3
2.4	Mirror Environments.....	2-7
2.5	Data Presentation and Interpretation Methods.....	2-12
2.6	Summary of Phase "A" Design.....	2-13
2.7	Summary of Mirror Model Comparisons.....	2-15
2.8	Actuator Local Effects.....	2-19
2.9	Recommendations.....	2-20
3	TRADE-OFF STUDIES.....	3-1
3.1	Baseline Design and Variation Parameters.....	3-1
3.2	Mirror Lightweighting.....	3-3
3.3	Parameter Variations.....	3-7
3.4	Summary and Conclusions.....	3-9

TABLE OF CONTENTS (Cont.)

Chapter		Page
4	BREADBOARD MIRROR.....	4-1
	4.1 Necessity for Breadboard Mirror.....	4-1
	4.2 Breadboard Mirror Dimensions.....	4-2
	4.3 Model Laws.....	4-3
	4.4 Conclusions.....	4-10
5	SUMMARY, CONCLUSIONS, AND RECOMMENDATIONS....	5-1
Appendix		
A	EQUIVALENT PLATE REPRESENTATION.....	A-1
	A.1 Introduction.....	A-1
	A.2 Unequal In-Plane Stress Resultants.....	A-1
	A.3 Backplate Hole Relatively Large.....	A-3
	A.4 Bending in Backplate.....	A-6
B	FORMULATION OF HONEYCOMBED MIRROR WEB.....	B-1
	B.1 Introduction.....	B-1
	B.2 Equivalent Shear Modulus.....	B-2

## LIST OF TABLES

Table		Page
2.1	Summary of Phase A Mirror Performance.....	2-14
2.2	Gravity Load Response.....	2-16
2.3	1 <sup>0</sup> F Soak Response.....	2-17
2.4	1 <sup>0</sup> F Transverse Gradient Response.....	2-17
2.5	1 <sup>0</sup> F Radial Gradient Response.....	2-17
3.1	Baseline Design.....	3-2
3.2	Limits in Cell Pattern Lightweighting.....	3-5
3.3	Mirror Lightweighting.....	3-6
3.4	Dependencies of Trade Variables.....	3-8
4.1	LST Breadboard—Fully Scaled.....	4-4
4.2	Integral Number of Cells in 20.5" Length.....	4-6
4.3	Model Laws.....	4-8
4.4	Relations Between Full Scale and Breadboard.....	4-9

## LIST OF ILLUSTRATIONS

Figure	Page
2.1 CER-VIT 101 Lightweight Mirror Blank - Phase "A" Design	2-2
2.2 60° Segment of 120" - Phase "A" Mirror - All Cells	2-6
2.3 60° Segment of 120" Phase "A" Mirror - Alternate Cells	2-8
2.4 Support Modelling Detail	2-9
2.5 60° Segment of 120" Phase "A" Mirror - Trade-Off Model	2-10
2.6 Optical Surface Displacements - 1g Transverse - All Webs	
2.7 Optical Surface Displacements - 1g Transverse Alternate Webs	2-23
2.8 Optical Surface Displacements - 1g Transverse Trade-Off Model	2-24
2.9 Deviations from Best-Fit Sphere - 1g Transverse - All Webs	2-25
2.10 Deviations from Best-Fit Sphere: 1g Transverse - Alternate Webs	2-26
2.11 Deviations from Best-Fit Sphere - 1g Transverse - Trade-Off Model	2-27
2.12 Stresses in Mirror Top Surface - 1g Transverse - All Cells	2-28
2.13 Stresses in Mirror Top Surface - 1g Transverse - Alternate Cells	2-29
2.14 Stresses in Mirror Top Surface - 1g Transverse - Trade-Off Model	2-30
2.15 Stresses in Mirror Equivalent Back Surface - 1g Transverse - All Cells	2-31
2.16 Local Back Surface - Stress Effects - 1g Transverse	2-32
2.17 Stresses in Mirror Equivalent Back Surface - 1g Transverse - Alternate Cells	2-33
2.18 Stresses in Mirror Equivalent Back Surface - 1g Transverse - Trade-Off Model	2-34
2.19 Maximum Cell Wall Stresses - 1g Transverse - All Cells	2-35
2.20 Maximum Cell Wall Stresses - 1g Transverse - Alternate Cells	2-36



LIST OF ILLUSTRATIONS (Continued)

Figure	Page
2.21 Stresses in Solid Support Area - Top Surface lg Transverse - All Cells	2-37
2.22 Stresses in Solid Support Area - Top Surface lg Transverse - Alternate Cells	2-38
2.23 Stresses in Solid Support Area - Bottom Surface lg Transverse - All Cells	2-39
2.24 Stresses in Solid Support Area - Bottom Surface lg Transverse - Alternate Cells	2-40
2.25 Stresses in Solid Support Area - Front Surface - lg Transverse - All Cells	2-41
2.26 Optical Surface Displacements - 1 <sup>o</sup> F Soak - All Webs	2-42
2.27 Optical Surface Displacements - 1 <sup>o</sup> F Soak - Alternate Cells	2-43
2.28 Optical Surface Displacements - 1 <sup>o</sup> F Soak - Trade-Off Model	2-44
2.29 Deviations from Best-Fit Sphere - 1 <sup>o</sup> F Soak - All Cells	2-45
2.30 Deviations from Best-Fit Sphere - 1 <sup>o</sup> F Soak - Alternate Cells	2-46
2.31 Deviations from Best-Fit Sphere - 1 <sup>o</sup> F Soak - Trade-Off Model	2-47
2.32 Top Surface Stresses - 1 <sup>o</sup> F Soak - All Cells	2-48
2.33 Top Surface Stresses - 1 <sup>o</sup> F Soak - Alternate Cells	2-49
2.34 Optical Surface Displacements - 1 <sup>o</sup> F Transverse Gradient - All Cells	2-50
2.35 Optical Surface Displacements - 1 <sup>o</sup> F Transverse Gradient - Alternate Cells	2-51
2.36 Optical Surface Displacements - 1 <sup>o</sup> F Transverse Gradient - Trade-Off Model	2-52
2.37 Deviations from Best-Fit Sphere - 1 <sup>o</sup> F Transverse Gradient - All Cells	2-53
2.38 Deviations from Best-Fit Sphere - 1 <sup>o</sup> F Transverse Gradient - Alternate Cells	2-54
2.39 Deviations from Best-Fit Sphere - 1 <sup>o</sup> F Transverse Gradient - Trade-Off Model	2-55
2.40 Top Surface Stresses - 1 <sup>o</sup> F Transverse Gradient - All Cells	2-56

LIST OF ILLUSTRATIONS (Continued)

Figure	Page
2.41 Top Surface Stresses - 1° F Transverse Gradient - Alternate Cells	2-57
2.42 Optical Surface Displacement - 1° F Radial Gradient - All Cells	2-58
2.43 Optical Surface Displacements - 1° F Radial Gradient - Alternate Cells	2-59
2.44 Optical Surface Displacements - 1° F Radial Gradient - Trade-Off Model	2-60
2.45 Deviations from Best-Fit Sphere - 1° F Radial Gradient - All Cells	2-61
2.46 Deviations from Best-Fit Sphere - 1° F Radial Gradient - Alternate Cells	2-62
2.47 Deviations from Best-Fit Sphere - 1° F Radial Gradient - Trade-Off Model	2-63
2.48 Top Surface Stresses - 1° F Radial Gradient - All Cells	2-64
2.49 Top Surface Stresses - 1° F Radial Gradient - Alternate Cells	2-65
2.50 Optical Surface Displacements - "Sperry Rand Thermal" - All Cells	2-66
2.51 Deviations from Best-Fit Sphere - "Sperry Rand Thermal" - All Cells	2-67
2.52 Top Surface Stresses - "Sperry Rand Thermal" - All Cells	2-68
2.53 Actuator Locations - Alternate Cell Model	2-69
2.54 Optical Surface Displacements - Actuator Cell Test	2-70
2.55 Optical Surface Displacements - Actuator Rib Test	2-71
3.1 Limits on Cell Patterns	3-11
3.2 Variations on Web Density 1g Transverse Load	3-12
3.3 Variations in Web Density 1g Transverse Load	3-13
3.4 Variations on Web Weight - 1G	3-14
3.5 Variations on Mirror Depth - 1G	3-15
3.6 Variatons on Mirror Depth - 1G	3-16
3.7 Variatons on Mirror Depth - 1G	3-17
3.8 Variations on Top Plate Thickness - 1G	3-18
3.9 Variations on Top Plate Thickness - 1G	3-19

LIST OF ILLUSTRATIONS (Continued)

Figure	Page
3.10 Variations on Top Plate Thickness - 1G	3-20
3.11 Local Cell Effects of Tool Pressure	3-21
3.12 Variations on Back Plate Thickness - 1G	3-22
3.13 Variations on Back Plate Thickness - 1G	3-23
3.14 Variations on Back Plate Thickness - 1G	3-24
3.15 Variations on Rim Plate - 1G	3-25
3.16 Variations on Rim Plate - 1G	3-26
3.17 Variations on Web Density - Various Thermal Loads	3-27
3.18 Variations on Mirror Depth - Thermal Loads	3-28
3.19 Variations on Top Plate Thickness - Thermal Loads	3-29
3.20 Variations on Back Plate Thickness - Thermal Loads	3-30
3.21 1° F Soak	3-31
3.22 1° F Transverse Gradient	3-32
3.23 1° F Radial Gradient	3-33
3.24 Actuator Locations - At Back of Mirror	3-34
3.25 Variation on Mirror Depth - 1# Actuator Force	3-35
3.26 Variations on Web Density - 1# Actuator Load	3-36
3.27 Variations on Back Plate Thickness - 1# Actuator Force	3-37
3.28 Variations on Top Plate Thickness - 1# Actuator Force	3-38
4.1 Basic Requirements for Breadboard Cell Layout	4-5
4.2 48" Breadboard Mirror	4-7
A.3.1 Hexagonal Truss Model	A-3
A.4.1 Finite Element End of Backplate - CPT Elements	A-9
A.4.2 Loadings Considered for Strain Energy Computation	A-10
A.4.3 Nodal Rotations	A-11
B.1 Basic Repeating Units for Lightweight Mirrors	B-3

## Chapter 1

### INTRODUCTION

Finite element structural analysis methodology has been developed to the point today that there are few problems in static, linear structures that do not lend themselves to ready treatment by any of the vast number of software packages. Mirror structures fall into this feasible category, but the demands of optical accuracy lead to the requirement of many degrees of freedom in the analysis. The large stiffness matrices and their rather substantial bandwidths can lead to considerable computer running time as well as high data preparation costs. This inhibits the proper evaluation of alternative designs and prevents the mirror designers from acquiring a "feel" for the affects of parameter variation.

The objectives of the studies reported herein are primarily three. The first is to develop an accurate model of a CERVIT 101 hexagonally-lightweighted 120" mirror as proposed for the "Phase A" configuration of the NASA Large Space Telescope. This mirror will be evaluated under a number of "unit" mechanical and thermal loads. The actual values of the loads are as yet uncertain, so that when these are known, the "unit" results may be appropriately scaled.

The second objective is to develop a number of simpler models which still retain most of the significant technical characteristics of the accurate model but whose computer running costs are substantially less. These models will be run with the same loading conditions as the "accurate" and the results will be compared. These first two objectives are reported in Chapter 2.

The third objective is to use the cheapest, but still technically significant, model for the variation of the mirror lightweighting parameters. This would determine which parameters contribute most to the mirror performance, and whether the current "Phase A" configuration might not be slightly improved. These results are reported in Chapter 3.

Chapter 4 contains a description of a "breadboard" mirror, 48 inches in diameter that was being considered for a technology test-bed for the full 120" reference. Various model laws are discussed and a design for the lightweighting configuration is proposed.

Chapter 5 completes the report with recommendations and conclusions.

Appendix A describes the development of models to represent the lightweighted mirror backplate, which otherwise due to the holes, would require considerable numbers of elements.

Appendix B outlines the formulation of the equivalent stiffness parameters for the mirror core to be used in the approximate "trade-off" model.

## Chapter 2

### LIGHTWEIGHT MIRROR MODELS AND RESULTS

#### 2.1 Description of Mirror

The primary mirror for the Large Space Telescope as proposed by the Phase "A" studies consists of a 120" CERVIT 101 substate in a hexagonally-lightweighted configuration. Figure 2.1 gives a general picture of the mirror details as well as documents the necessary dimensional parameters.

It is evident that the hexagonal cell lightweighting method conforms well to the three point edge support configuration. The mirror supports consist of cylindrical trunnions which in turn are carried by A-frames to the spacecraft structure. The area of the mirror around the support is not lightweighted and this may cause significant uncertainties in manufacture, figuring and perhaps in structural performance.

The proposed cell wall thickness of 0.2" may also lead to strength problems. The mirror is approximately 18 inches deep, and the final lightweighting procedure uses angled tools which must pass through the back plate hole. The long arm of the tool will most certainly flex and thus result in considerable variations in the cell wall thicknesses and possible cutting through of the walls. This is one of the largest sources of manufacturing risk.

It is recognized, however, that the mirror mechanical design is strictly preliminary, and one that fulfills mainly the optical requirements. Much structural stiffness optimization may be possible, and it is one of the purposes of this study to determine some of the improvements possible. Since

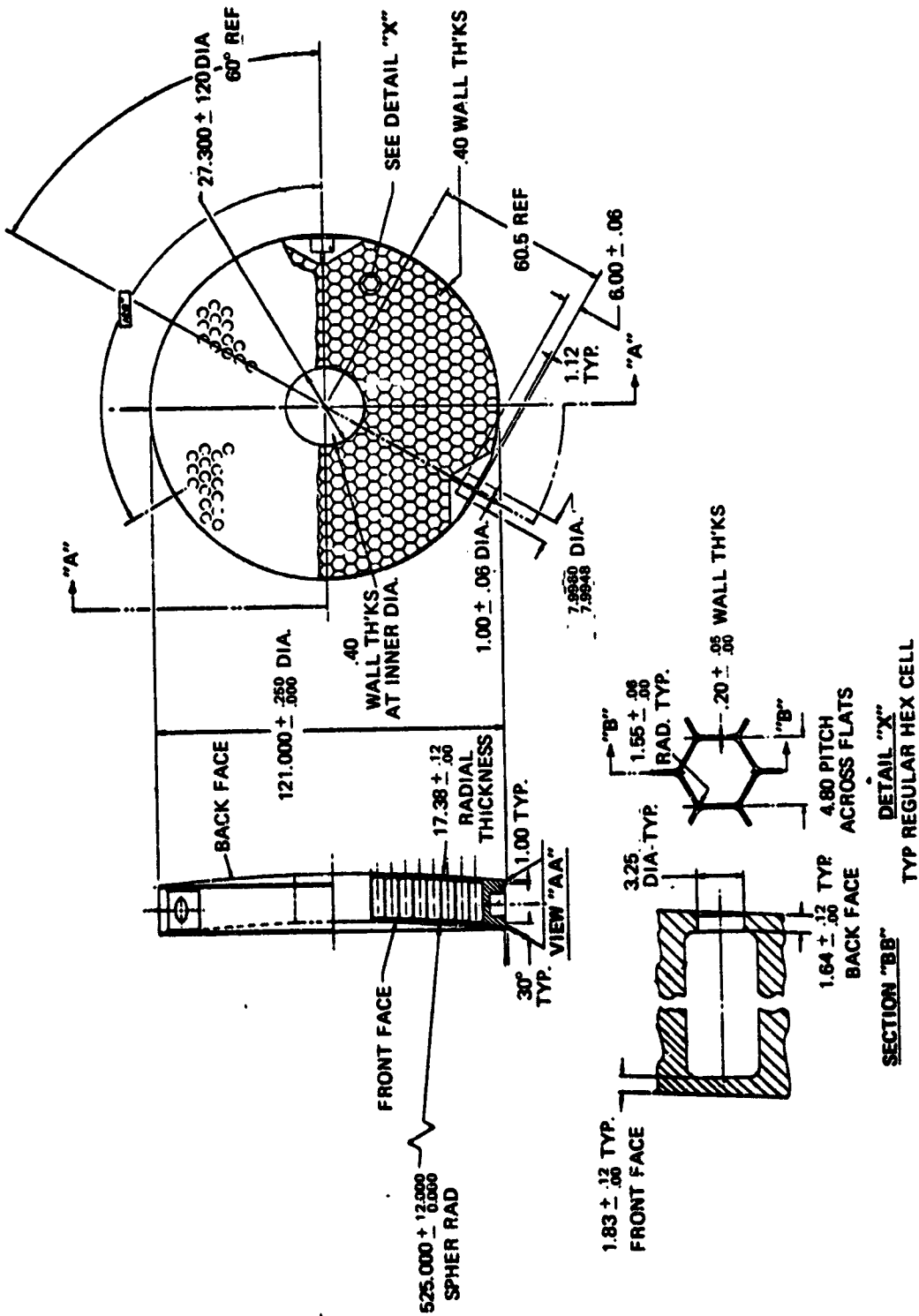


Figure 2.1. CER-VIT 101 Lightweight Mirror - Phase "A" Design  
(All units shown in inches.)

ORIGINAL PAGE IS  
OF POOR QUALITY

substantial weight savings may accrue from a proper structural optimization as well, it is worthwhile studying this, the heaviest single LST component, in some detail.

## 2.2 Methods of Mirror Structural Modelling

For the longest time, the structural design of optical mirrors consisted of the rule of thumb that "the thickness of the mirror should be one-sixth of the diameter." With the dimensions fixed by custom, the structural analysis seemed superfluous. Apart from convenience in casting or handling the blank, there seemed to be no justification for these proportions.

Couder<sup>(1)\*</sup> made considerable progress in the field when he realized that a mirror blank was basically a plate structure. Since his experiments had to be done with thin plates, much thinner than six to one, he did not observe the transverse shear deformations which are quite significant as the depth of the plate increases. Reissner<sup>(2)</sup> formulated the behavior of deep plates and this was recently applied to thick mirrors by Selke.<sup>(3)</sup>

Analytic solutions required uniform thickness mirrors and rather well-behaved boundary conditions, so that the implementation of these methods was rather limited. At about the time that the issue of mirror structural performance and its prediction became quite critical, the finite element method was developed and was soon applied to various mirror problems. Following the path of the analytical approaches, the finite element method first used bending elements, and later bending plus shear elements. When higher order three-dimensional solid isoparametric elements were developed, these were quickly implemented for the analysis of solid mirrors.<sup>(4)</sup> The curved-sided characteristic of these elements made them especially ideal for the modelling of astronomical mirrors.

---

\*See Bibliography



At about the same time, considerable interest also arose in the development of lightweight reflectors, mainly for space applications. To maintain strength and stiffness while reducing weight, the best strategy entailed reduction of the material from near the neutral axis where it was relatively ineffective for supporting bending loads. This resulted in sandwich-type structures where the continuous reflecting surface was supported by a grid of plates. In the case of CERVIT, the sandwich structure was obtained by carving out a solid blank. In the ULE case, face and back plates were fused to a previously assembled core.

These mirrors could possibly be coarsely modelled by bending and shear elements, but this would give very little feeling for the actual stresses experienced. The approach therefore was taken to model each of the web and flange plates individually wherever they appeared.<sup>(5)</sup> This method gives moderately good over-all results, but should not be used if highly detailed local information is desired. In those cases, where fillet stress information, for example, is important, three-dimensional solid elements must be used.

The factor of cost of analysis becomes quite important, however, in large lightweighted mirrors with many cells. The effort of preparation of input, the cost of the computer runs, and the effort of data interpretation is considerable unless steps are taken to assume symmetry conditions. Sometimes these are not possible, and the full mirror model is mandatory. It makes sense then to attempt to simplify the model as much as possible without losing significant amounts of valuable information. It is one of the purposes of this investigation to determine where the limits of these simplifications lie.

### 2.3 Description of Mirror Models Used

Since it was primarily necessary to model the existing Phase "A" mirror (see Figure 2.1) in sufficient detail to permit high confidence in the results, a rather complex finite element layout was initially chosen. Every web and flange element of the lightweight structure was individually represented as a bending/stretching plate element, although loading and support conditions permitted the reduction of the full mirror to a 60° symmetry segment (see Figure 2.2).

The support area, which had been left an un-lightweighted solid, was designed with a cylindrical trunnion support which resulted in a very complicated configuration. This region was modelled with three-dimensional isoparametric hexahedral and prismatic elements and boundary-matched to the plate elements (see Figure 2.4). The mirror back-plate which has holes at each cell, was represented by an equivalent solid plate structure using the method outlined in Appendix A. This mirror model was called "EXACT".

With only one-sixth of the mirror modelled, the number of nodes obtained were 554 and elements 762. While this is not a particularly sizable problem, the bandwidth of the stiffness matrix remained quite large and considerable effort was expended to reduce this. The costs of data preparation, computer running, and data interpretation were quite substantial, however, so that a simpler model became desirable.

One such possibility was to model groups of cells as one cell, adjusting the cell wall thicknesses, however, to maintain the relative web stiffness. Since the local bending deflection across each cell had not been modelled anyway, this would not change the high-frequency component of the mirror surface displacements. The cells were modelled twice as large, with twice as thick cell walls, and the edge support details (see

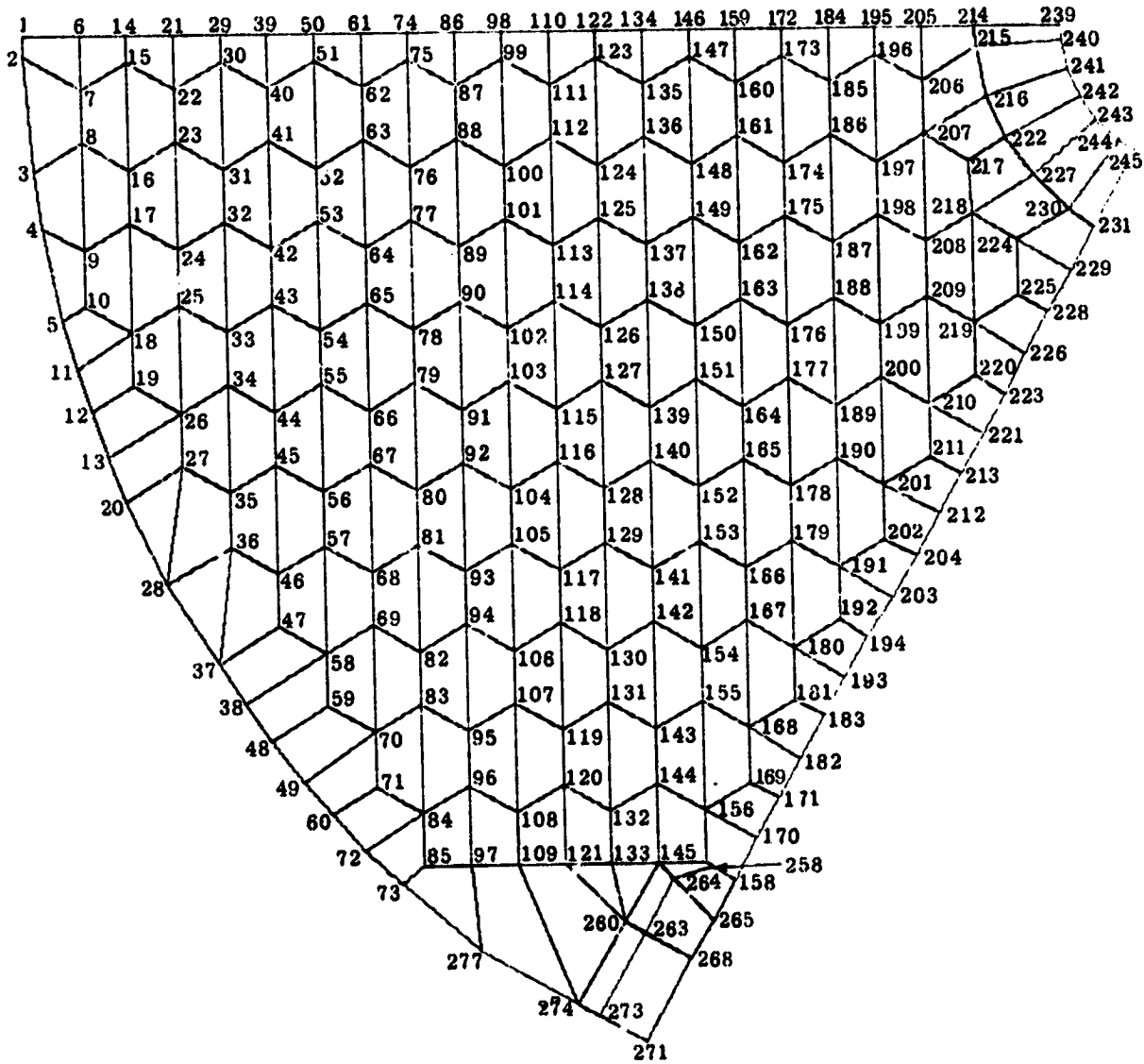


Figure 2.2. 60° Segment of 120" -  
 Phase "A" Mirror - All Cells  
 Top Surface Node Numbers Shown  
 Total Nodes: 554  
 Total Elements: 762

ORIGINAL PAGE IS  
 OF POOR QUALITY

Figure 2.4) could be maintained quite faithfully. This resulted in a reduction to 236 nodes and 263 elements (see Figure 2.3). This mirror model was called the "ALTERNATE WEB".

This model reduced the problem complexity substantially, but not to a level of reasonably simple data preparation, short computer runs, quick computer turnaround, and simple data interpretation. A further major model simplification was needed.

The next model represented a major change from the earlier. The honeycombed web was represented by an equivalent three-dimensional solid element (as per Appendix B), but the top and bottom flange plates were retained (see Figure 2.5). This also allowed the model to be used for parametric studies with only minor modifications necessary. The support was reduced to a single prismatic element. The number of nodes was reduced to 50 and the number of elements was 56. This model was not expected to behave perfectly in all instances, but the limits of its applicability were to be established. It succeeded very well in the reduction of preparation, running, turnaround, and data interpretation times. This model was called the "TRADE-OFF MODEL".

In the studies following, all of these models were subjected to the same loading conditions, and the results were compared.

It should be noted that in all of the finite element studies reported herein, the ICES-STRUDL II system was employed.

#### 2.4 Mirror Environments

At the time of the studies, it was not known precisely the types of environments that the mirror would experience in going through manufacture, test, launch and operation. It was decided, therefore, to subject the mirror only to unit

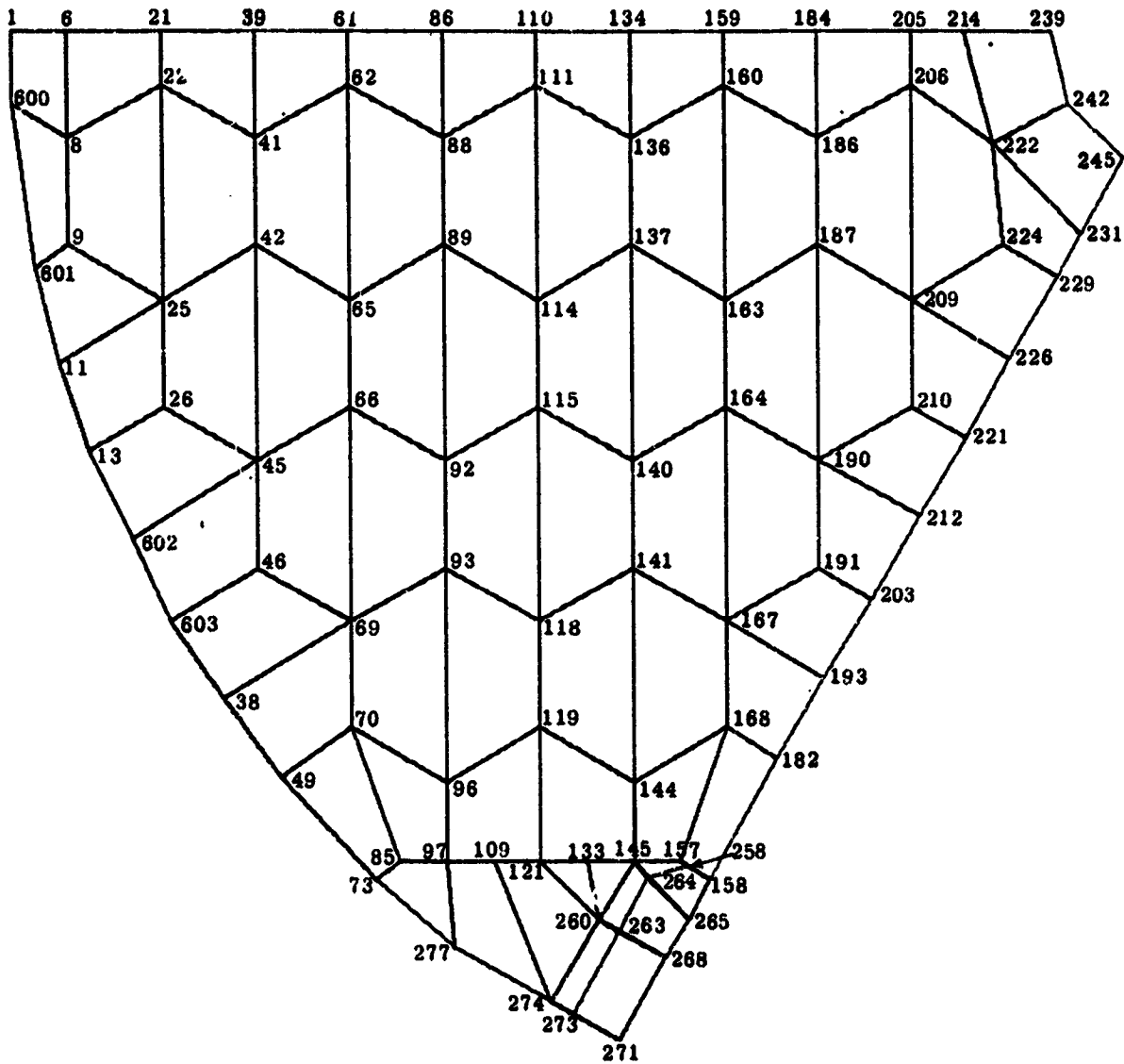


Figure 2.3. 60° Segment of 120" Phase "A" Mirror -  
 Alternate Cells  
 Top Surface Node Numbers Shown  
 Total Nodes: 236  
 Total Elements: 263

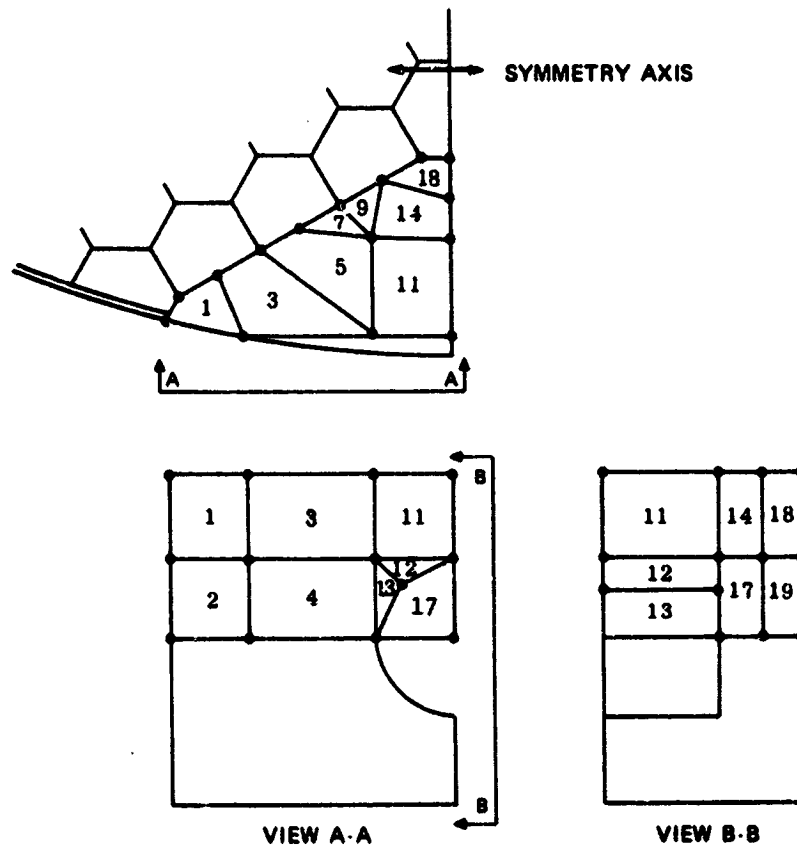


Figure 2.4, Support Modelling Detail  
 Hexahedral and Prismatic Isoparametric  
 Solid Finite Elements

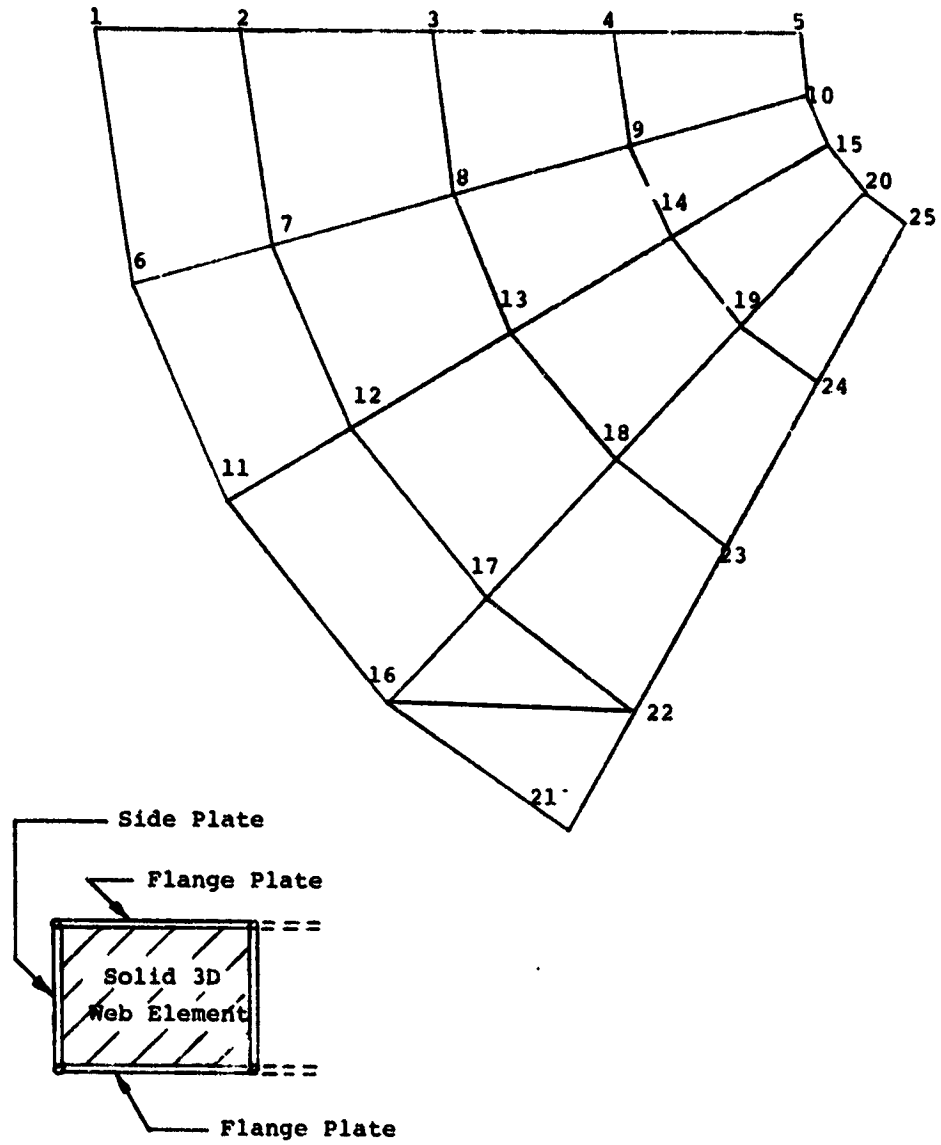


Figure 2.5. 60° Segment of 120" Phase "A" Mirror -  
 Trade-Off Model  
 Top Surface Node Numbers Shown  
 Total Nodes: 50  
 Total Elements: 56

inertial and thermal loadings which then could be scaled when the real inputs were available. These loadings were further restricted to those that were consonant with the one-sixth mirror segment modelled. The loadings studied were the following.

- a. 1-g applied along the optical axis: this result could be used for evaluation of the test, the launch, and the zero-g effects.
- b. 1°F soak: the entire mirror undergoes a uniform temperature change from the final figuring and test temperatures.
- c. 1°F transverse gradient: there is a gradient of 1°F from optical surface to the back of the mirror. This represents the effect of staring into cold space.
- d. 1°F radial gradient: there is a gradient of 1°F from the inside hole of the mirror to the outer band. This represents the effect of heat transfer through the outer rim to the telescope tube.
- e. "Sperry Rand Thermal": this data on a probable thermal distribution supplied by Sperry Support Division, Inc. was applied only to the "EXACT" model.
- f. Actuator test: the difference in response of the mirror to actuators located across a cell versus a single joint was studied on the intermediate "ALTERNATE WEB" model since this one would exaggerate that behavior.



## 2.5 Data Presentation and Interpretation Methods

The results of the various studies were tabulated and plotted in the following ways.

- a. Optical surface displacements: raw deflection of the top layer of nodes relative to the mirror supports.
- b. Deviations from best-fit sphere: the optical surface displacements were added to the original spherical reflecting surface, and a new best-fit sphere was computed. These deviations represent the differences between this sphere and the deformed surface. A root-mean-square of these deviations was also computed and tabulated.
- c. Stresses in Top Surface: iso-stress contours have been plotted for a number of cases. These are primarily in-plane, as the bending component was found to be very small and was eventually dropped from the model altogether. The stress magnitudes are nodally averaged.
- d. Stresses in mirror equivalent back surface: iso-stress contours have been plotted for stresses in the plate substituting for the plate with the lightweighting hole. A comparison of this "pseudo-stress" with the actual backplate stresses determined by exact analysis was made, and the results were found to be comparable within the limits of finite element stress results (see Figure 2.16).
- e. Stresses in cell walls: peak stresses in the cell walls were plotted. Since these were not consistently near the top or bottom surfaces, these

results are somewhat diffuse. They were not obtained for the "TRADE-OFF" model since there is little meaning in this.

- f. Stresses in solid support area: nodal-averaged stresses were indicated on various views of the three-dimensional solid element support area. While the figures show surface layer stresses, the interior values were not seriously different, and could only be properly presented by three-dimensional holography.

## 2.6 Summary of Phase "A" Design

The results of the "EXACT" or "cell webs" model are summarized in Table 2.1. The maximum deflection, the peak-to-peak deviation from the best-fit sphere (also known as the half-optical path difference), the RMS of the deviations from the best-fit sphere (useful for Strehl ratio calculations), and the peak tensile stress are recorded for each of the loading environment cases. The number in the right-hand corner of each box refers to the figure on which the relevant data is graphically presented. The order of the figures in this chapter is arranged so that the different model types can be best compared.

With the operating wavelength of the telescope assumed to be in the visible range (5500 Å), the value of  $\lambda$  can be approximated by  $20 \times 10^{-6}$  inches. This value is compared now to the magnitude of the displacements, keeping in mind that a design goal has been stated at  $\lambda/40$  or  $0.5 \times 10^{-6}$  inches RMS.

It is clear from these results that the mirror may not rest for polishing purposes on its operating supports alone. An RMS error of  $3\lambda$  would then result in the zero-g condition. Thus it is absolutely mandatory to consider additional supports

Table 2.1. SUMMARY OF PHASE "A" MIRROR PERFORMANCE  
60° ALL PLATES

Loading Case	Max $\Delta$	Peak to Peak	RMS	Peak Tensile Stress
1g Transverse	$322 \times 10^{-6}$ in. (2.6)	$297 \times 10^{-6}$ in. (2.9)	$66 \times 10^{-6}$ in.	30 psi/g (2.15)
1°F Soak	$0.17 \times 10^{-6}$ (2.26)	$0.061 \times 10^{-6}$ (2.29)	$0.007 \times 10^{-6}$	$80 \times 10^{-6}$ psi (2.32)
1°F Transverse Grad.	$2.4 \times 10^{-6}$ (2.34)	$0.48 \times 10^{-6}$ (2.37)	$0.056 \times 10^{-6}$	$300 \times 10^{-6}$ psi (2.40)
1°F Radial Grad.	$0.33 \times 10^{-6}$ (2.42)	$0.24 \times 10^{-6}$ (2.45)	$0.04 \times 10^{-6}$	$1500 \times 10^{-6}$ psi (2.48)
'Sperry Temperatures'	$16.7 \times 10^{-6}$ (2.50)	$2.95 \times 10^{-6}$ (2.51)	$0.446 \times 10^{-6}$	$4000 \times 10^{-6}$ psi (2.52)

for manufacturing purposes and the 1-g net effect on the zero-g figure must be proven to be acceptable. This can probably be done analytically if done with care.

A 30 psi tension per g of acceleration may be a problem if launches are anticipated with TITAN III vehicles where the net g sometimes reaches 10. It is not too easy to be dogmatic here since the working stress for CERVIT has never been firmly established. This latter can only be done through a proper fracture mechanics test and analysis procedure. The fracture strength is sometimes rumored to be around 1000 psi, but results have not been published, and a good factor of safety is most desirable.

It is assumed that the "Sperry Temperatures" represent a reasonable first order approximation to the actual thermal operating conditions. Under those conditions it appears that the RMS value does not exceed the  $\lambda/40$  limit, although it should really be somewhat less to allow for other sources of figure error. It should also be noted that the thermoelastic calculation was based on an idealized (manufacturer supplied) thermal expansion coefficient ( $.277 \times 10^{-7}$  in/in/ $^{\circ}$ F). Some preliminary reports indicate that this may be a highly optimistic value, although no hard data is available at this time. Since the mirror performance depends so highly on this parameter and its variation through the mirror and over temperature ranges, it is vital that real test results from the real mirror blank be introduced into the thermoelastic calculations.

## 2.7 Summary of Mirror Model Comparisons

Tables 2.2 through 2.5 summarize the comparisons between the three modelling methods. Again as before, the contour figure numbers are shown in parentheses after the performance number. In some cases the box is blank, indicating that the

Table 2.2. GRAVITY LOAD RESPONSE (IN.)

Element Model	Max Δ	Peak to Peak	RMS	Tensile Stress
'Exact'	$322 \times 10^{-6}$ (2.6)	$297 \times 10^{-6}$ (2.9)	$66 \times 10^{-6}$	30 psi (2.15)
Alt. Webs	$348 \times 10^{-6}$ (2.7)	$329 \times 10^{-6}$ (2.10)	$86 \times 10^{-6}$	25 psi (2.17)
Trade-off	$323 \times 10^{-6}$ (2.8)	$258 \times 10^{-6}$ (2.11)	$56 \times 10^{-6}$	40 psi (2.18)

Table 2.3. 1°F SOAK RESPONSE (IN.)

Element Model	Max Δ	Peak to Peak	RMS	Tensile Stress
'Exact'	$1.7 \times 10^{-7}$ (2.26)	$.61 \times 10^{-7}$ (2.29)	$.069 \times 10^{-7}$	$80 \times 10^{-6}$ (2.32)
Alt. Webs	$1.7 \times 10^{-7}$ (2.27)	$.70 \times 10^{-7}$ (2.30)	$.087 \times 10^{-7}$	$40 \times 10^{-6}$ (2.33)
Trade-off	$2.0 \times 10^{-7}$ (2.28)	$2.6 \times 10^{-7}$ (2.31)	$.43 \times 10^{-7}$	—

Table 2.4. 1° F TRANSVERSE GRADIENT—RESPONSE (IN.)

Element Model	Max Δ	Peak to Peak	RMS	Tensile Stress
'Exact'	$24 \times 10^{-7}$ (2.34)	$4.8 \times 10^{-7}$ (2.37)	$.56 \times 10^{-7}$	$300 \times 10^{-6}$ (2.40)
Alt. Webs	$24 \times 10^{-7}$ (2.35)	$4.1 \times 10^{-7}$ (2.38)	$.62 \times 10^{-7}$	$400 \times 10^{-6}$ (2.41)
Trade-off	$32 \times 10^{-7}$ (2.36)	$.56 \times 10^{-7}$ (2.39)	$.11 \times 10^{-7}$	—

Table 2.5. 1° F RADIAL GRADIENT—RESPONSE (IN.)

Element Model	Max Δ	Peak to Peak	RMS	Tensile Stress
'Exact'	$3.3 \times 10^{-7}$ (2.42)	$2.4 \times 10^{-7}$ (2.45)	$.39 \times 10^{-7}$	$1500 \times 10^{-6}$ (2.48)
Alt. Webs	$3.0 \times 10^{-7}$ (2.43)	$1.7 \times 10^{-7}$ (2.46)	$.39 \times 10^{-7}$	—
Trade-off	$2.9 \times 10^{-7}$ (2.44)	$2.9 \times 10^{-7}$ (2.47)	$.54 \times 10^{-7}$	—

data found was not sufficiently conclusive to be reliably presented.

Table 2.2 indicates that the simpler models come reasonably close to yielding the same data as the "EXACT" model. These results are also verified qualitatively through a comparison of the shapes of the contour diagrams.

Table 2.3 indicates that while the "ALTERNATE WEB" model represents the 1<sup>o</sup>F soak behavior very similarly to the "EXACT", the "TRADE-OFF" model does relatively poorly in the peak-to-peak and RMS results. The stress results were rather inconclusive in the "TRADE-OFF" case as well.

Table 2.4 shows again that while the maximum deflections of the transverse thermal load can be comparable, the peak-to-peak and RMS results appear to have higher "noise/signal" ratios and are less conclusive. This is evident from the contour results as well.

The radial gradient data presented in Table 2.5 appears to be relatively consistent from model to model. This can also be deduced from the contour results.

In summary, it can be said that although many of the cases exhibit considerable divergences between the models, the very worst maximum deflection difference is about 30%, and with the average very much less than that. The peak-to-peak results of the "EXACT" and "ALTERNATE WEB" models agree well in all cases, but in two instances there is a difference of about half of an order of magnitude between the "EXACT" and the "TRADE-OFF" model. The results have been double-checked and it has been concluded that this is due to the nature of the displacement functions in the solid finite elements used in the "TRADE-OFF" model. A higher order element will cure this but at a considerable computational price. The same conclusions may be made for the RMS results.

These divergences of results do not condemn the "TRADE-OFF" model, however. Trends of behavior can be established, and the amplitude of that trend re-established from comparison with the results from an "EXACT" model benchmark. It should be recalled, moreover, that the "TRADE-OFF" model is the only one capable of obtaining even approximate results in a short period of time, and the only economical model for studies involving more than one design configuration. Its value is thus demonstrated, although it should be used with somewhat more than average care.

## 2.8 Actuator Local Effects

Actuators may be located either to span a cell, and have their effect divided across 6 nodes, or they may be located at the intersection of three cell walls alone. The displacement effect of this choice was studied on the alternate web model, as this tends to exaggerate the response (see Figure 2.53). Since the mirror model represents one-sixth of the whole, in reality the effect of six symmetrically placed actuators is being studied.

The results (see Figures 2.54 and 2.55) indicate that the actuator placed across the cell tends to produce a much smoother response surface with less localized effects than the cell wall intersection case. This makes the former much more desirable for correcting low spatial-frequency surface errors, while the converse is true for the latter.



## 2.9 Recommendations

As can be seen from many of the "deviations" plots, isolated but large peaks or valleys can be found at or near the supports. Since the interest of the program lies in the main reflecting surface area of the mirror, the contour intervals chosen were based on the interior surface performance, and the highly localized peaks are indicated only by their magnitude. These peaks do enter, however, into the best-fit sphere calculations, and if they are to be suppressed, strong rationale must be supplied.

These peaks can be traced to two major factors--mechanical design and mathematical modelling. With the type of mirror support detail indicated, it is expected that some degree of support disturbance would be observed. The magnitude of that disturbance depends highly on the compliance of the telescope mechanical system beyond the support location. In view of the uncertainties in that area, it was decided to model the supports so as to allow radial displacements only. This introduces a "clamping" phenomenon which, however, is seen to damp away quite quickly. It does result in "inflection" contours near the support, and possibly the peak numbers.

The other possible factor in the extreme values observed, is that of grid fineness in the solid elements. While a large number of solid elements were used in the model, the grid may not be fine enough to smooth out all of the fluctuations that occur. A model that would interpolate between existing element nodes would require almost an order of magnitude more nodes since all three dimensions must be involved. Since running costs are already exorbitant, it is probably wise to stop here.

If the extreme peaks are interpreted as grid size effects, they could be suppressed for the best-fit calculations and the peak to peak and rms values would be reduced. It is more likely that the mirror supports are the cause and in this case a large number of parametric modelling studies are necessary to establish optimal support compliances. It is probable, however, that even the best compliance will result in considerable support effects and in the final analysis masking of this area of the reflector might be necessary. The magnitude of that mask may be best established experimentally.

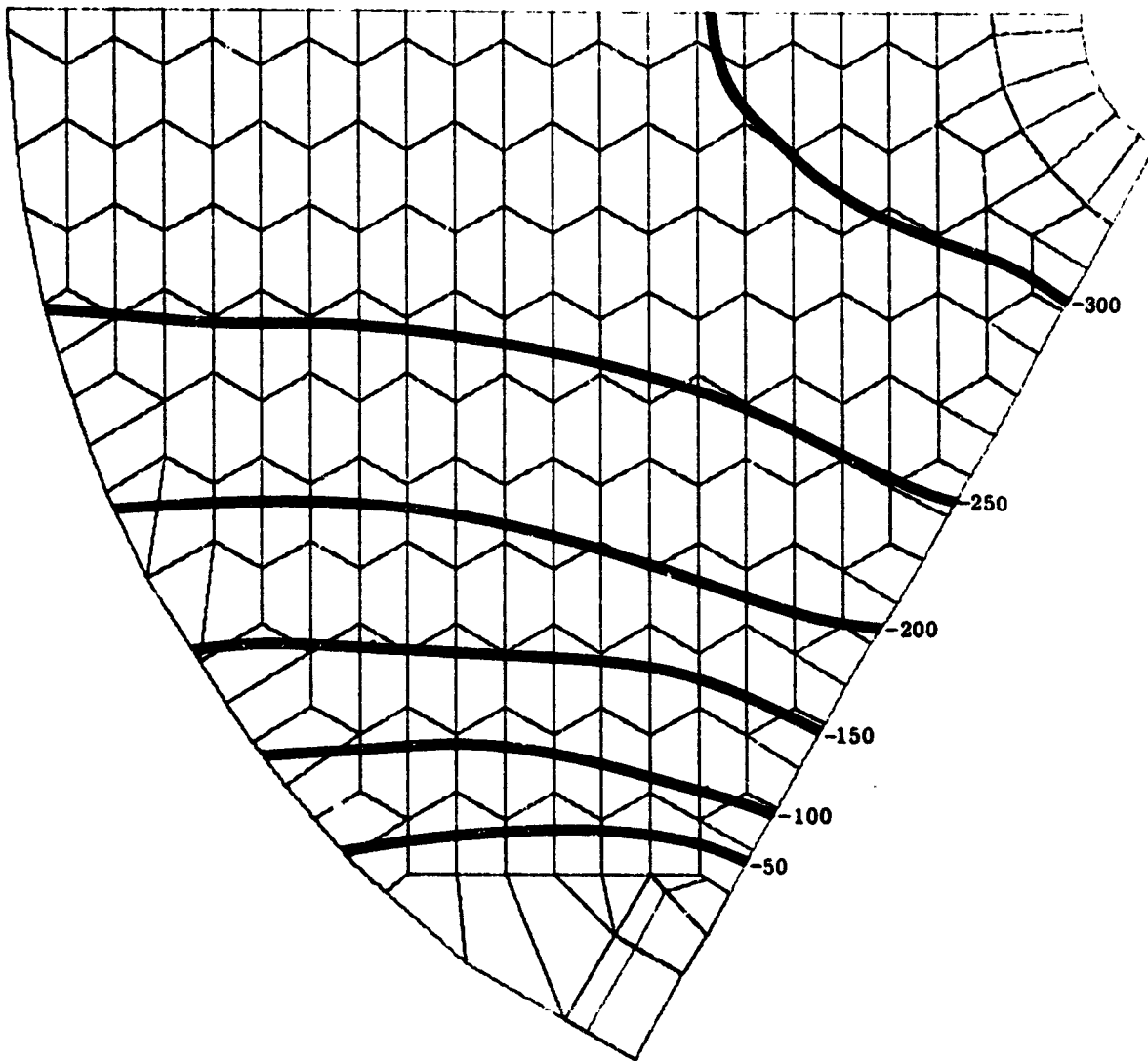


Figure 2.6. Optical Surface Displacements -  
lg Transverse - All Webs  
Scale: Displacements plotted  $\times 10^6$  inches

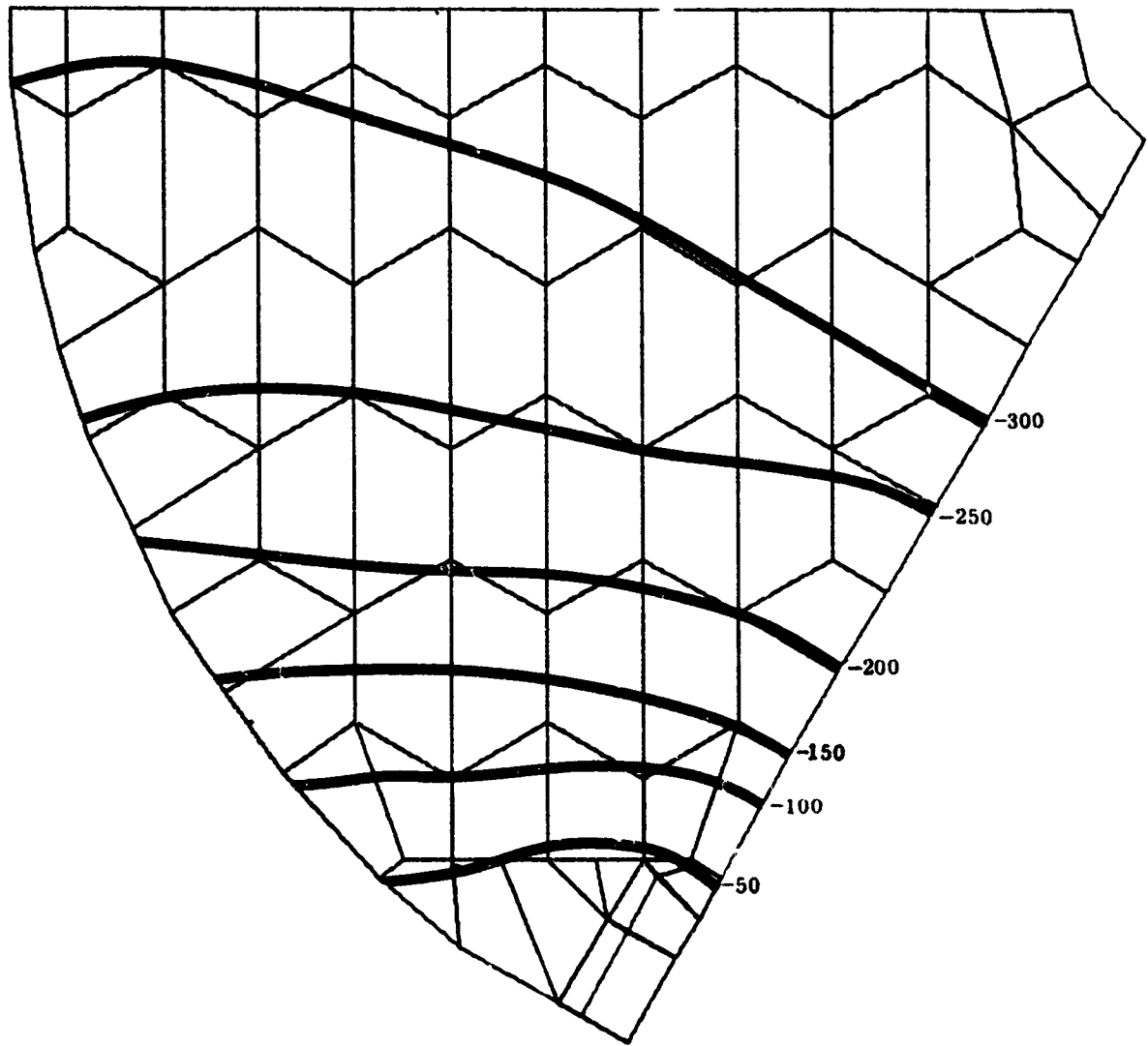


Figure 2.7. Optical Surface Displacements -  
lg Transverse - Alternate Webs  
Scale: Displacements plotted  $\times 10^6$  inches



Figure 2.8. Optical Surface Displacements -  
lg Transverse - Trade-Off Model  
Scale: Displacements x  $10^6$  inches

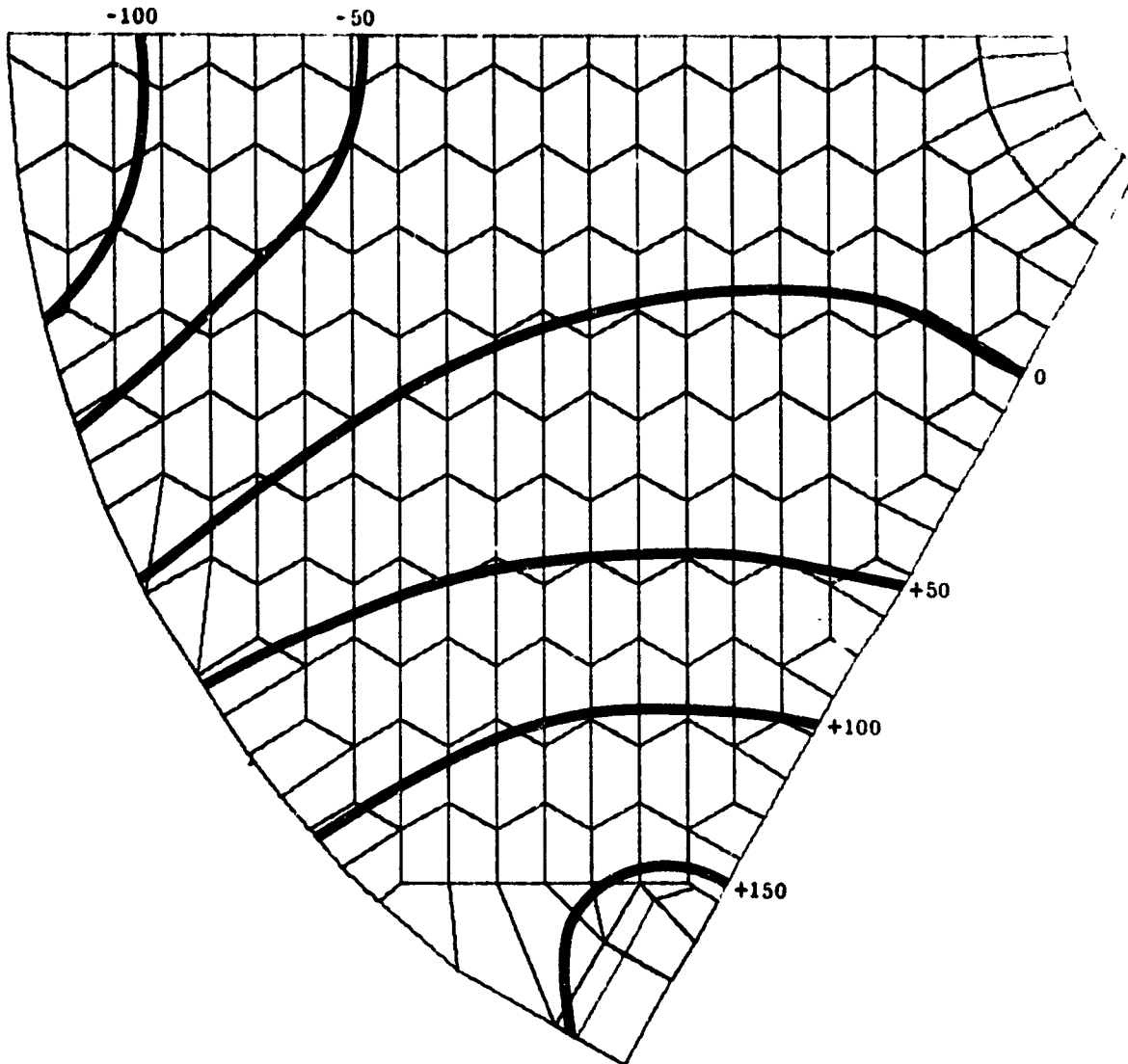


Figure 2.9. Deviations from Best-Fit Sphere -  
1g Transverse - All Webs  
Scale: Deviations x 10<sup>6</sup> inches

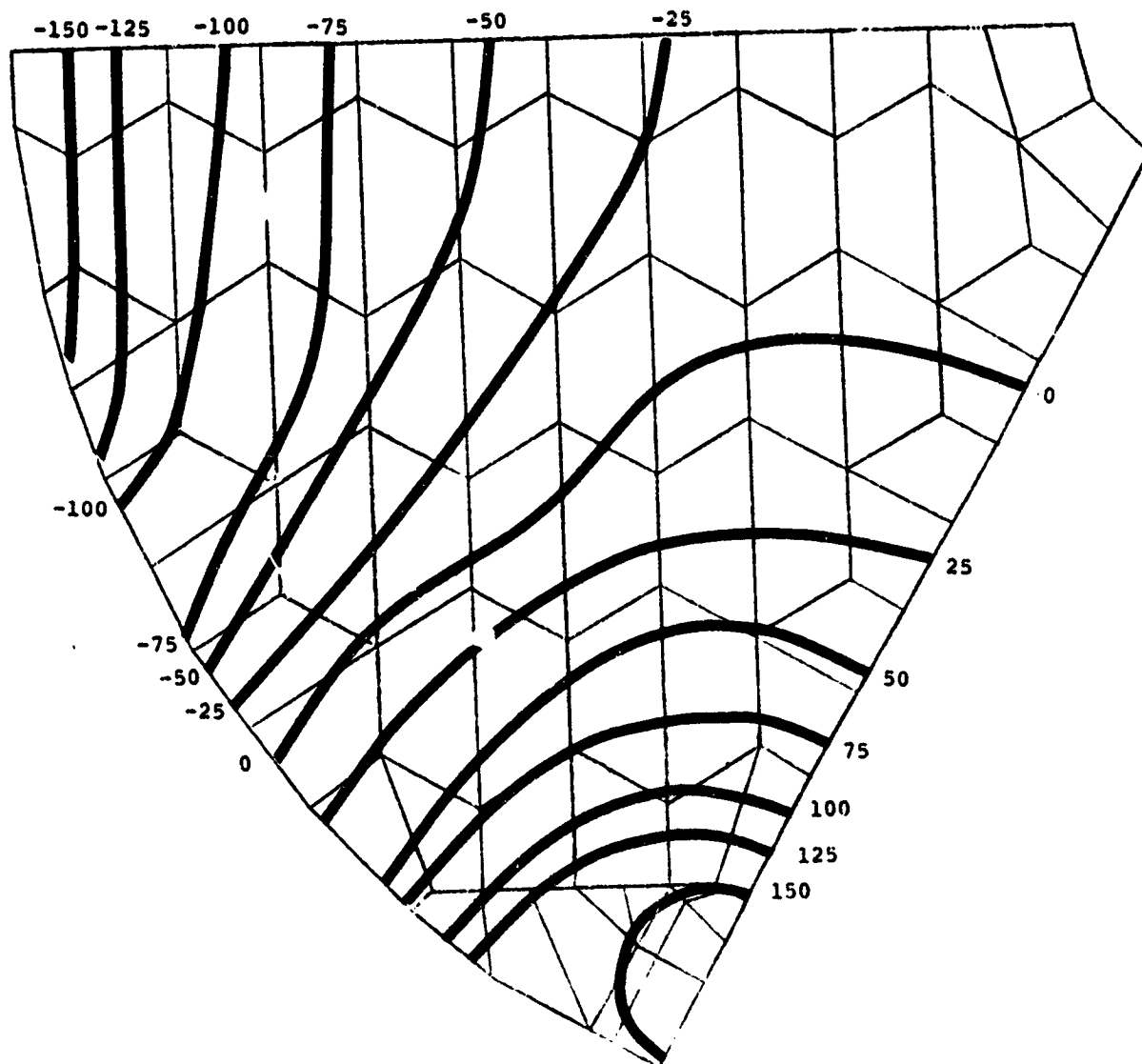


Figure 2.10 Deviations from Best-Fit Sphere -  
 1g Transverse - Alternate Webs  
 Scale: Deviations x 10<sup>6</sup> inches

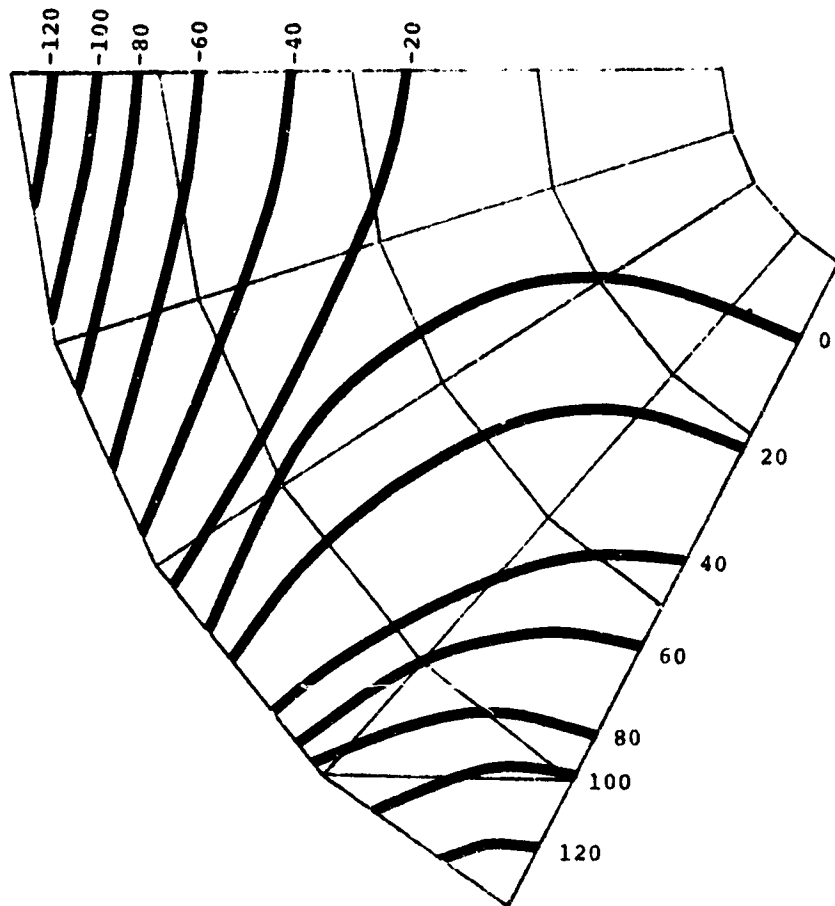


Figure 2.11. Deviations from Best-Fit Sphere -  
 1g Transverse - Trade-Off Model  
 Scale: Deviations x 10<sup>6</sup> inches



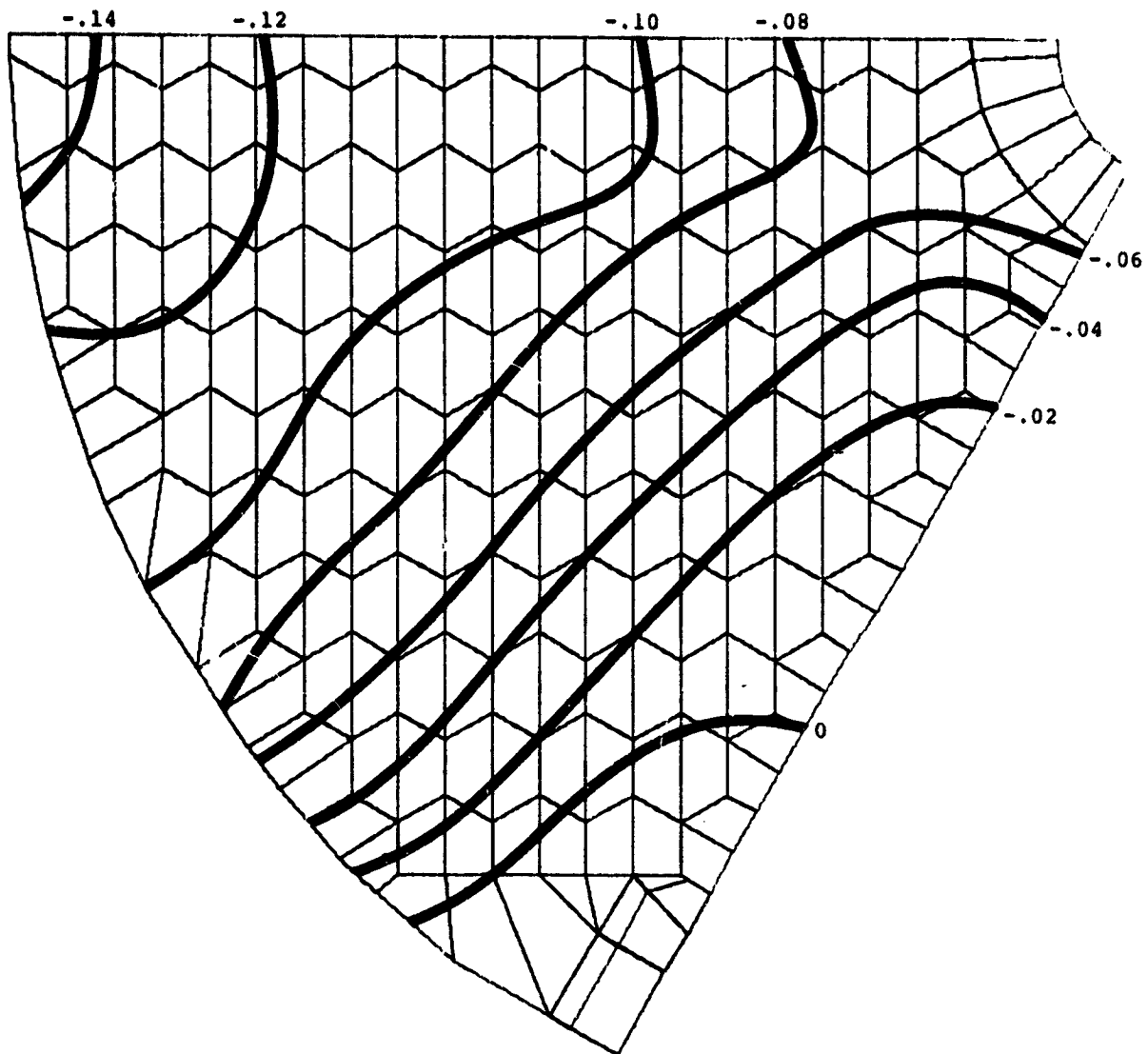


Figure 2.12. Stresses in Mirror Top Surface -  
lg Transverse - All Cells  
Scale: Stresses x 10<sup>2</sup> psi (Positive Tensile)

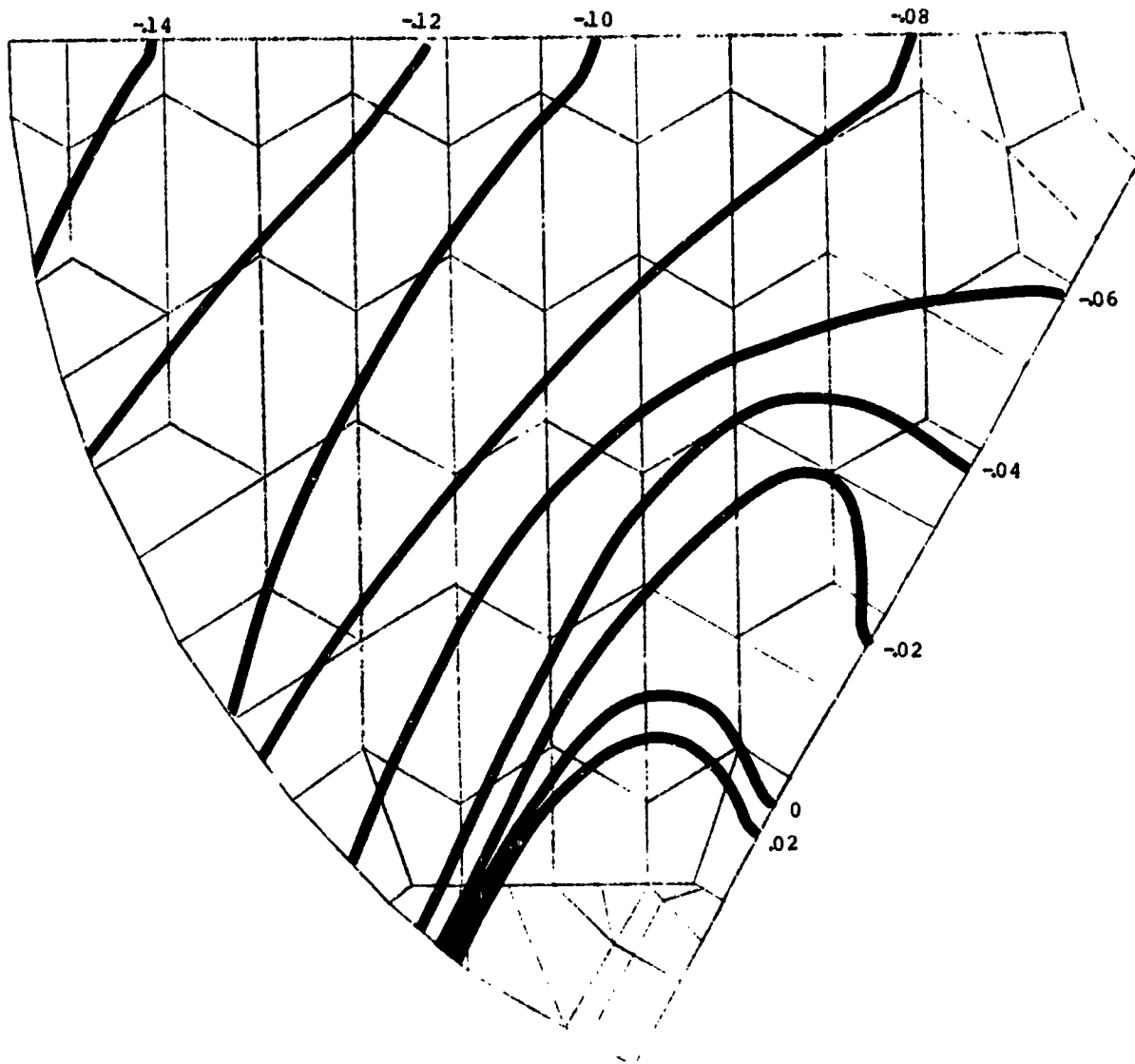


Figure 2.13. Stresses in Mirror Top Surface -  
 1g Transverse - Alternate Cells  
 Scale: Stresses x 10<sup>2</sup> psi (Positive Tensile)

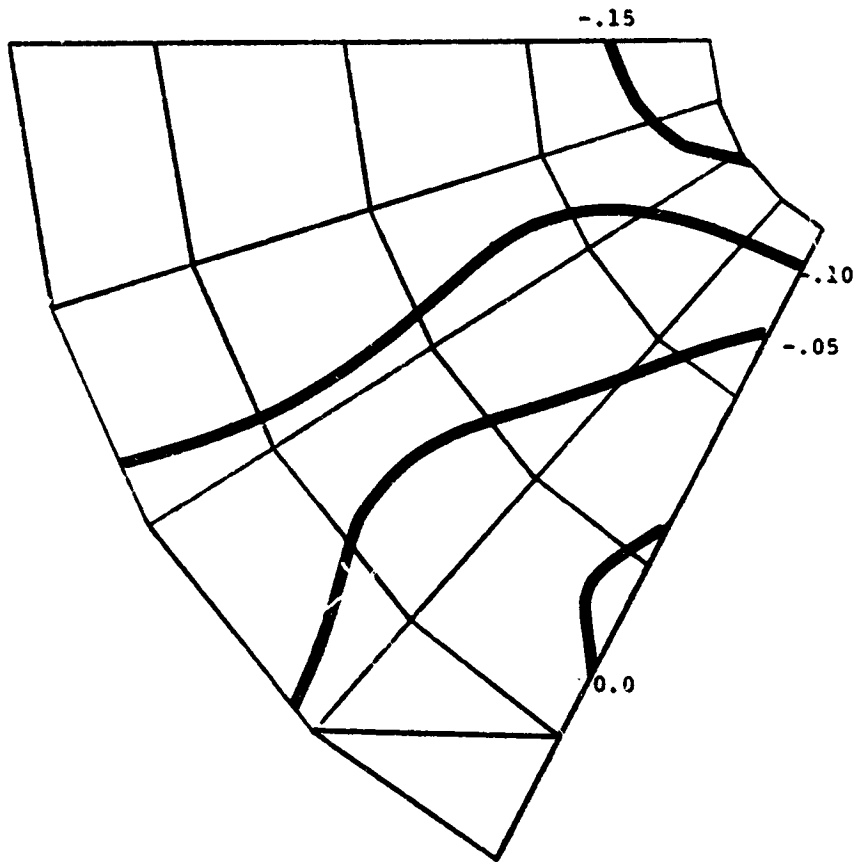


Figure 2.14. Stresses in Mirror Top Surface -  
lg Transverse - Trade-Off Model  
Scale: Stresses x 10<sup>2</sup> psi (Positive Tensile)

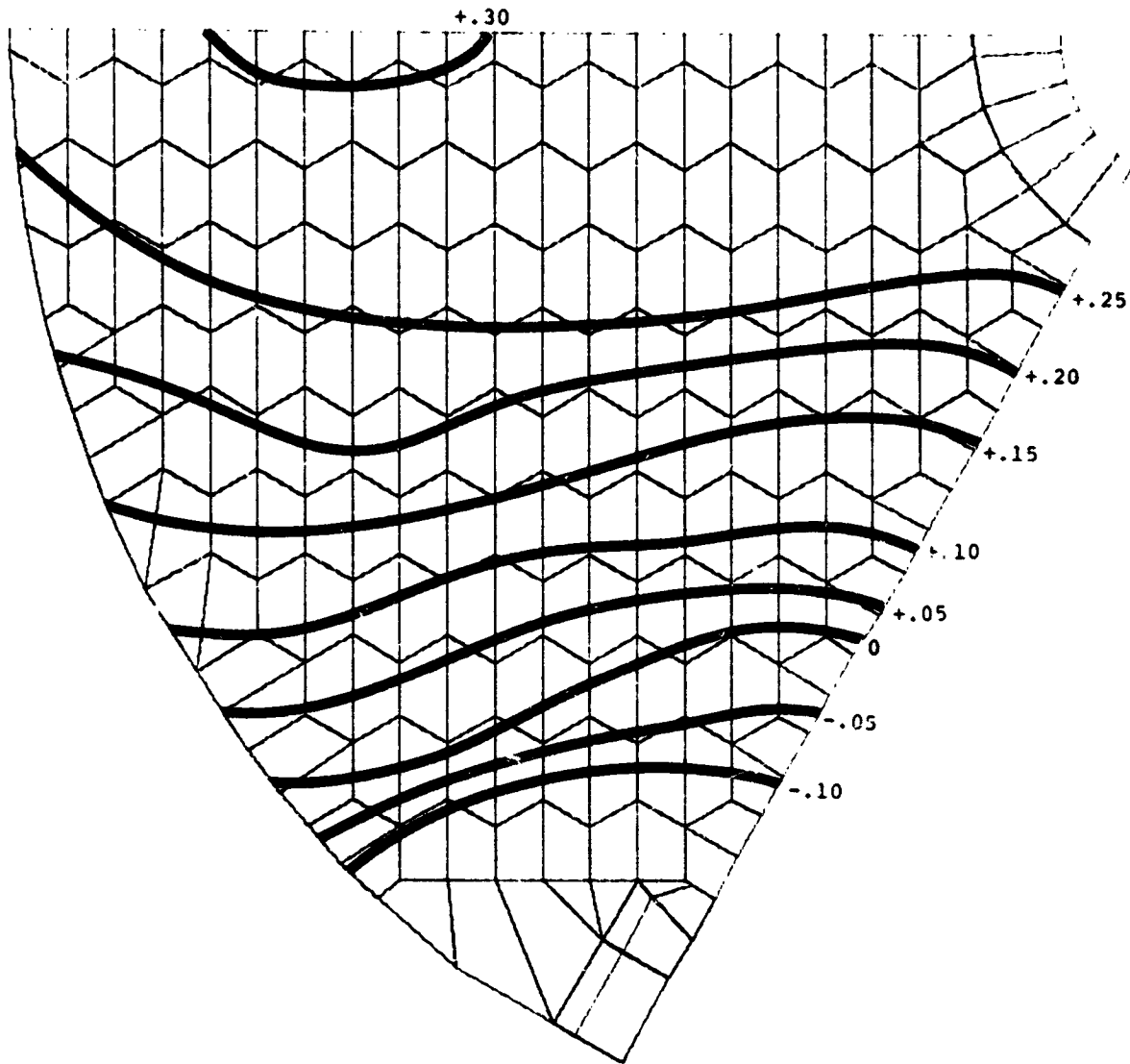


Figure 2.15. Stresses in Mirror Equivalent Back Surface -  
lg Transverse - All Cells  
Scale: Stresses Plotted  $\times 10^2$  psi  
(Positive Tensile)

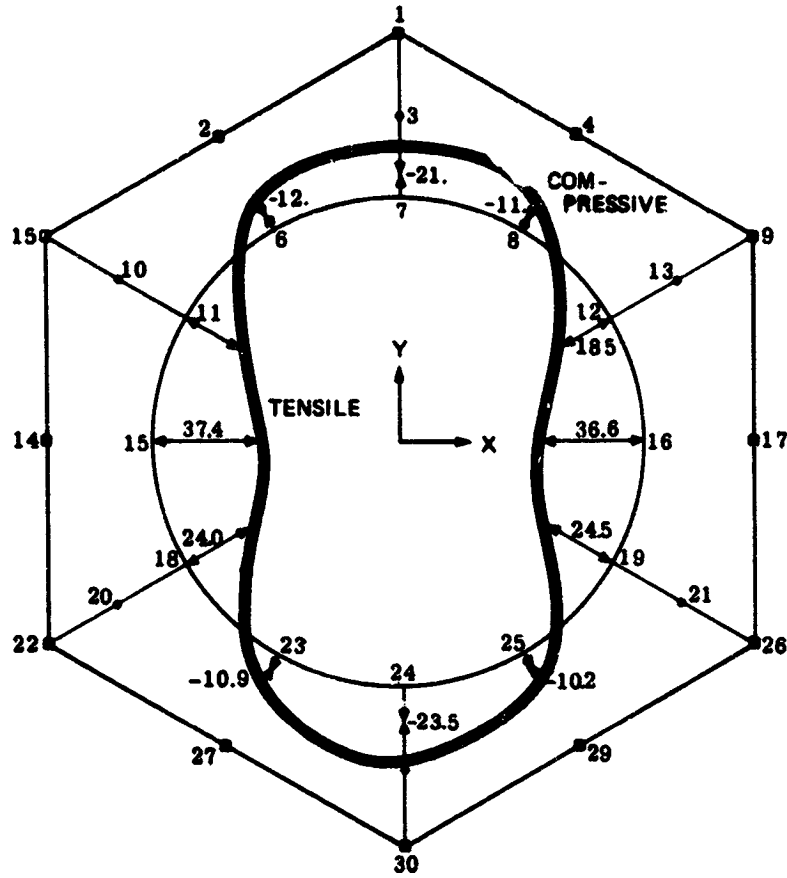


Figure 2.16. Local Back Surface - Stress Effects -  
 1g Transverse Results from Displacements  
 Applied to Boundary Joints.  
 Equivalent results 30 psi tension  
 Scale Stresses in psi (Positive Tensile)

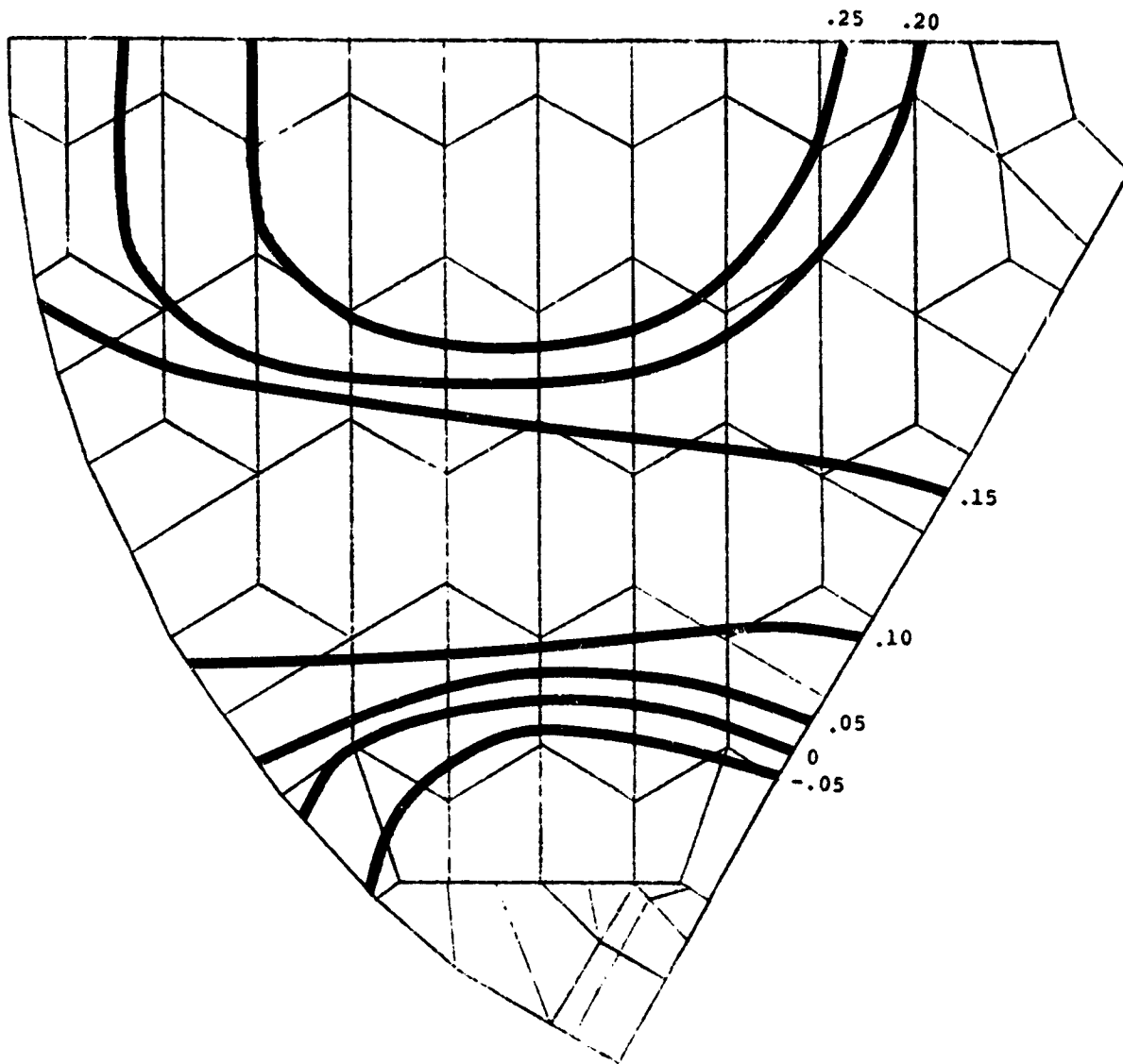


Figure 2.17. Stresses in Mirror Equivalent Back Surface -  
 1g Transverse - Alternate Cells  
 Scale: Stresses Plotted  $\times 10^2$  psi  
 (Positive Tensile)

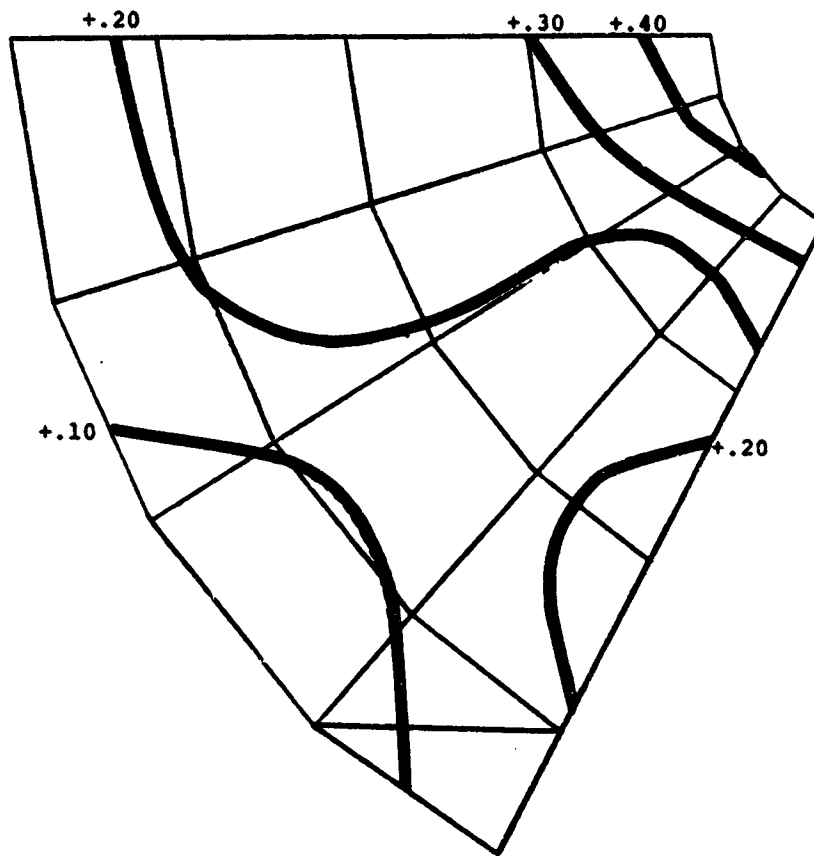


Figure 2.18. Stresses in Mirror Equivalent Back Surface -  
lg Transverse - Trade-Off Model  
Scale: Stresses Plotted  $\times 10^2$  psi  
(Positive Tensile)

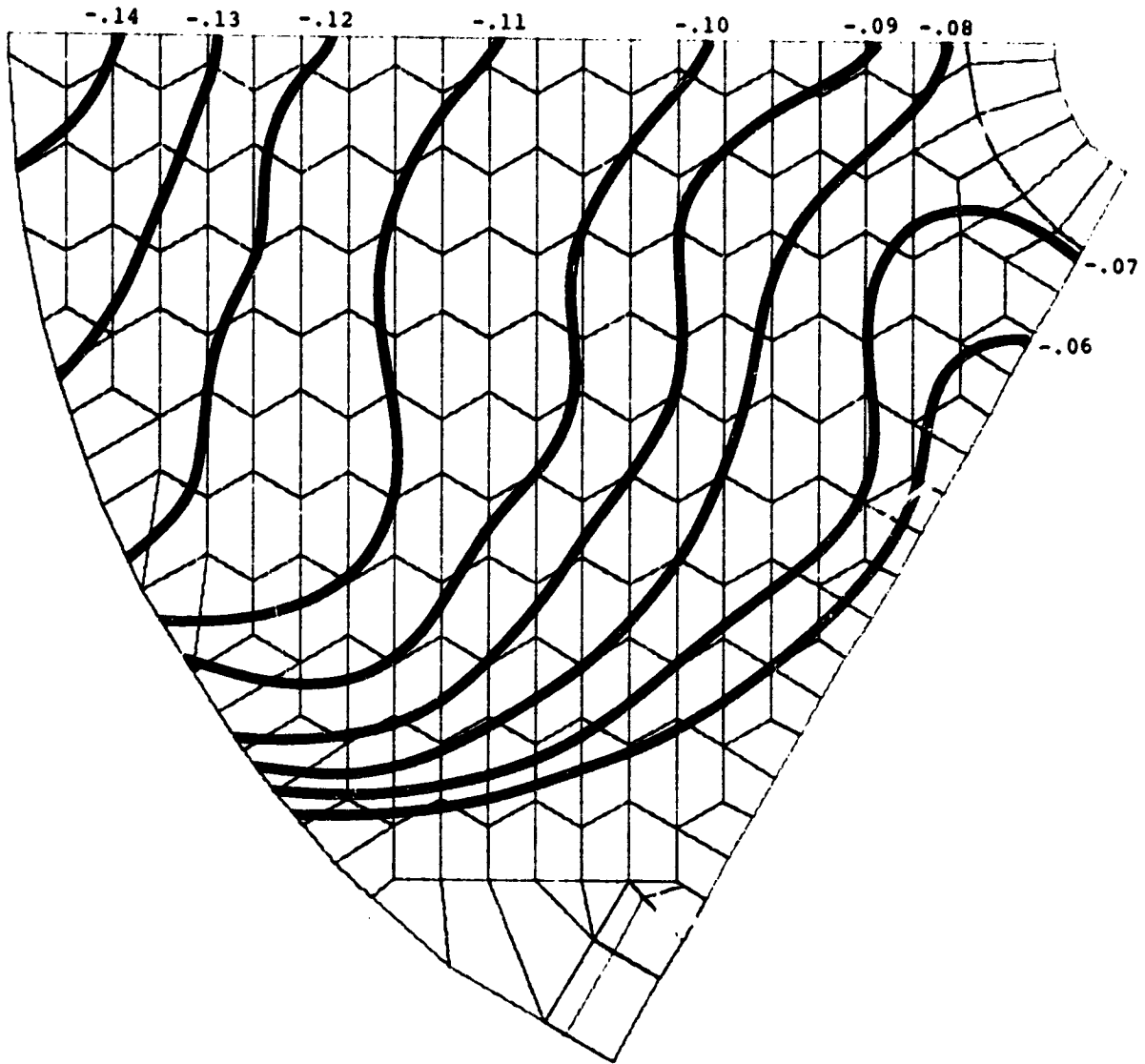


Figure 2.19. Maximum Cell Wall Stresses -  
lg Transverse - All Cells  
Scale: Stresses Plotted  $\times 10^2$  psi  
(Positive Tensile)



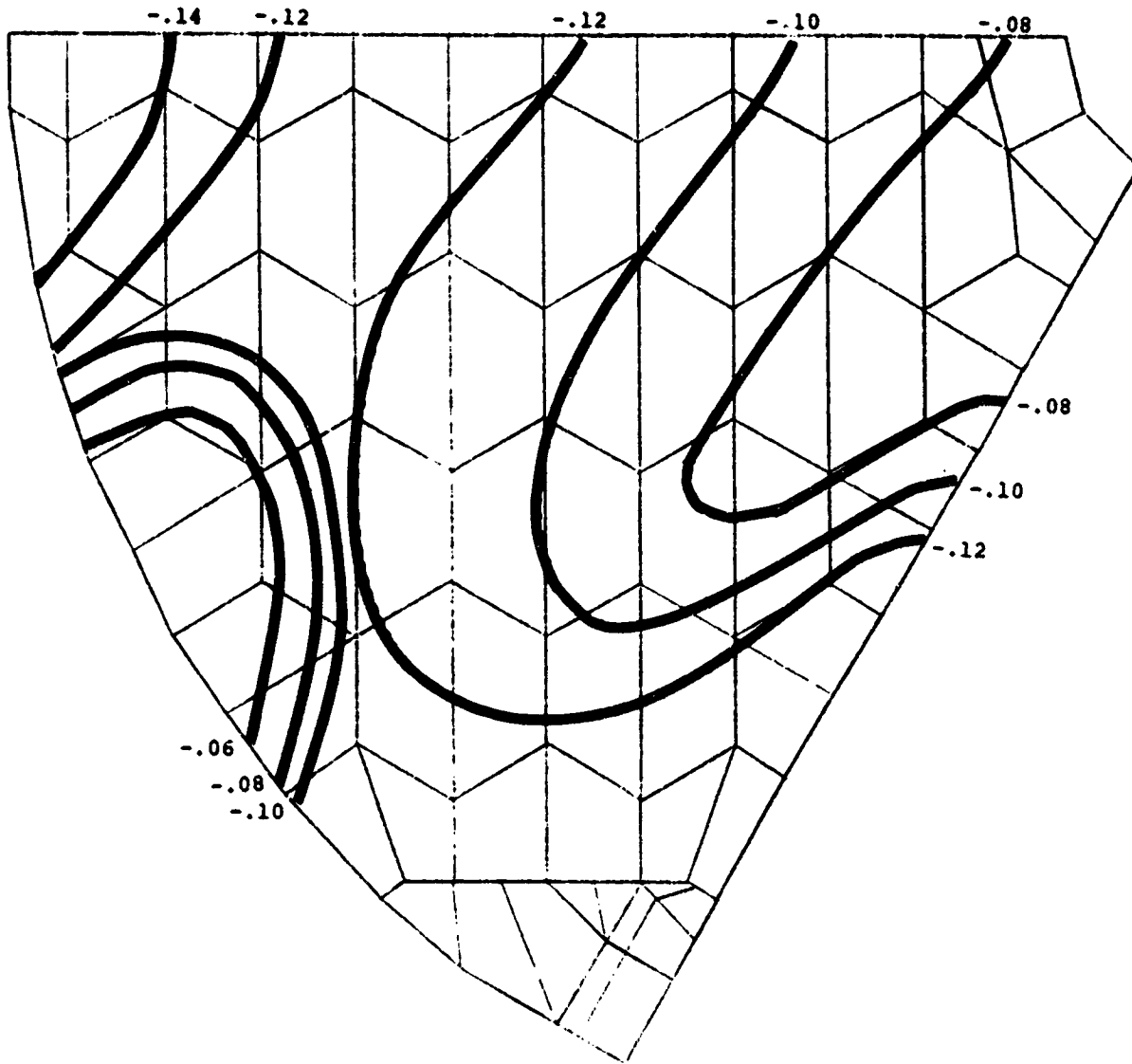


Figure 2.20. Maximum Cell Wall Stresses -  
 1g Transverse - Alternate Cells  
 Scale: Stresses Plotted  $\times 10^2$  psi  
 (Positive Tensile)

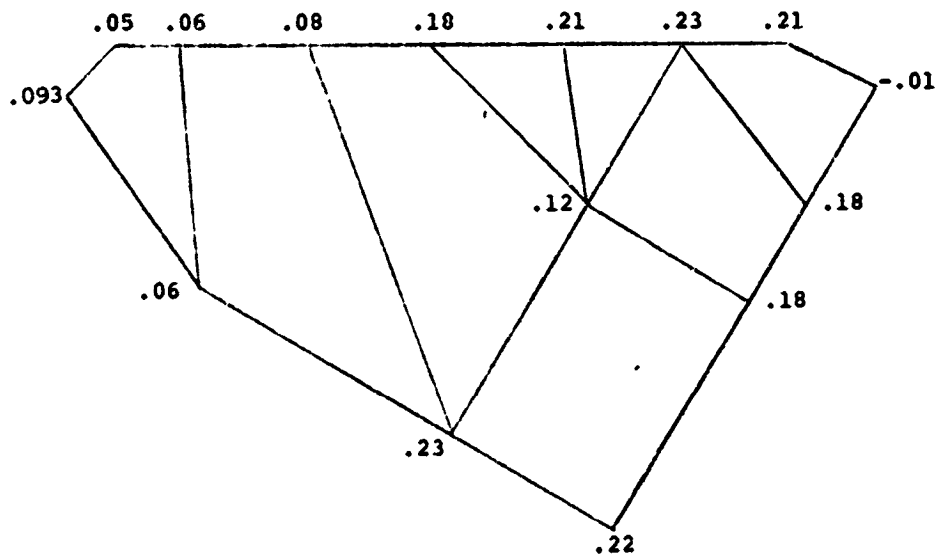


Figure 2.21. Stresses in Solid Support Area - Top Surface  
 lg Transverse - All Cells  
 Scale: Stresses x 10<sup>2</sup> psi  
 (Positive Tensile)

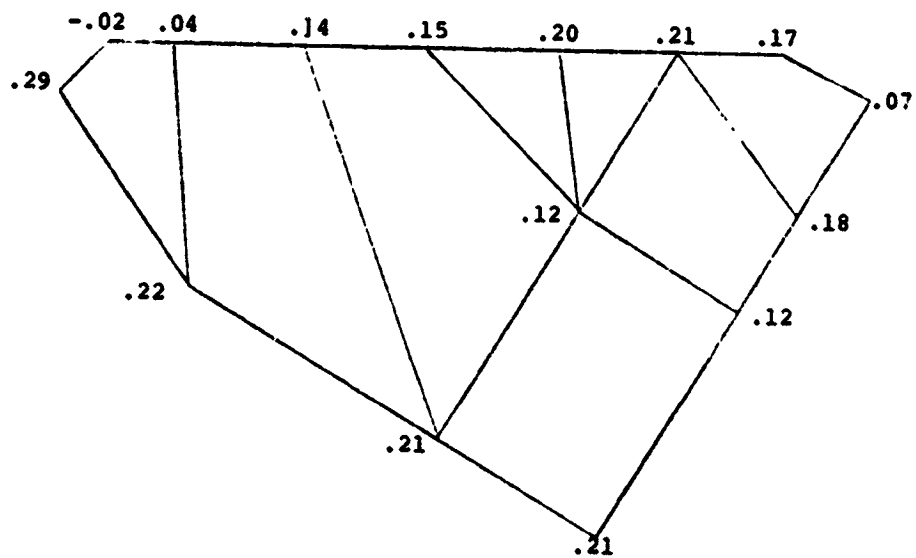


Figure 2.22. Stresses in Solid Support Area - Top Surface  
 lg Transverse - Alternate Cells  
 Scale: Stresses x 10<sup>2</sup> psi  
 (Positive Tensile)

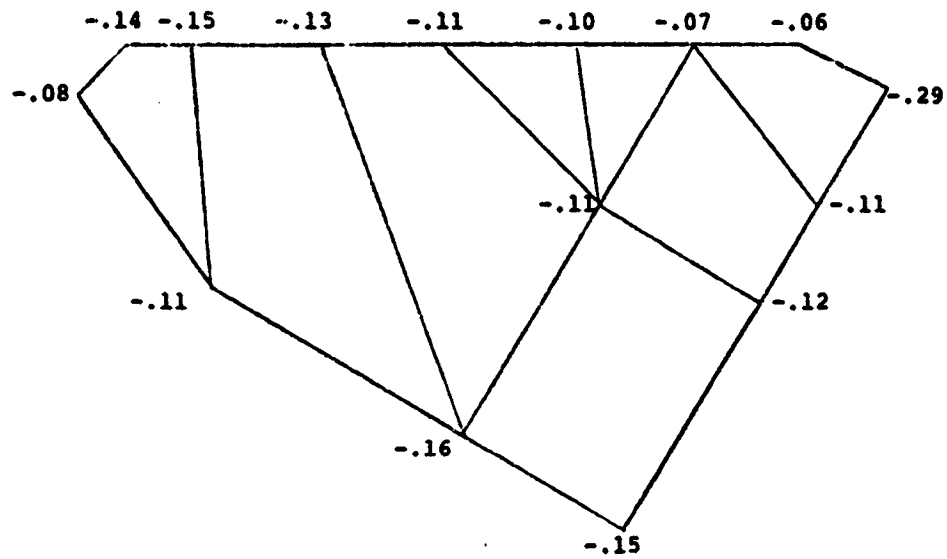


Figure 2.23. Stresses in Solid Support Area - Bottom Surface lg Transverse - All Cells  
 Scale: Stresses x 10<sup>2</sup> psi  
 (Positive Tensile)

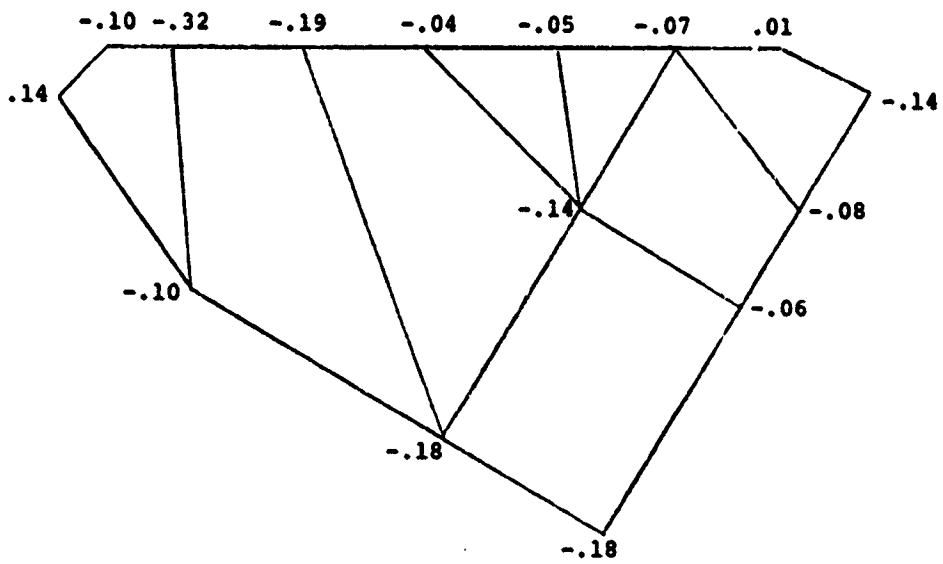


Figure 2.24. Stresses in Solid Support Area - Bottom Surface lg Transverse - Alternate Cells  
 Scale: Stresses x 10<sup>2</sup> psi  
 (Positive Tensile)

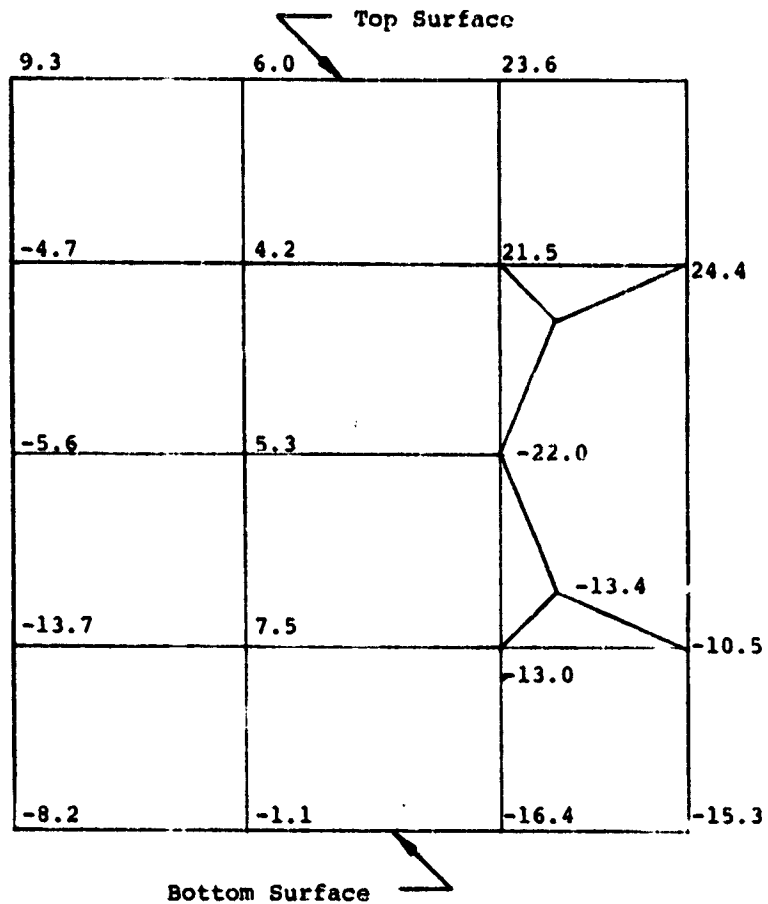
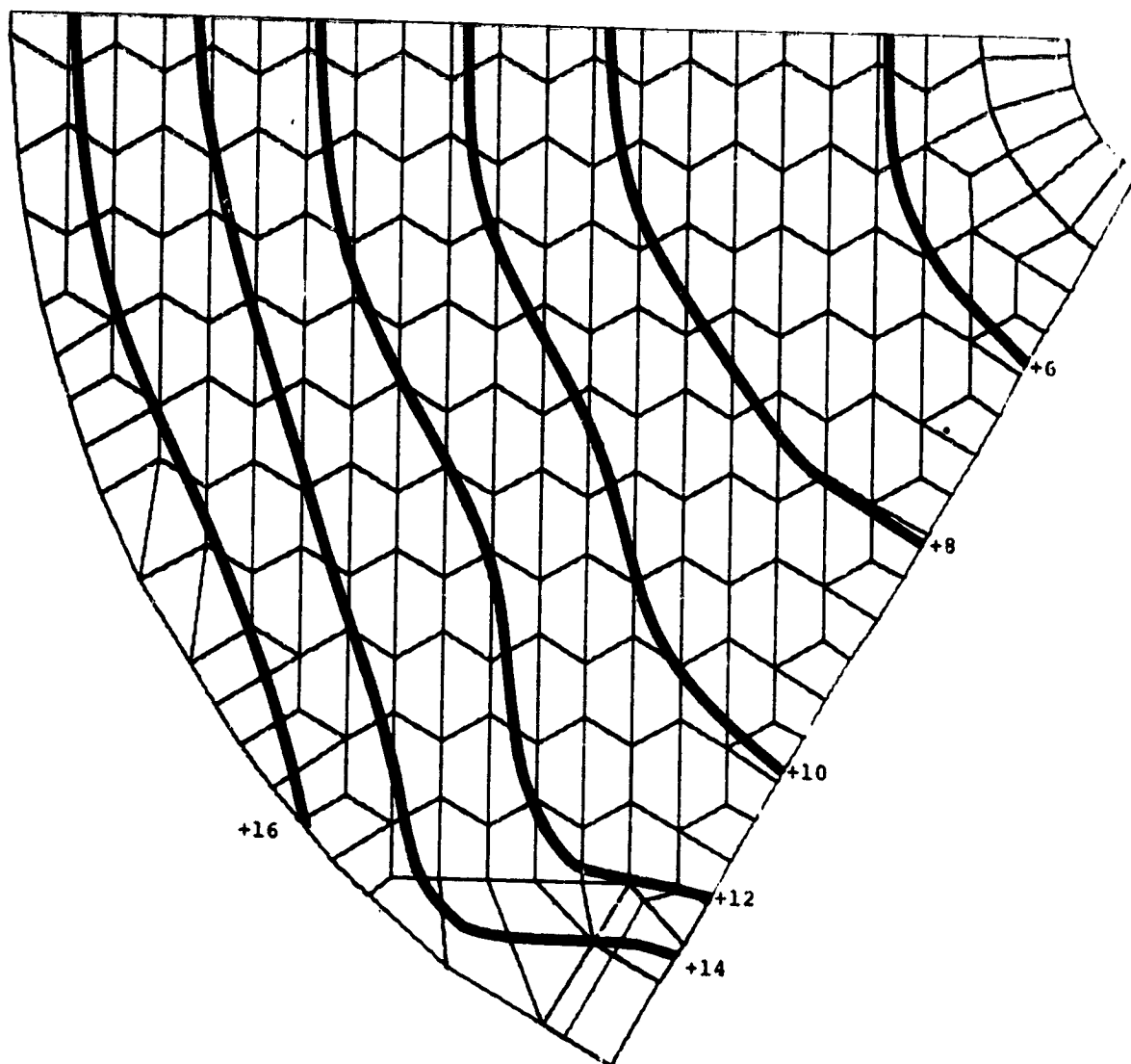


Figure 2.25. Stresses in Solid Support Area - Front Surface - lg Transverse - All Cells  
 Scale: Stresses in psi (Positive Tensile)  
 Stresses in Interior of Solid Range Around 10 psi



60° All Plates 120" Mirror

Figure 2.26. Optical Surface Displacements -  
 1<sup>o</sup>F Soak - All Webs  
 Scale: Displacements x 10<sup>8</sup> in.

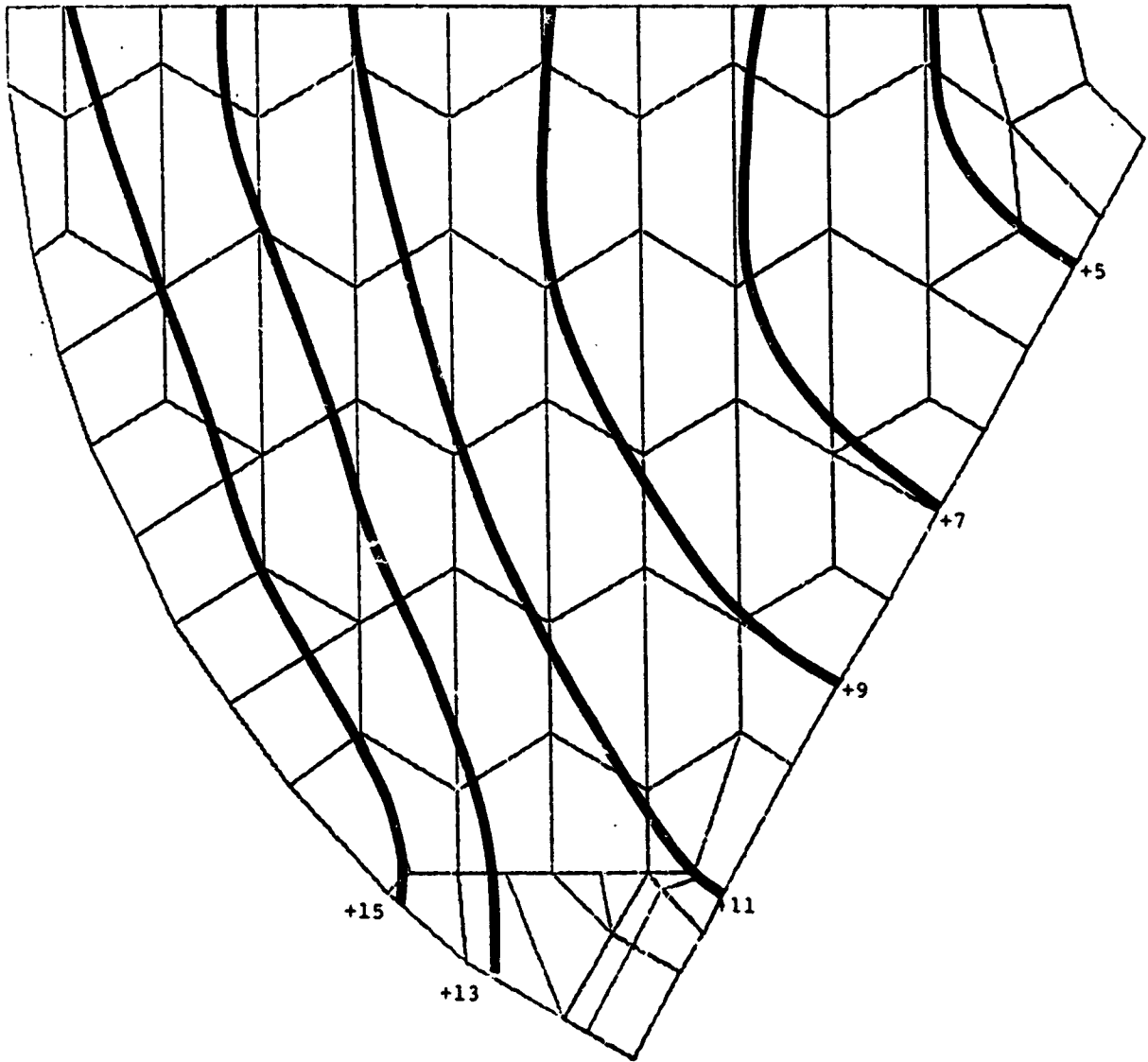


Figure 2.27. Optical Surface Displacements -  
 1<sup>o</sup>F Soak - Alternate Cells  
 Scale: Displacements x 10<sup>8</sup> in.



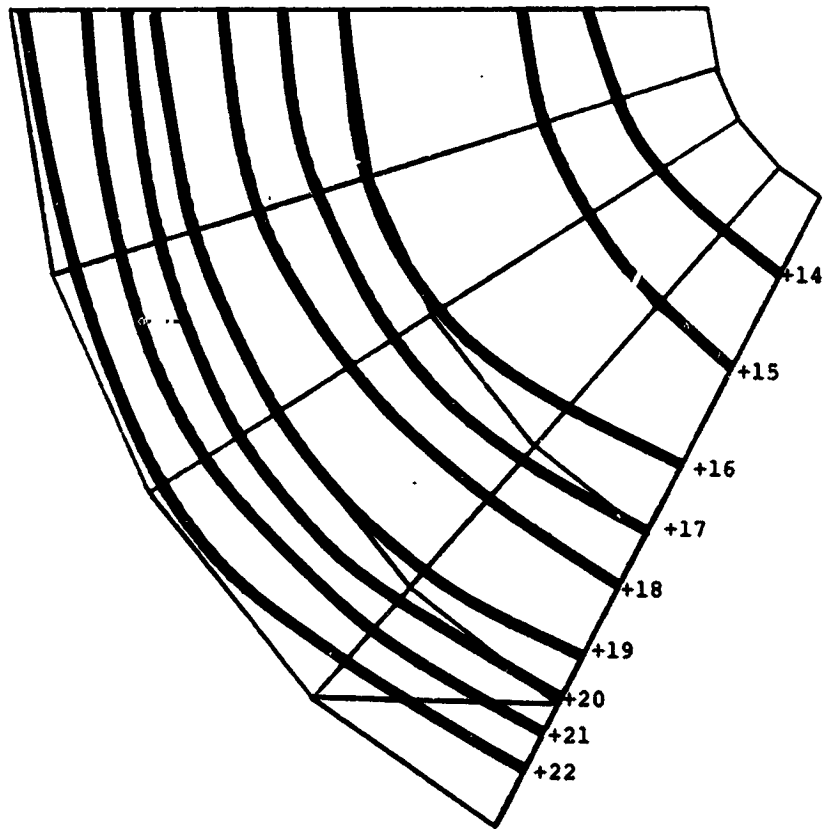


Figure 2.28. Optical Surface Displacements -  
1<sup>o</sup>F Soak - Trade-Off Model  
Scale: Displacements x 10<sup>8</sup> in.

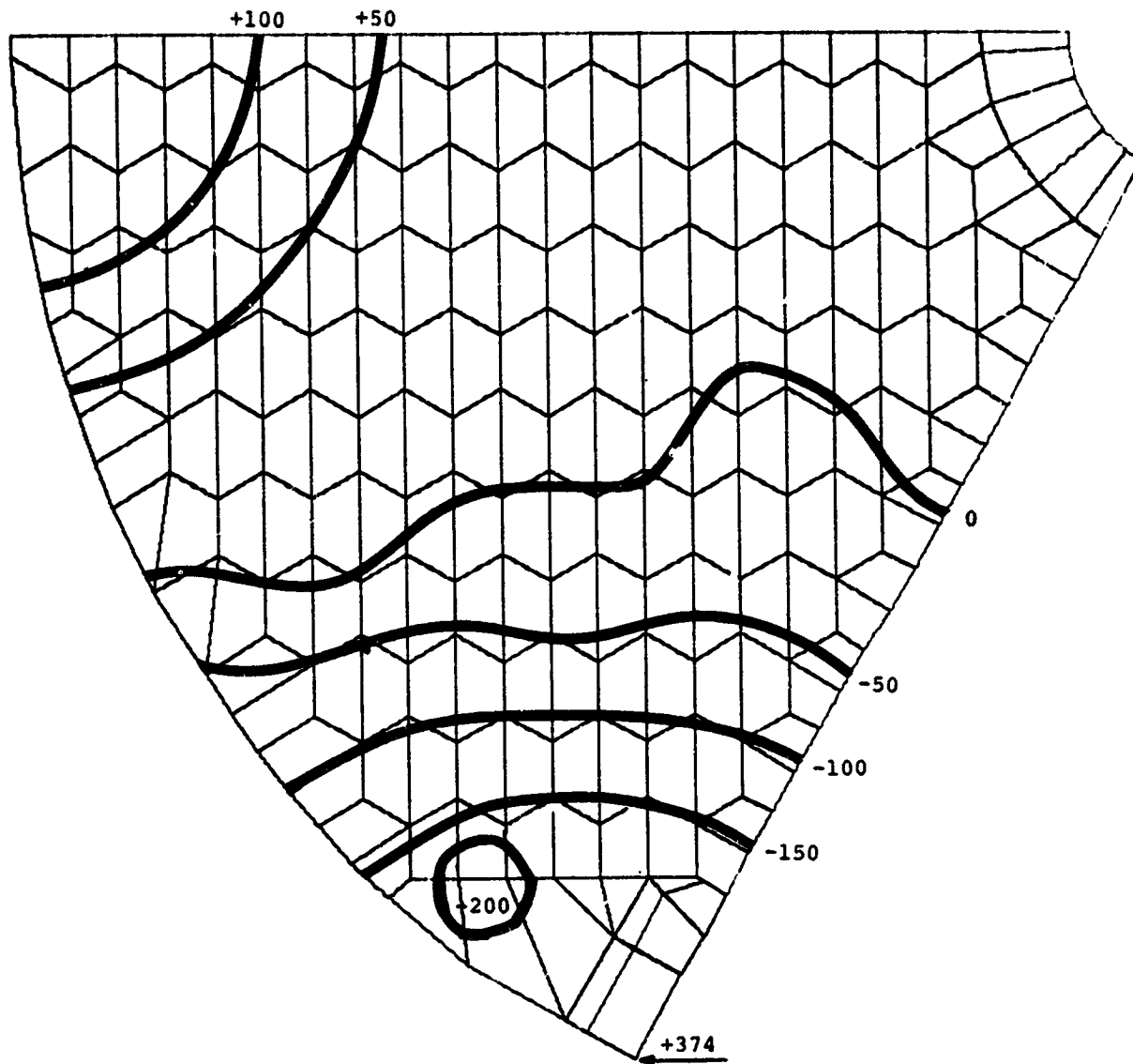


Figure 2.29. Deviations from Best-Fit Sphere -  
 1°F Soak - All Cells  
 Scale: Deviations x 10<sup>10</sup> inches

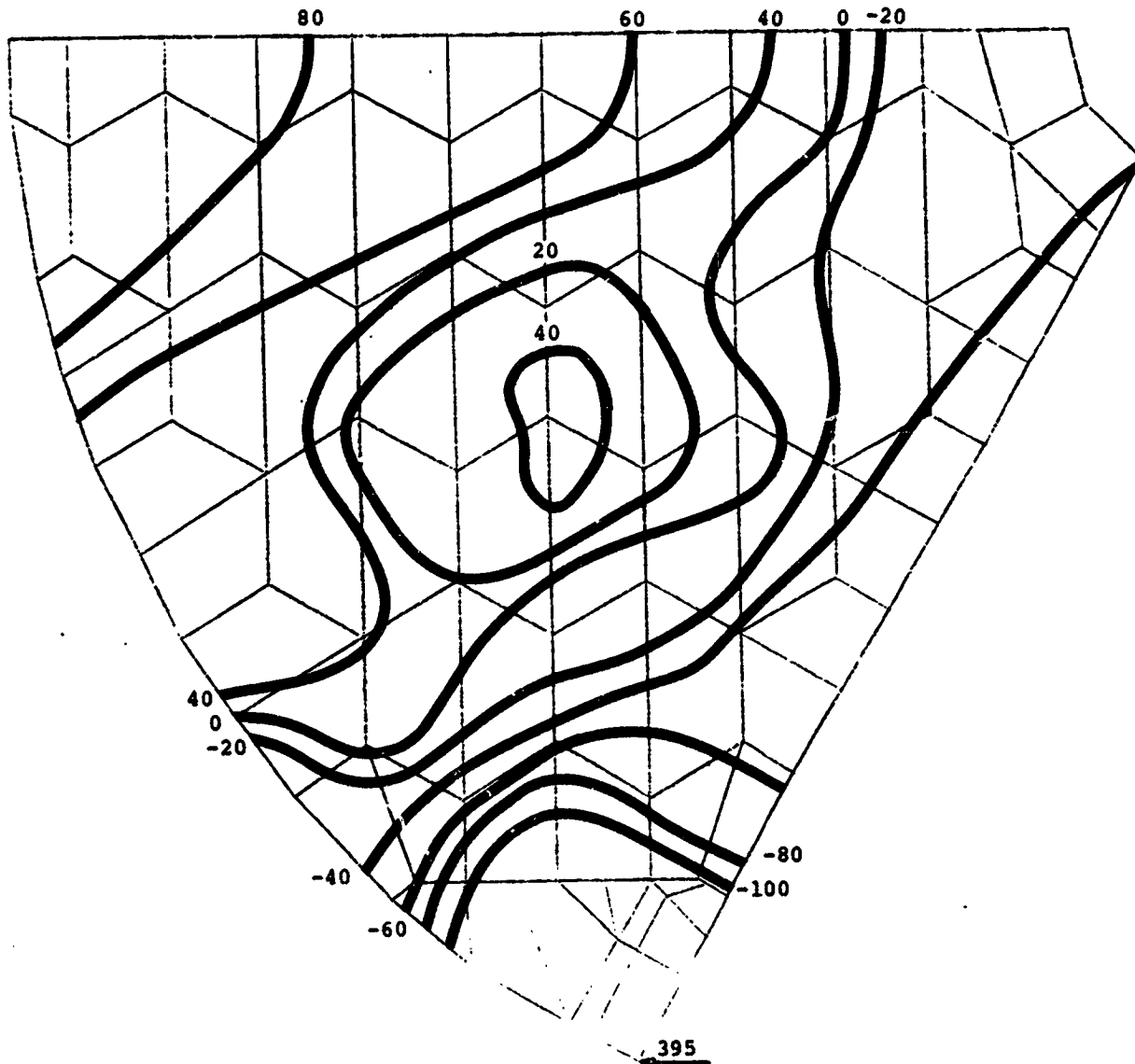


Figure 2.30. Deviations from Best-Fit Sphere -  
 10°F Soak - Alternate Cells  
 Scale: Deviations x 10<sup>10</sup> inches

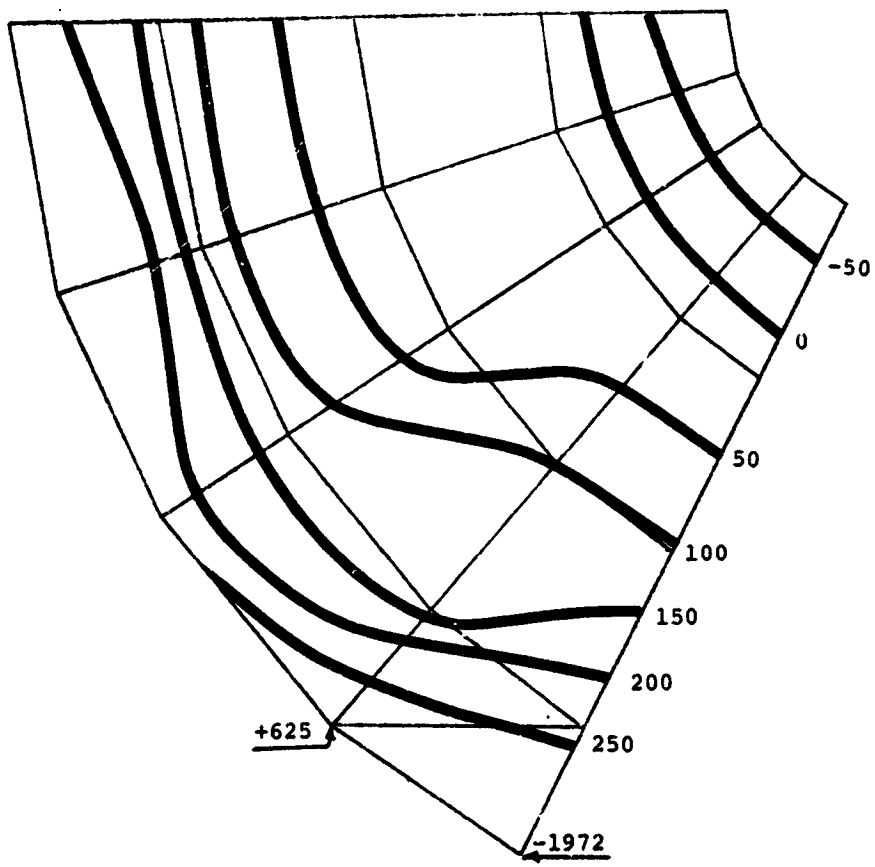


Figure 2.31. Deviations from Best-Fit Sphere -  
 1°F Soak - Trade-Off Model  
 Scale: Deviations x 10<sup>10</sup> inches

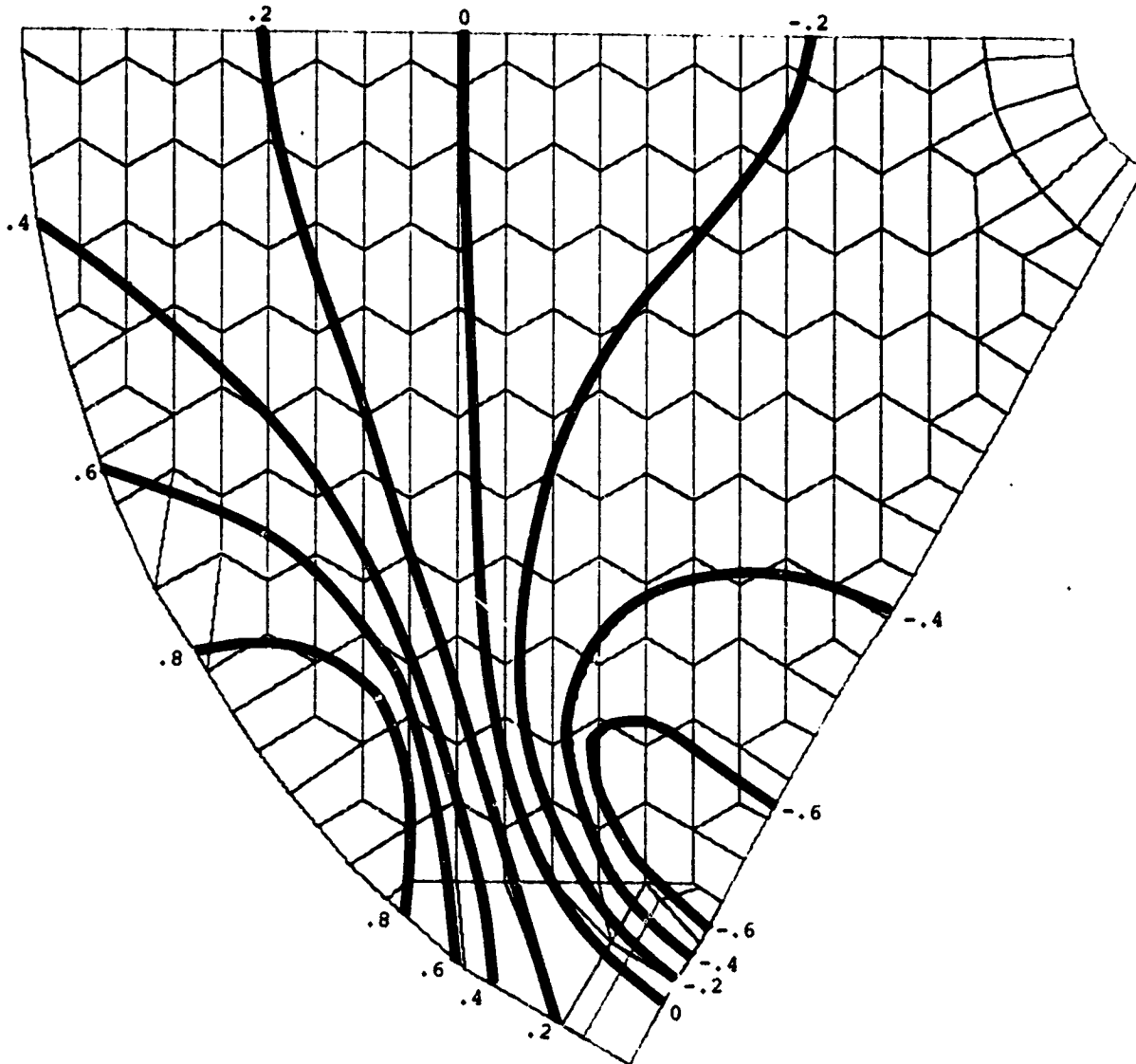


Figure 2,32. Top Surface Stresses - 1<sup>o</sup>F Soak - All Cells  
 Scale: Stresses x 10<sup>4</sup> psi

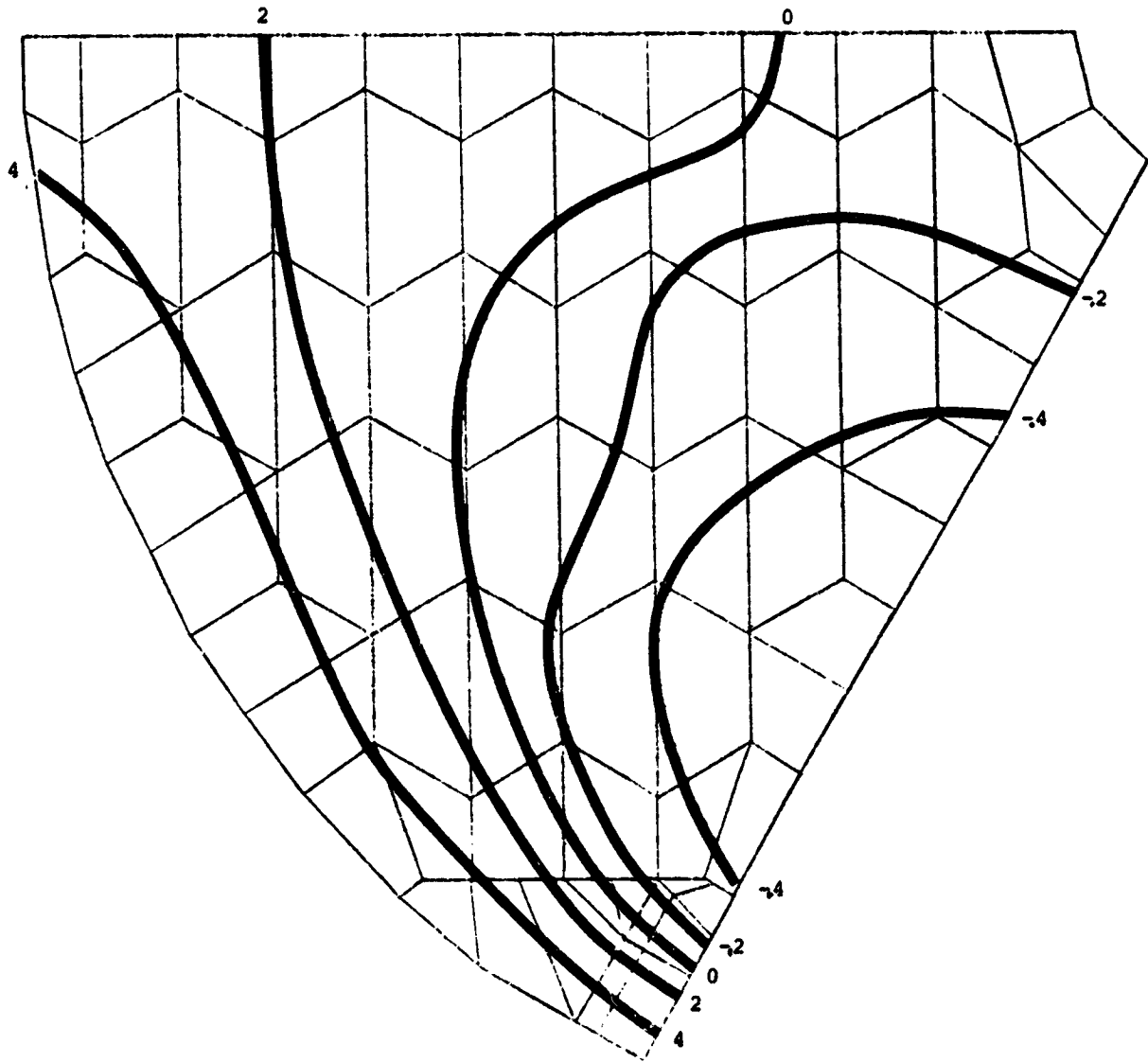


Figure 2.33. Top Surface Stresses 1° F Soak -  
 Alternate Cells  
 Scale: Stresses x 10<sup>4</sup> psi  
 (Positive Tensile)

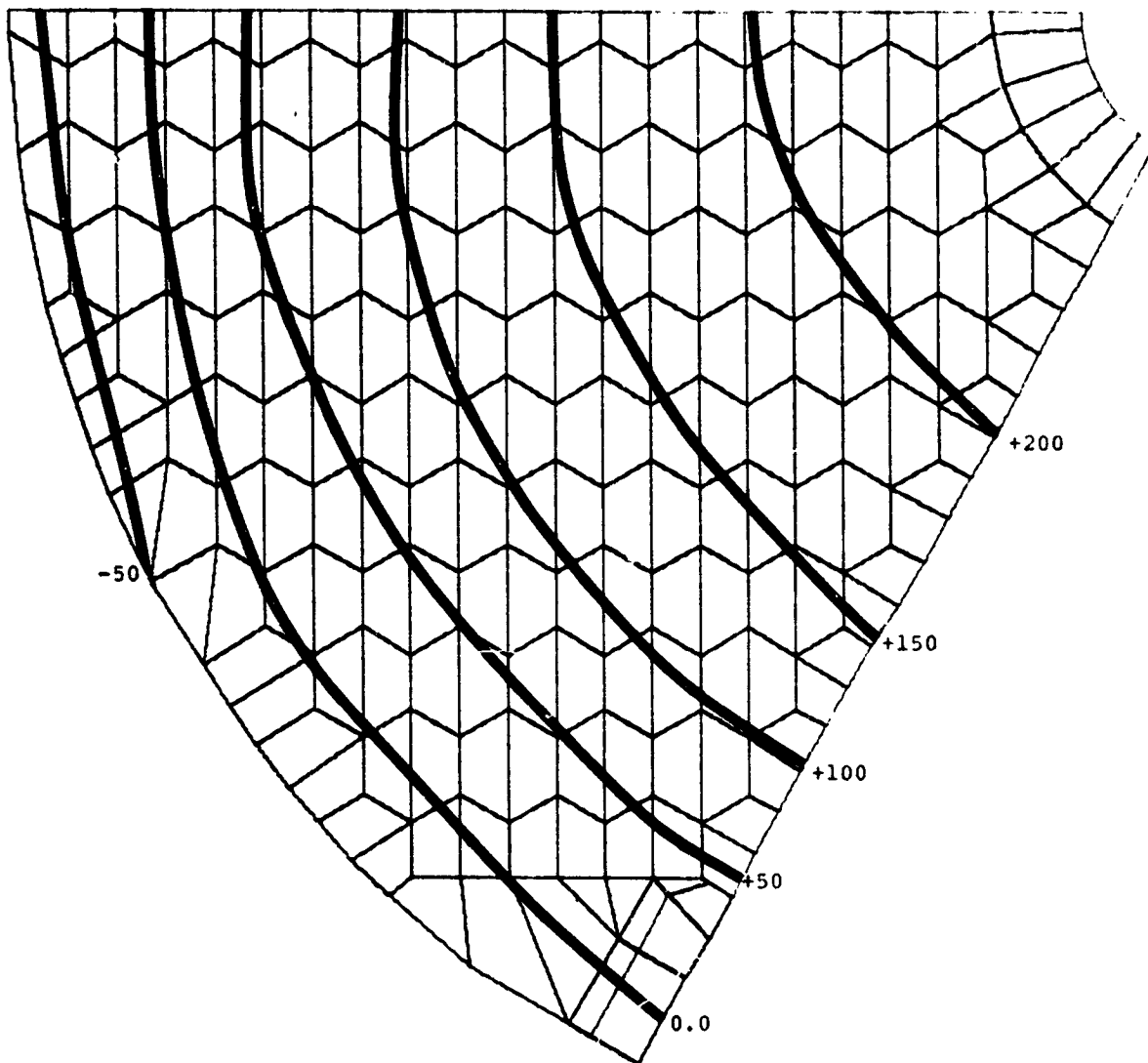


Figure 2.34. Optical Surface Displacements -  $1^{\circ}\text{F}$  Transverse  
Gradient - All Cells  
Scale: Displacements  $\times 10^8$  in.  
(Positive Upward)

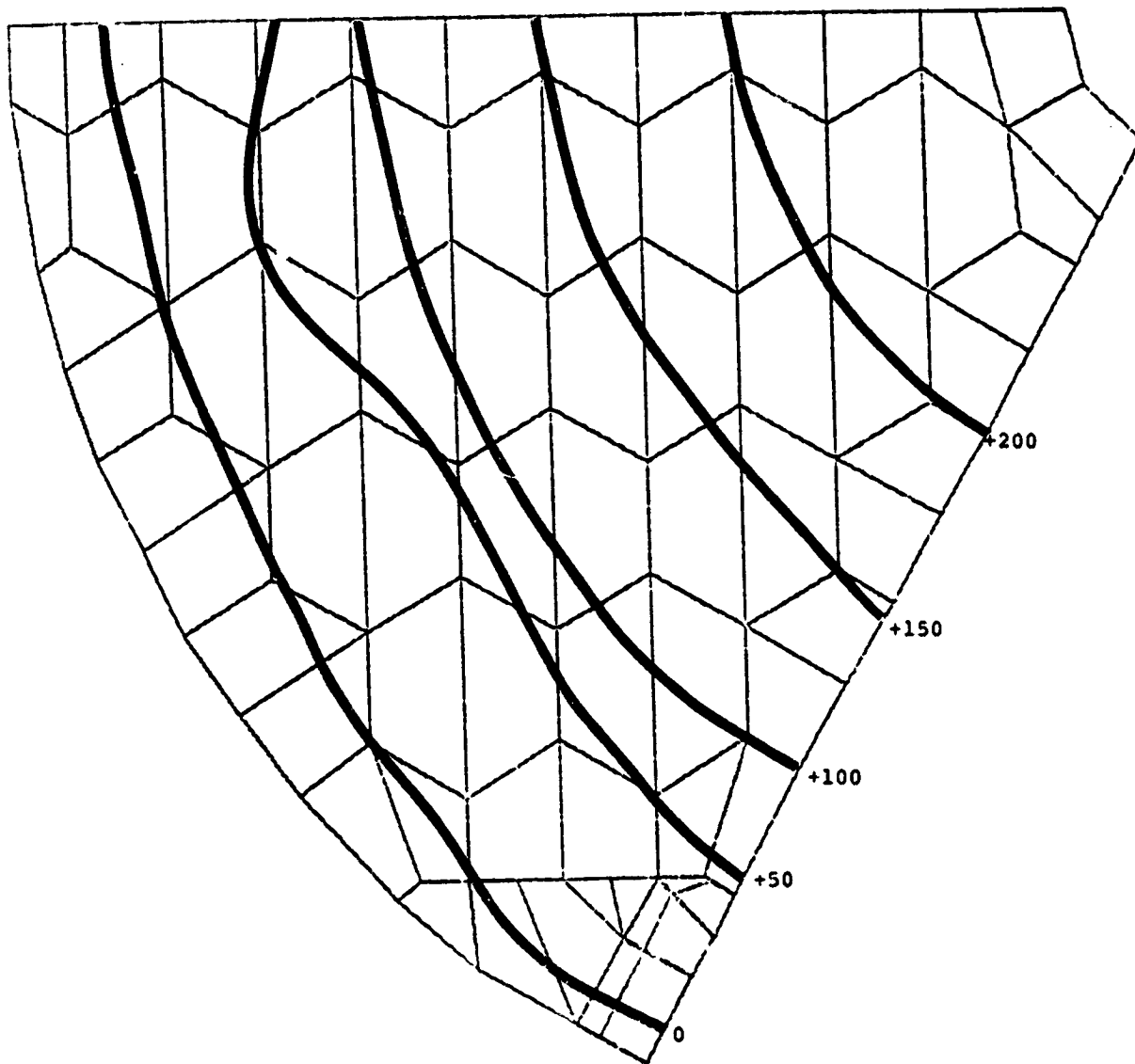


Figure 2.35. Optical Surface Displacements -  $1^{\circ}$ F Transverse  
 Gradient - Alternate Cells  
 Scale: Displacements  $\times 10^8$  in.  
 (Positive Upward)



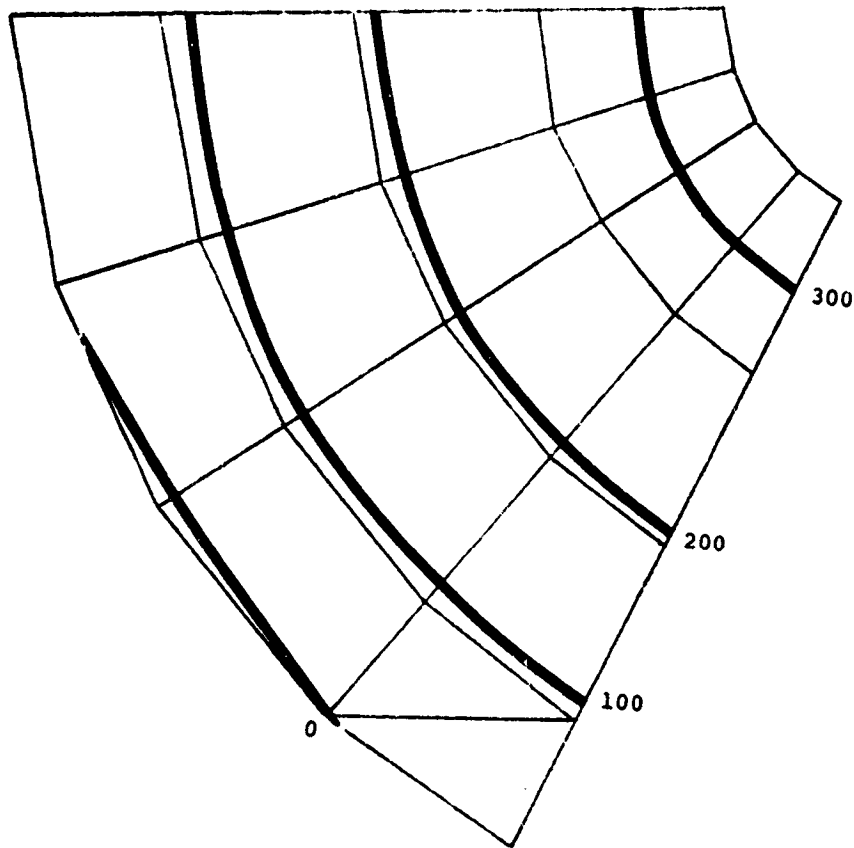


Figure 2.36. Optical Surface Displacements -  $1^{\circ}$ F Transverse  
Gradient - Trade-Off Model  
Scale: Displacements  $\times 10^8$  in.  
(Positive Upward)

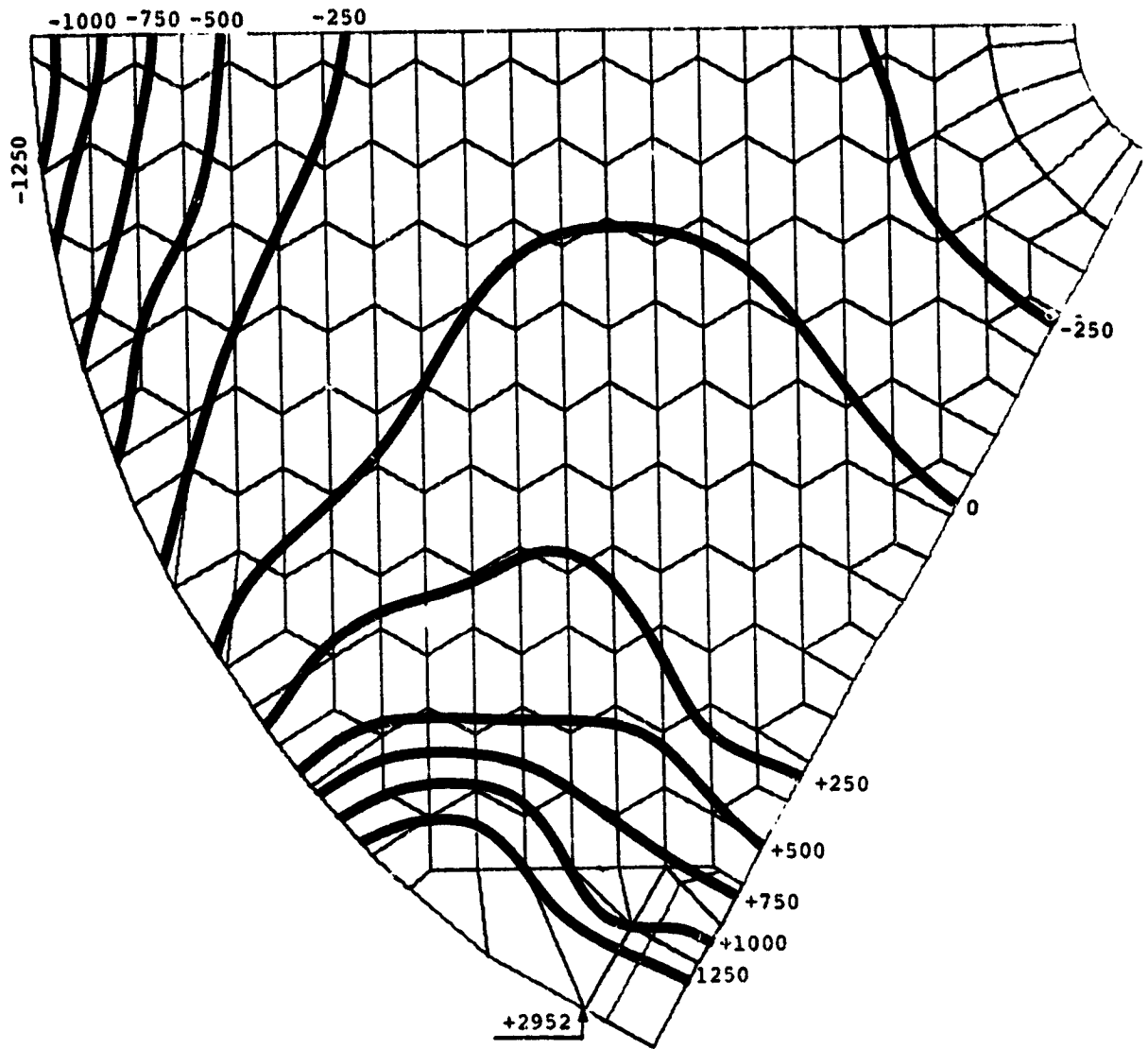


Figure 2.37. Deviations from Best-Fit Sphere -  
 $10^6$  Transverse Gradient - All Cells  
 Scale: Deviations  $\times 10^{10}$  in.  
 (Positive Upward)

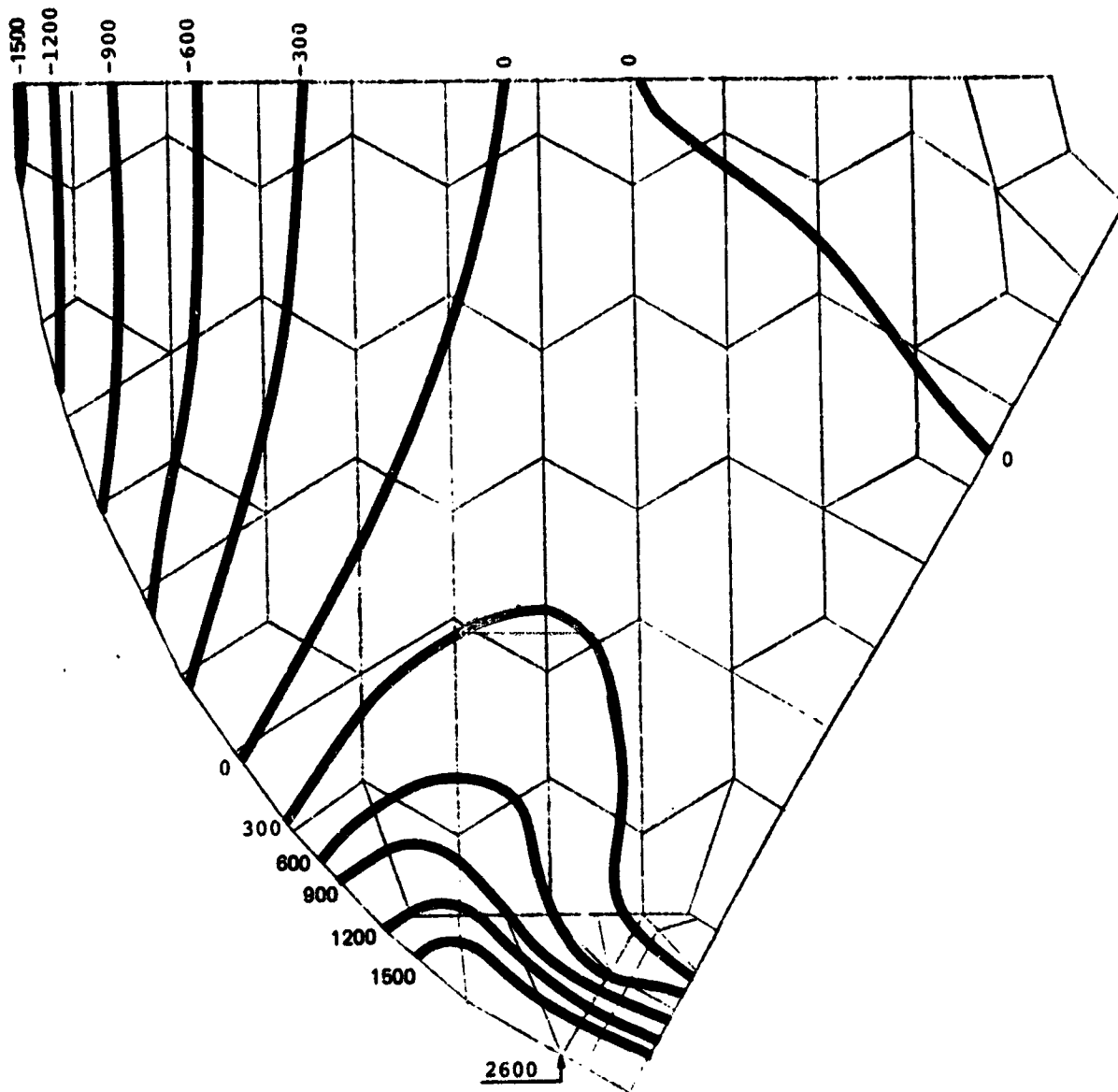


Figure 2.38. Deviations from Best-Fit Sphere -  
 $1^{\circ}\text{F}$  Transverse Gradient - Alternate Cells  
 Scale: Deviations  $\times 10^{10}$  in.

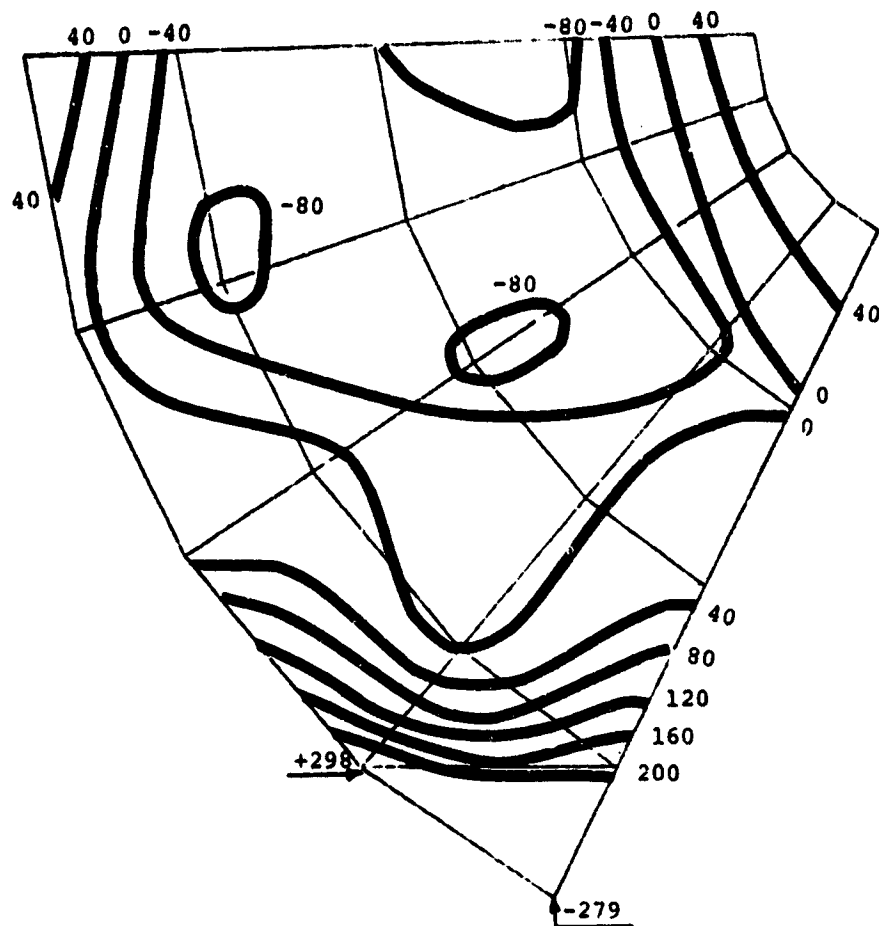


Figure 2.39. Deviations from Best-Fit Sphere -  
 $1^{\circ}\text{F}$  Transverse Gradient - Trade-Off Model  
 Scale: Deviations  $\times 10^{10}$  in.  
 (Positive Upward)

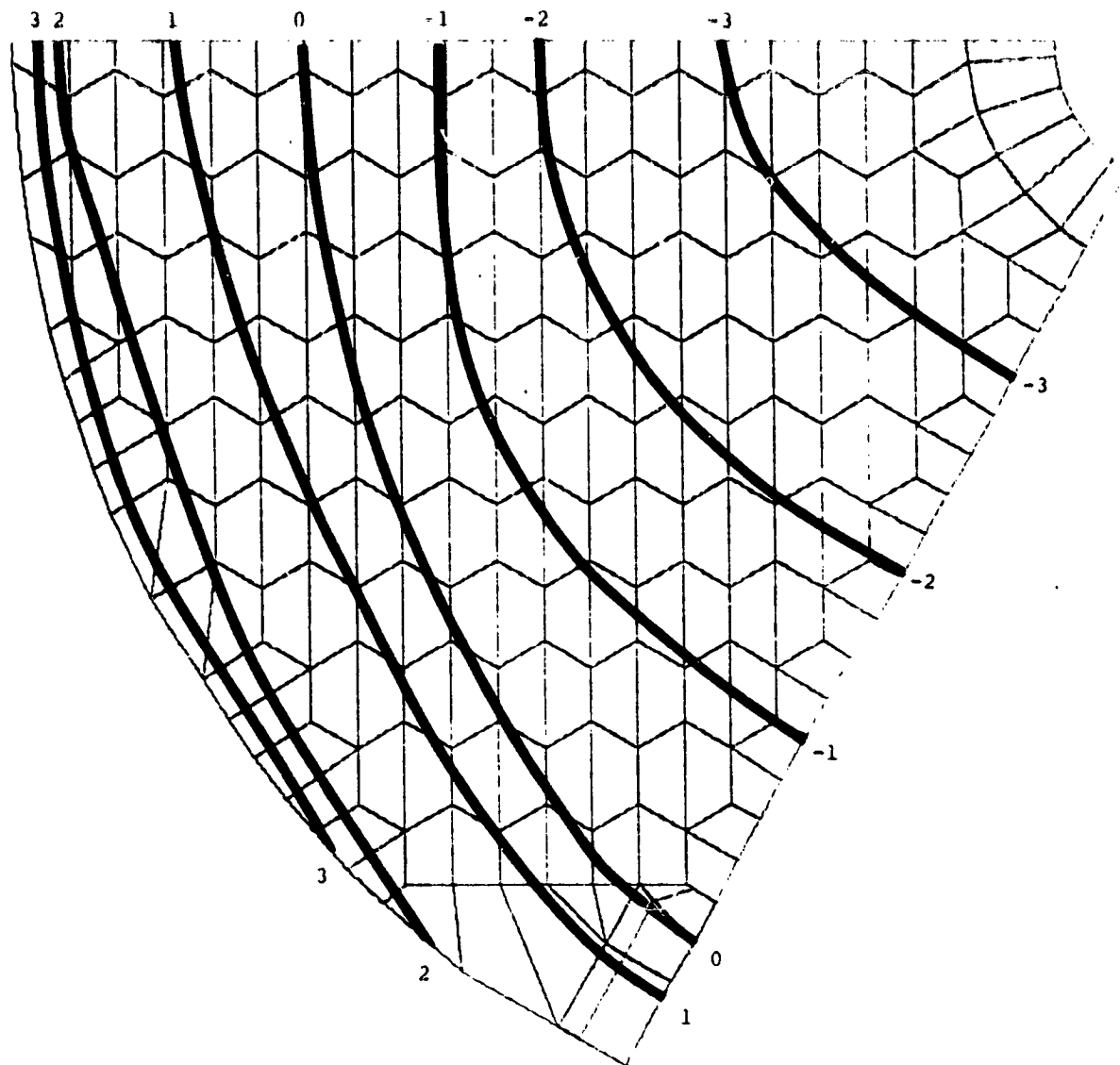


Figure 2.40. Top Surface Stresses -  $1^{\circ}\text{F}$  Transverse  
 Gradient - All Cells  
 Scale: Stresses  $\times 10^{-4}$  psi  
 (Positive Tensile)

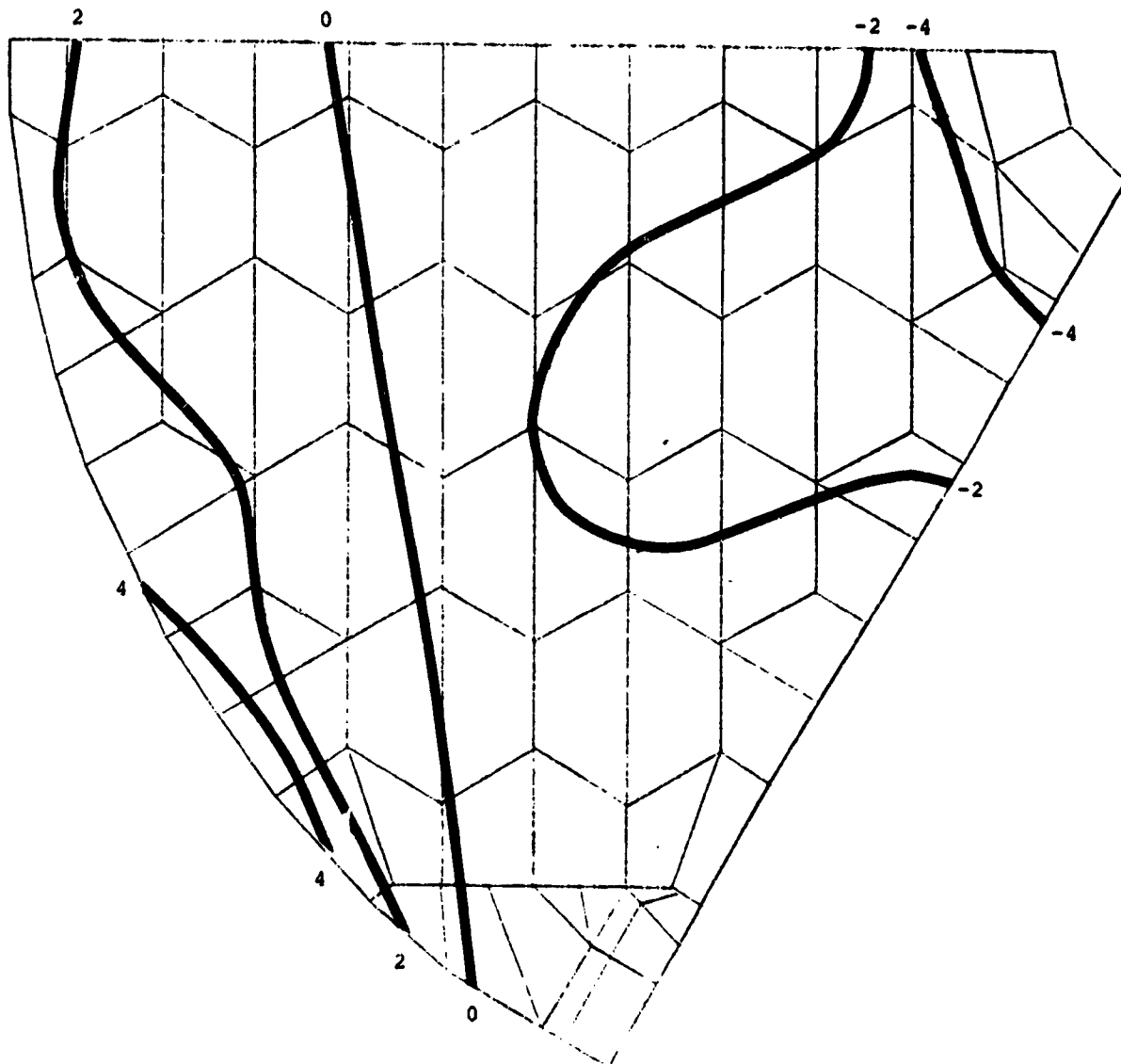


Figure 2.41. Top Surface Stresses - 1<sup>o</sup>F Transverse  
 Gradient - Alternate Cells  
 Scale: Stresses x 10<sup>-4</sup> psi  
 (Positive Tensile)

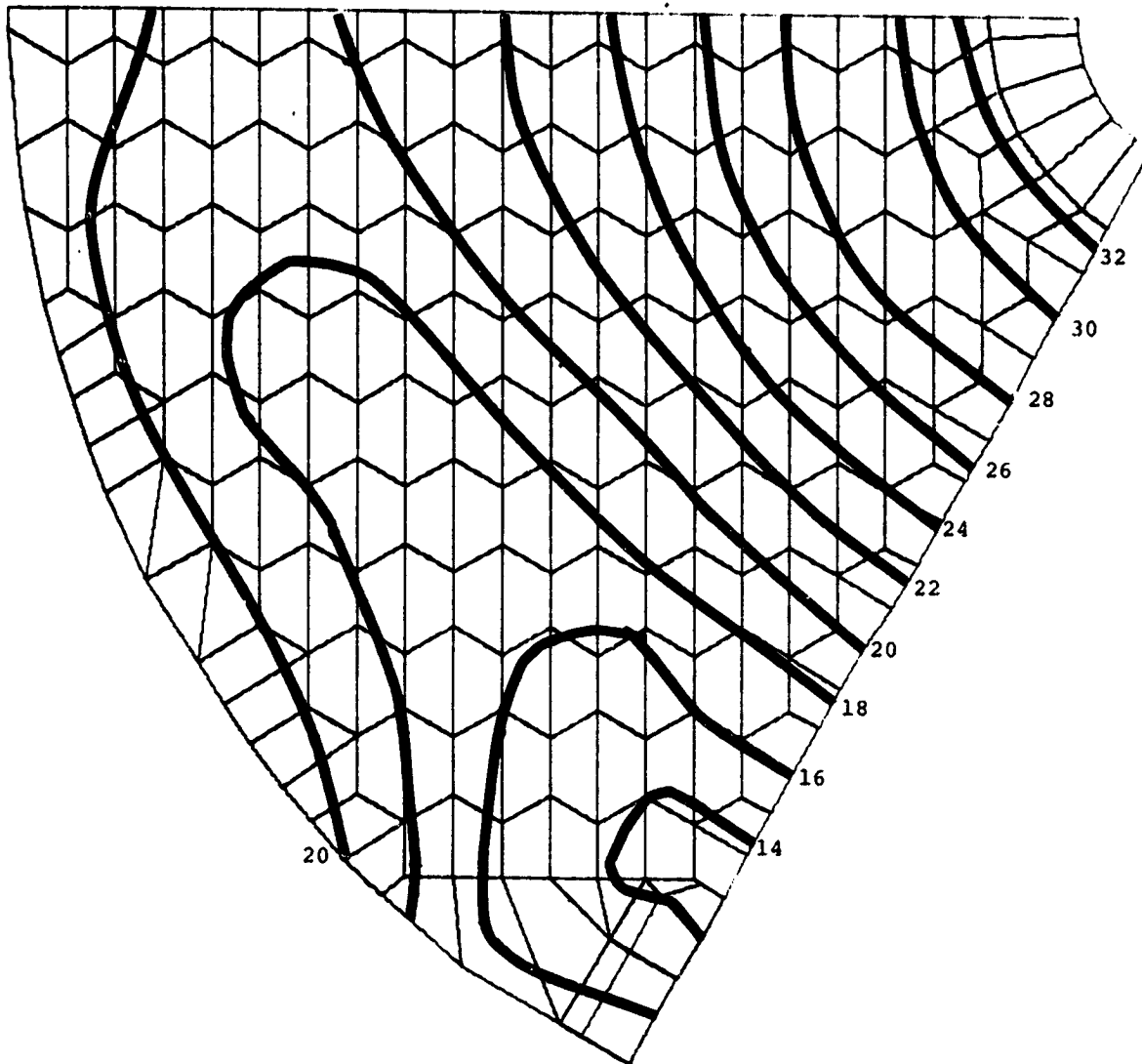


Figure 2.42. Optical Surface Displacements -  
1°F Radial Gradient - All Cells  
Scale: Displacements x 10<sup>8</sup> in.  
(Positive Upward)

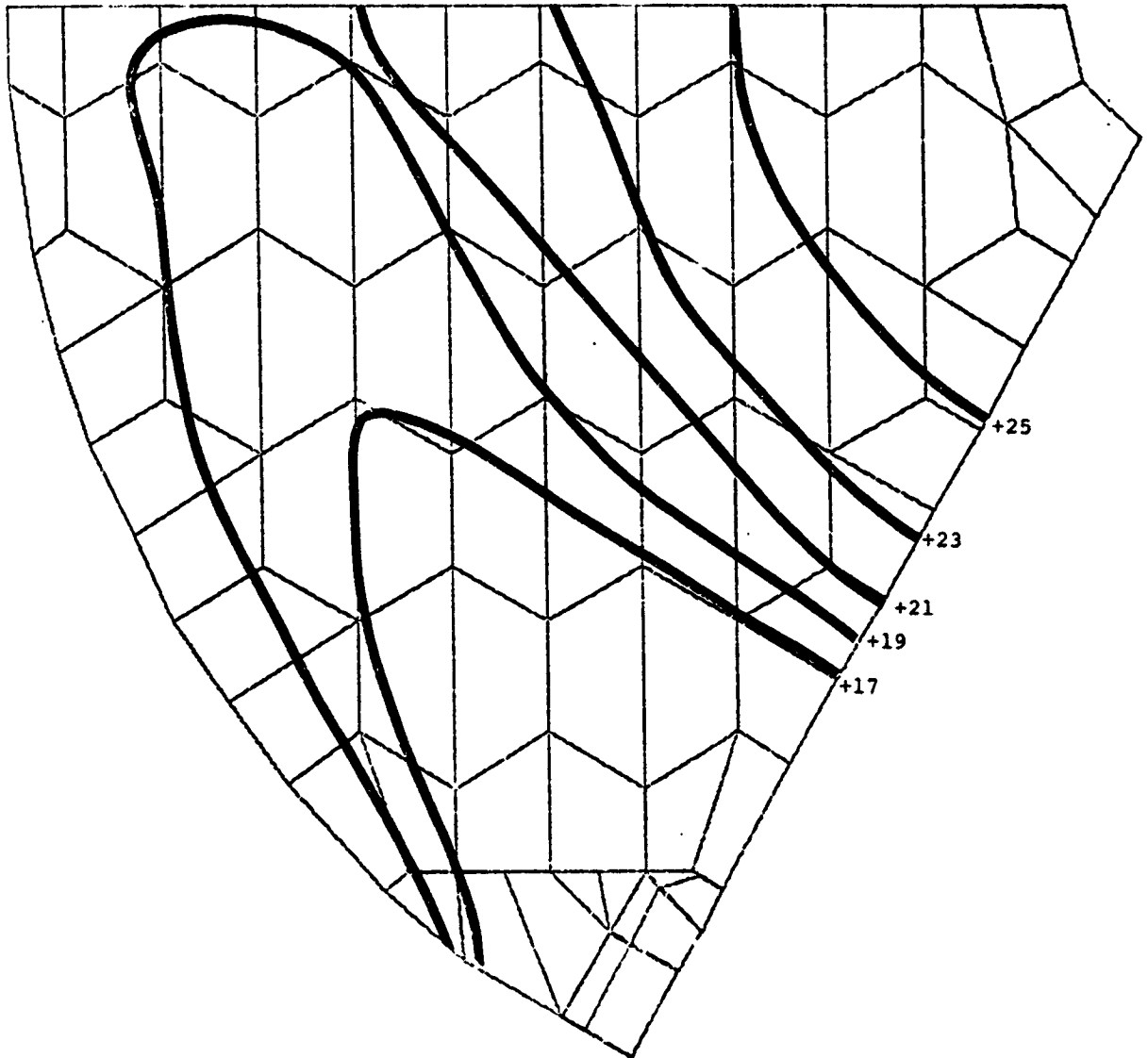


Figure 2.43. Optical Surface Displacements -  
1°F Radial Gradient - Alternate Cells  
Scale: Displacements x 10<sup>8</sup> in.  
(Positive Upward)



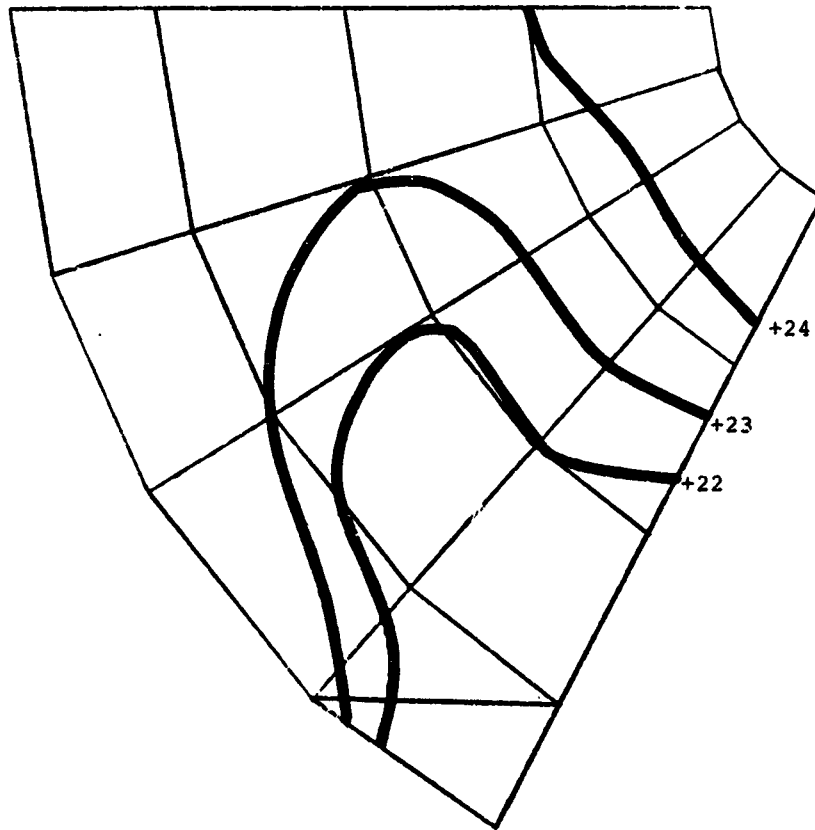


Figure 2.44. Optical Surface Displacements -  
1<sup>o</sup>F Radial Gradient - Trade-Off Model  
Scale: Displacements x 10<sup>8</sup> in.  
(Positive Upward)

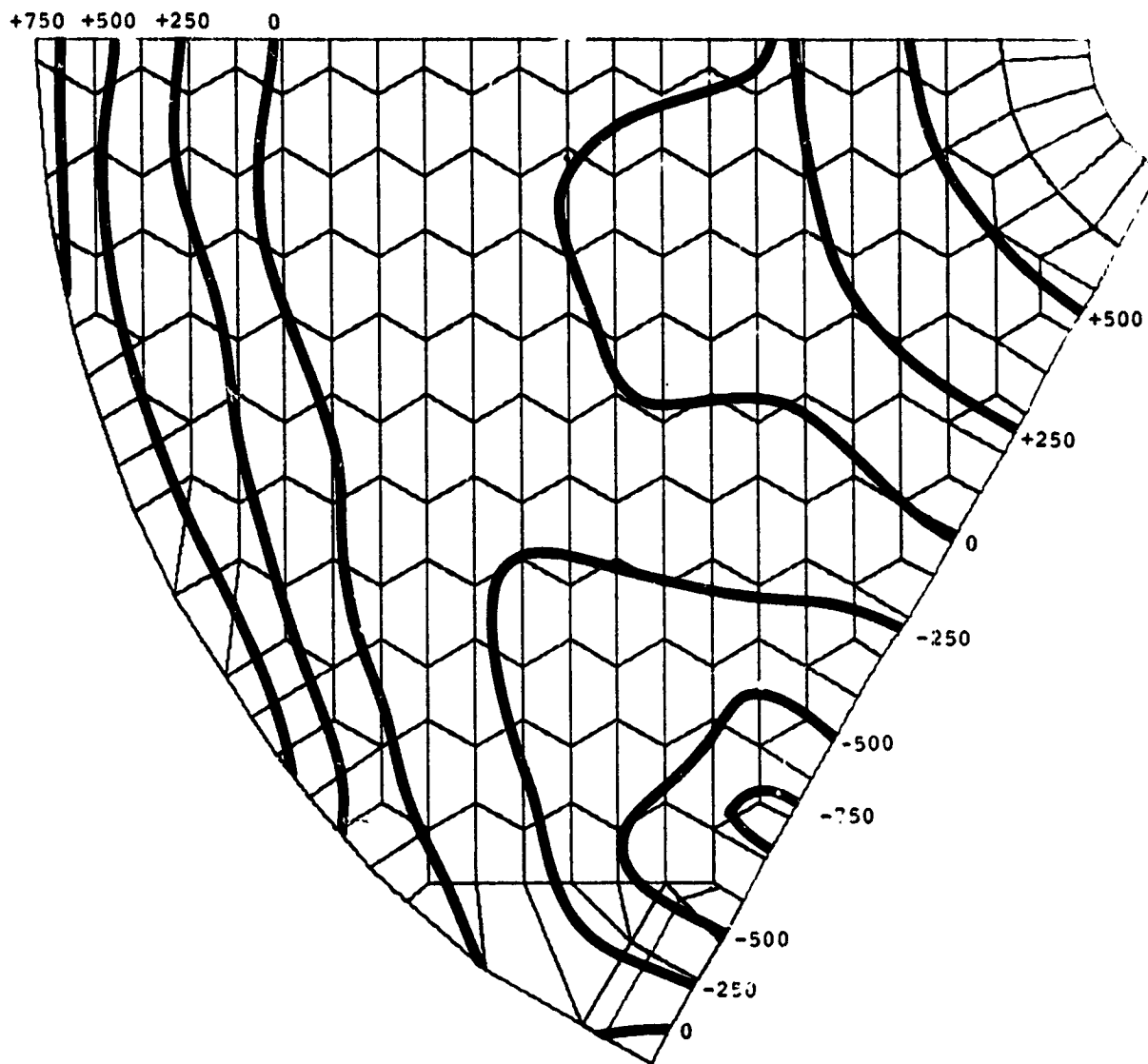


Figure 2.45 Deviations from Best-Fit Sphere -  
 $1^{\circ}\text{F}$  Radial Gradient - All Cells  
 Scale: Deviations  $\times 10^{10}$  in.  
 (Positive Upward)

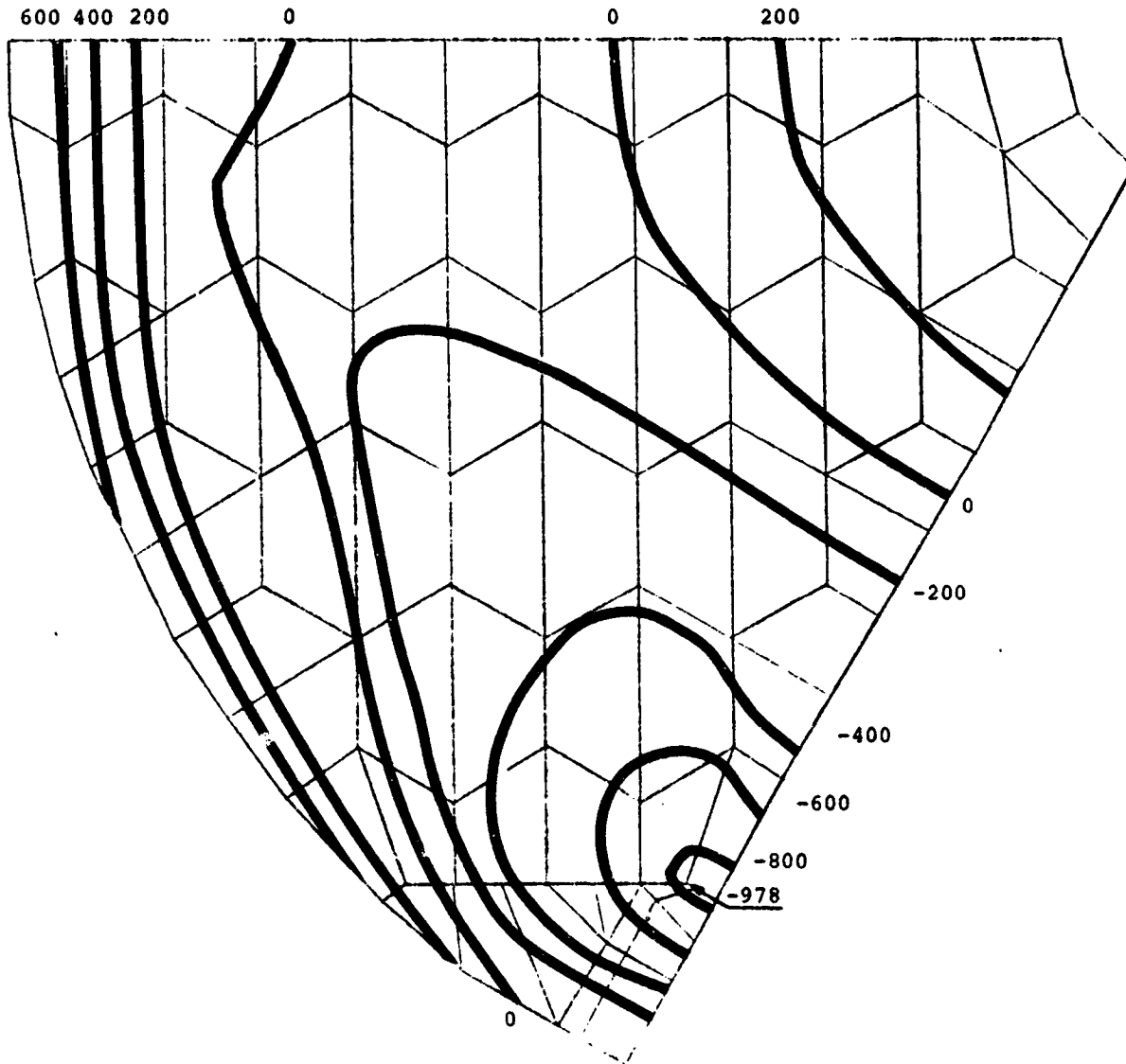


Figure 2.46. Deviations from Best-Fit Sphere -  
 $1^{\circ}\text{F}$  Radial Gradient - Alternate Cells  
 Scale: Deviations  $\times 10^{10}$  in.  
 (Positive Upward)

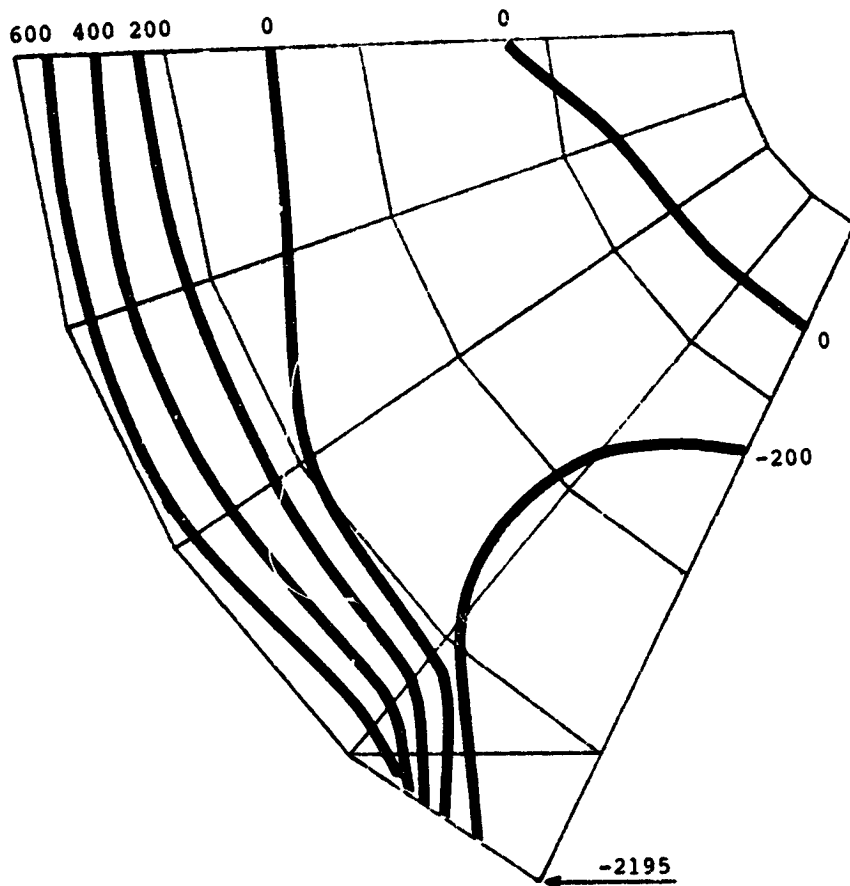


Figure 2.47. Deviations from Best-Fit Sphere -  
 1<sup>st</sup> Order Radial Gradient - Trade-Off Model  
 Scale: Deviations  $\times 10^{10}$  in.  
 (Positive Upward)

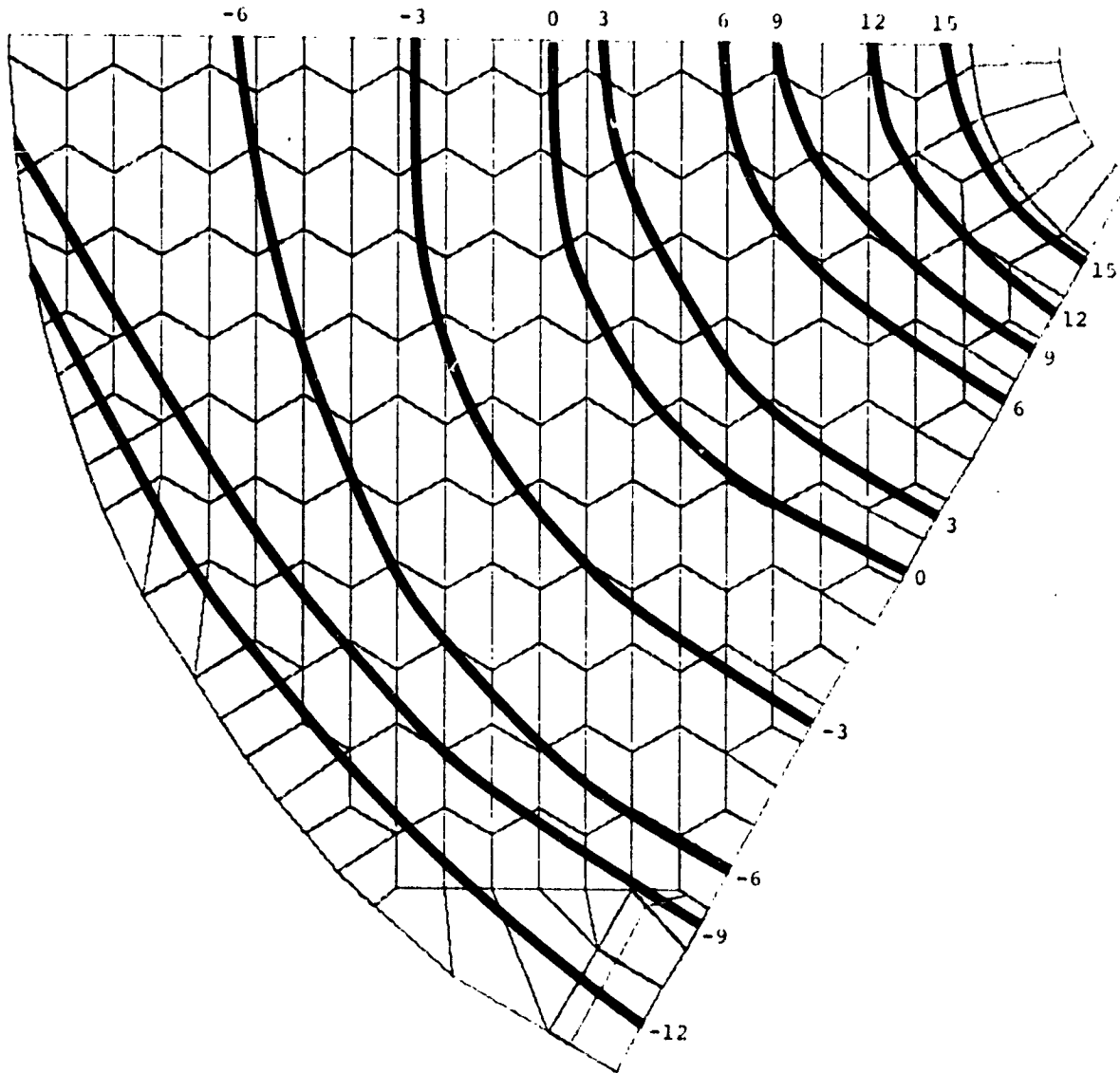


Figure 2.48. Top Surface Stresses -  $1^{\circ}\text{F}$  Radial  
 Gradient - All Cells  
 Scale: Stresses  $\times 10^{-4}$  psi

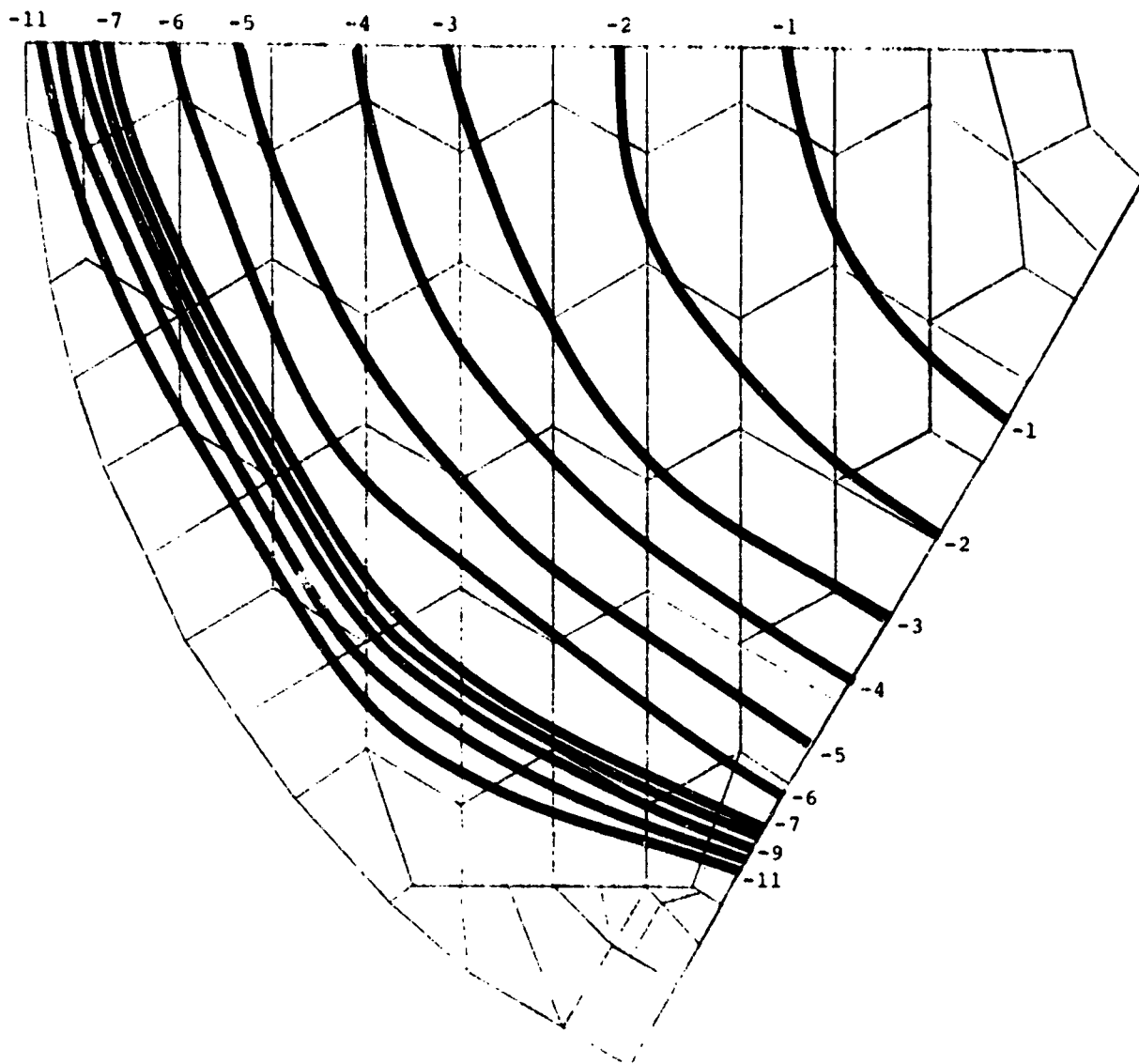


Figure 2.49. Top Surface Stresses -  $1^{\circ}\text{F}$  Radial  
 Gradient - Alternate Cells  
 Scale: Stresses  $\times 10^{-4}$  psi  
 (Positive Tensile)

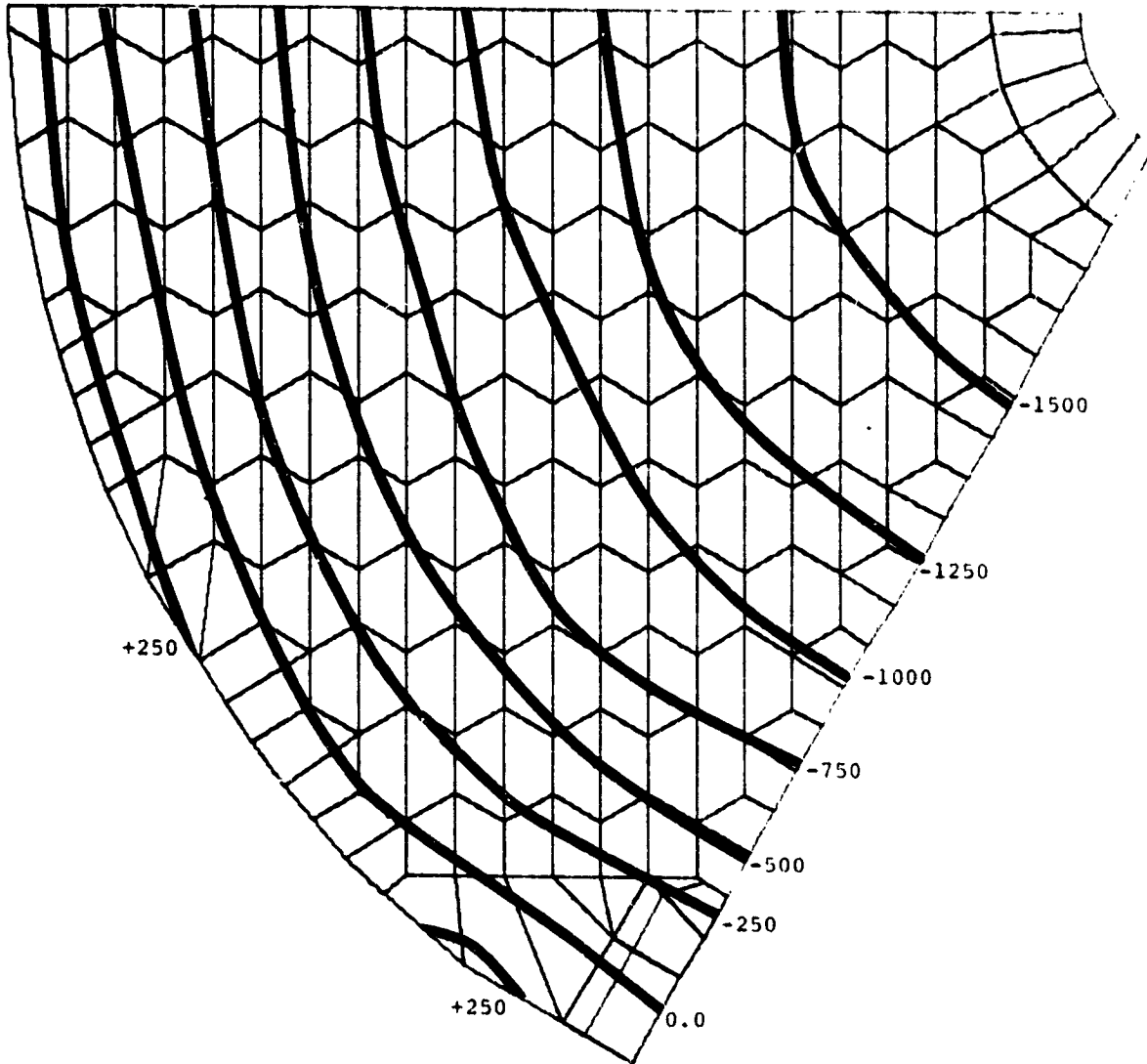


Figure 2.50. Optical Surface Displacements -  
"Sperry Rand Thermal" All Cells  
Scale: Displacements  $\times 10^8$  in.  
(Positive Upward)

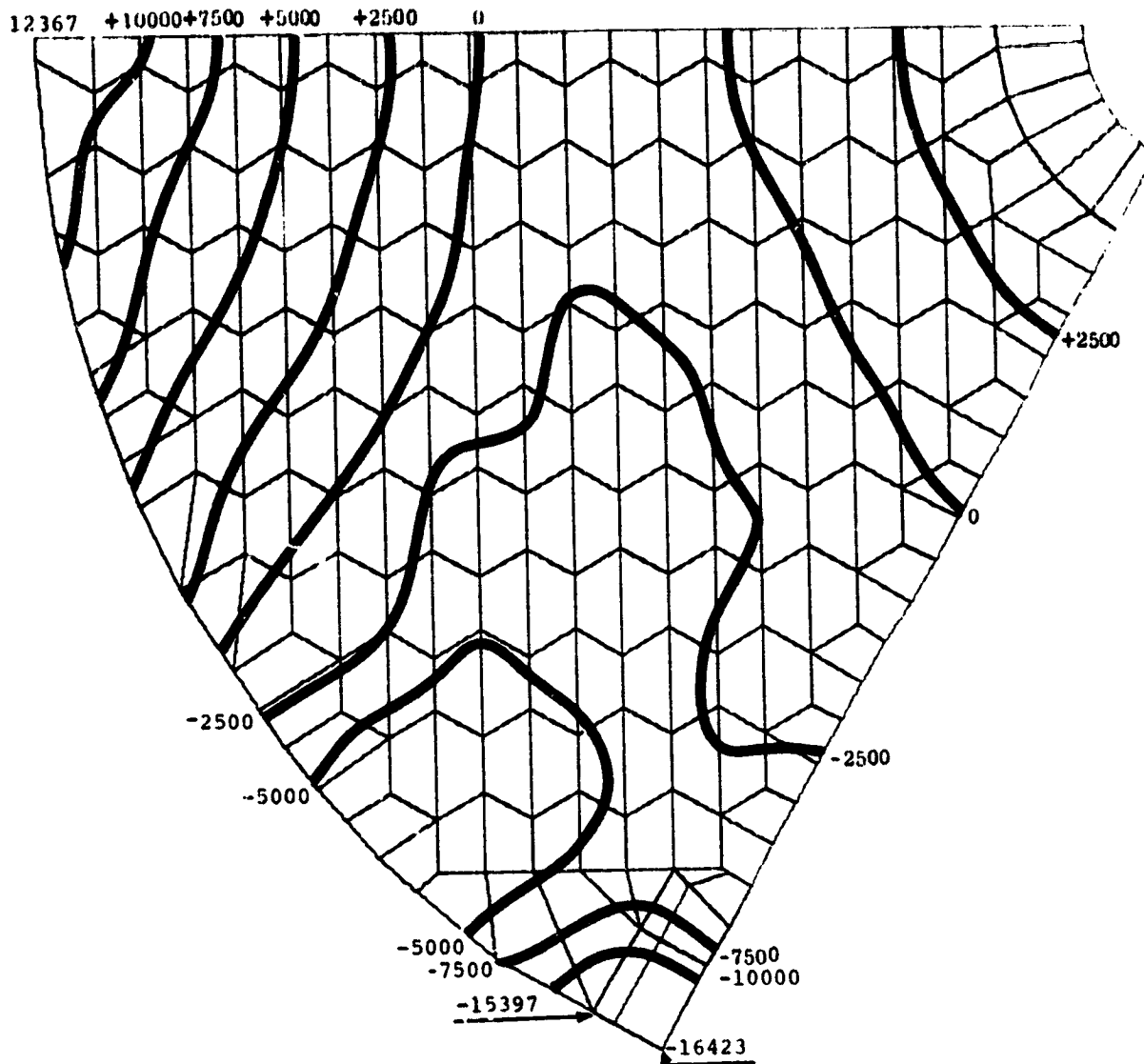


Figure 2.51. Deviations from Best-Fit Sphere -  
 "Sperry Rand Thermal" - All Cells  
 Scale: Deviations  $\times 10^{10}$  in.  
 (Positive Upward)



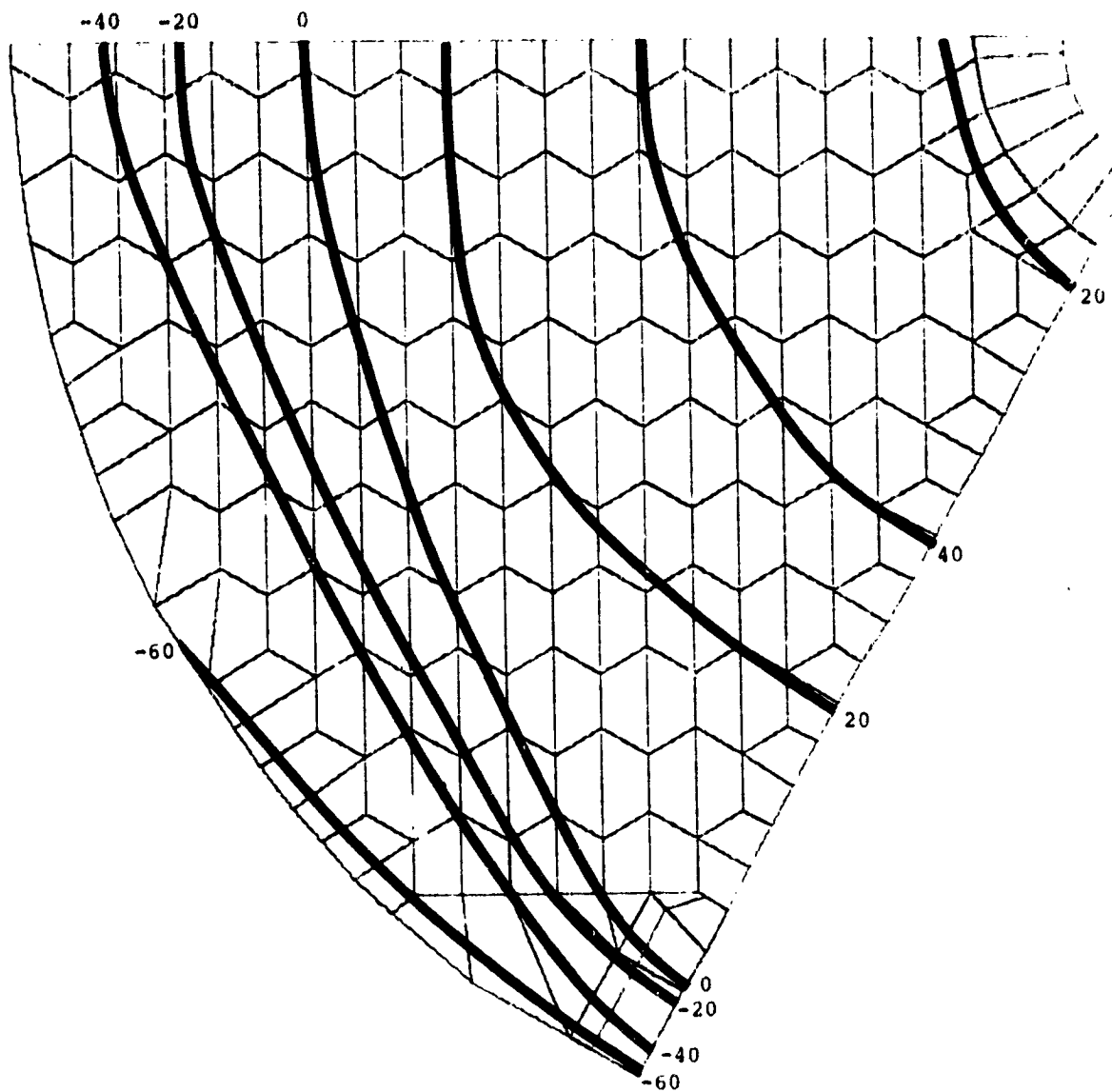
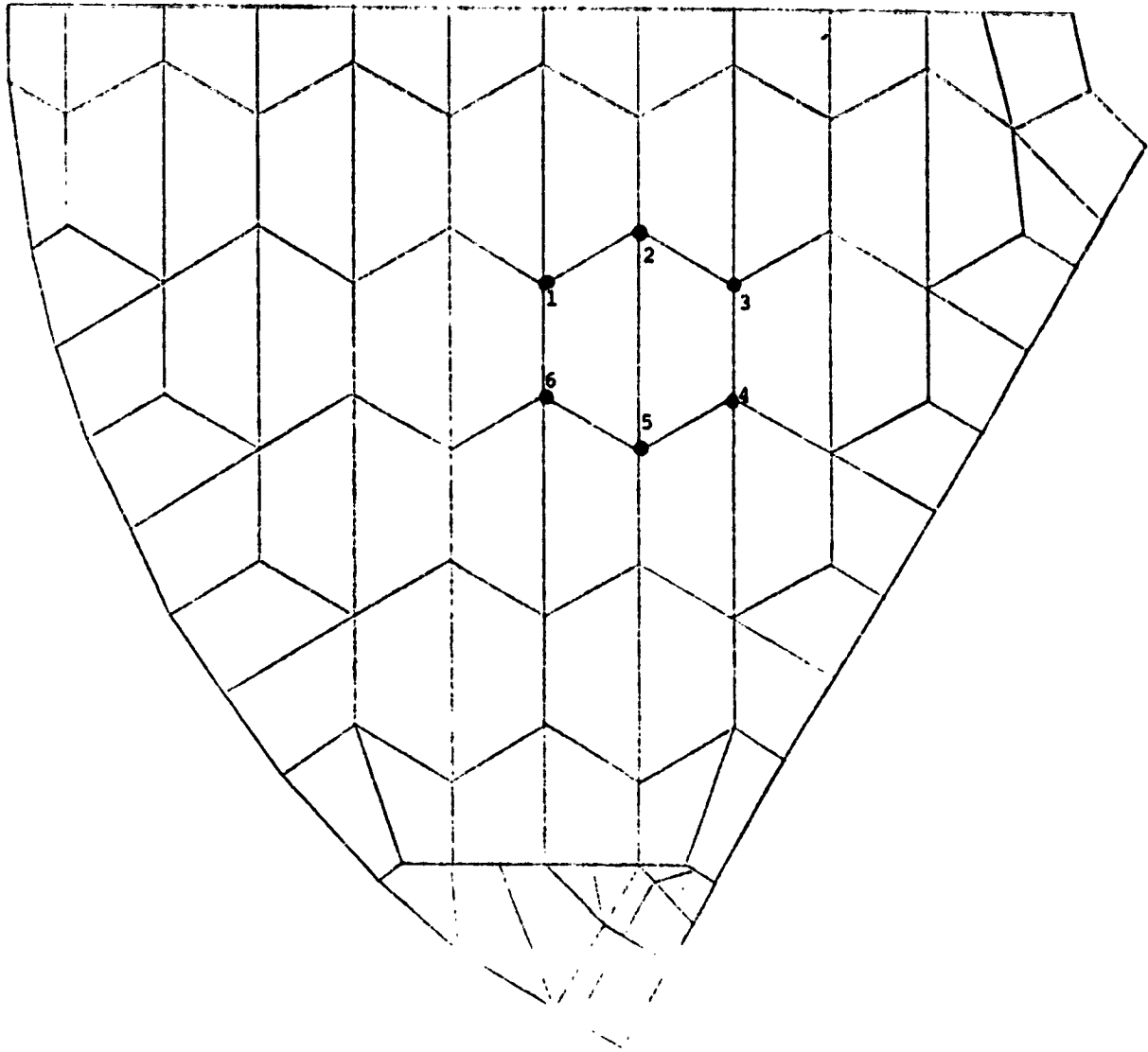


Figure 2,52. Top Surface Stresses -  
 "Sperry Rand Thermal" - All Cells  
 Scale: Stresses x  $10^{-4}$  psi  
 (Positive Tensile)



**Figure 2.53. Actuator Locations - Alternate Cell Model**  
**For Cell Test: 1 lb. Actuator Force**  
**Distributed Over Nodes 1**  
**through 6 at Back of Mirror**  
**For Rib Test: 1 lb. Actuator Force at**  
**Node 6 only**

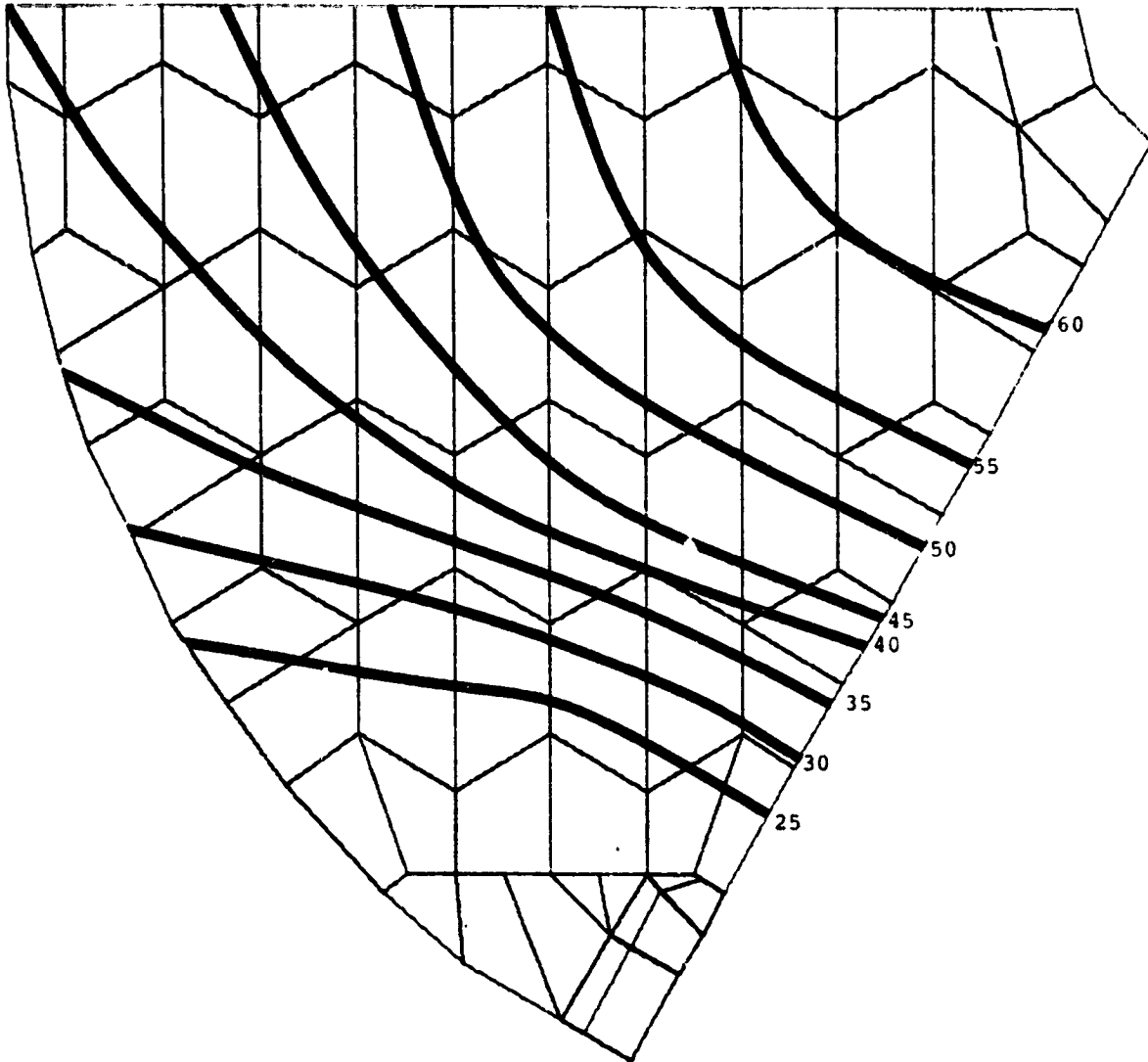


Figure 2.54. Optical Surface Displacements -  
Actuator Cell Test  
Note: Mirror Loaded by Six Actuators  
Scale: Displacements x  $10^8$  inches  
(Positive Upward)

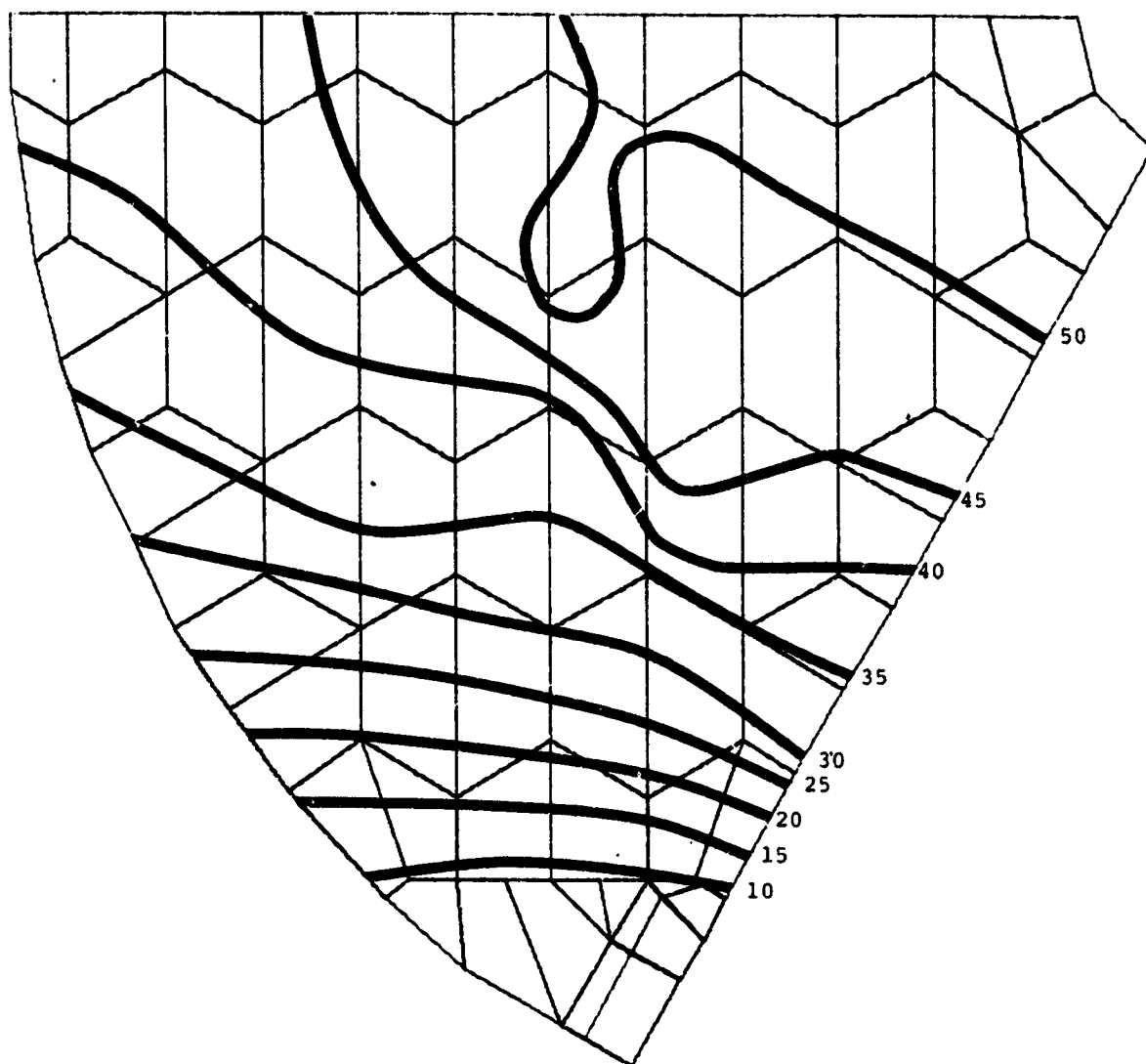


Figure 2.55. Optical Surface Displacements -  
 Actuator Rib Test  
 Note: Mirror Loaded by Six Actuators  
 Scale: Displacements  $\times 10^8$  inches  
 (Positive Upward)

Chapter 3  
TRADE-OFF STUDIES

3.1 Baseline Design and Variation Parameters

In the previous chapter, a "trade-off" finite element model was developed for the mirror and its use for a number of applications justified. In this chapter the design parameters will be varied over a considerable range to detect the directions in which optimization studies should move.

Table 3.1 lists the current "baseline design" dimensions. The variables that might be varied in a trade-off study include the following:

- a. mirror depth
- b. top plate thickness
- c. bottom plate thickness
- d. cell type
- e. cell size
- f. cell wall thickness
- g. rim plate thickness
- h. back plate hole diameter

The mirror depth, top plate thickness and bottom plate thickness are all relatively independent variables and will be studied parametrically in the following sections. As can be seen in Appendix B, the cell type, the cell size and the cell wall thickness are all relatively interdependent and can quite readily be represented by the single parameter of "average web density" or "percent of web weight removed".

TABLE 3.1

BASELINE DESIGN

Mirror Thickness	17.38"
Hex Cells - Pitch	4.8"
Wall Thickness	0.2"
Top Plate	1.83"
Back Plate	1.64"
Back Plate Hole	3.25" $\phi$
Rim Plates	0.4"
Diameter	122" $\phi$
Hole	23.5"
Radius of Curve	525"
CERVIT	
E = 13,400,000 psi	
Poisson = .252	
Alpha = $.277 \times 10^{-7}$ in/in/ $^{\circ}$ F	

The rim plate thickness is expected not to have sufficiently large variational impact, although a few trial studies will be attempted as well. The back plate hole diameter is probably a very strong parametric variable, but because its impact is primarily on stresses, a highly complex model is necessary, which it is not reasonable to study within the time and resource constraints. It is assumed therefore that the ratio of backplate hole diameter to cell size remains a constant. Thus the "pseudo back-plate" as per Appendix A is constrained to be valid.

The loadings under which the parameters will be varied are

- a. 1 g transverse
- b. 1°F soak
- c. 1°F transverse gradient
- d. 1°F radial gradient
- e. unit actuators

Nominal values of the material properties are assumed.

### 3.2 Mirror Lightweighting

The process by which a CERVIT blank becomes a lightweighted mirror includes four major manufacturing steps. Using first a geological type core-drill, ranging in diameter from one to four inches, a cylindrical section is removed each cell location. This establishes the diameter of the mirror backplate hole. Then with the help of an orbital grinder the hole is undercut and the cell is enlarged. This may already involve the use of patterns to obtain approximate cell shapes. Because of the nature of this type of machining, however, the fillet radii are quite large and considerable amount of material remains behind.

The following step uses an angled "golf-stick" grinding tool with a small radius (usually 0.75 in.) which is then used to remove the last major amount of material. Typically, the remaining fillet radii are 0.75 in. Finally the cells are chem-milled to minimize the surface stress levels. Chem-milling may also be used to "super-lightweight" the mirror if cell wall thicknesses of less than 0.3 are desired.

Each of these steps is successively more expensive per volume of material removed than the previous, and it is of interest to determine the volumes in each step with hexagonal square and triangular types of lightweighting cells. Assuming the baseline design, which has a "web weight removed" of about 91%, the other dimensions of the baseline mirror, and an 0.75 diameter "golf-stick" tool, a simple geometrical calculation can be made to determine the volume to be removed by each lightweighting step as a function of the type of cell desired. Table 3.2 summarizes these findings. The first column lists the volume removable by that particular step; the second, the cumulative volume removed. It is clearly evident that the hexagonal cell configuration will be the least expensive to produce, since it obtains most of its lightweighting through the cheaper steps. It is also evident that if the same cell wall thickness and "golf-stick" tool diameters are used, the square and triangular cells cannot be lightweighted to the same degree as the hexagonal. This can also be seen graphically in Figure 3.1 which indicates as well the deflection and weight relationships associated with the various types of lightweighting under a 1 g performance load.

Once a certain goal of mirror lightweighting has been established, then a number of possibilities can be found, depending on the size of cell desired, cell wall thickness that can be afforded, etc. Table 3.3 shows some of these possibilities.



TABLE 3.2

LIMITS IN CELL PATTERN LIGHTWEIGHTING

Baseline Design      4.8" Pitch  
                          0.2" Wall  
                          0.1" Chem-Mill  
                          3.25" Back Pl Hole (core drill)  
                          0.75" Fillet Radius

Procedure Step	Cell Type					
	Hexagonal		Square		Triangular	
	% Rem.*	Cum	% Rem.	Cum	% Rem.	Cum
Coring	42	(42)	36	(36)	28	(28)
Orbital	35	(77)	30	(66)	23	(51)
"Golf-Stick"	5	(82)	15	(81)	28	(79)
Chem-Mill	8	(90)	8	(89)	8	(87)
Fillets	1	(91)	2	(91)	4	(91)

\* % Removed of total web volume by step

TABLE 3.3  
WEB LIGHTWEIGHTING

Web Pl/Pitch	% Web Removed	Weight	Actual Web Pl/Pitch Values	Locally Limited
1/40	95	4300	.1/4. .15/6. .2/8. .25/10.	
1/30	93.3	4460	.1/3. .15/4.5 .2/6. .25/7.5 .30/9.0	
* 1/24	91.6	4670	.1/2.4 .15/3.6 .2/4.8 .25/6. .30/7.2	
1/20	90	4860	.1/2.0 .15/3. .2/4.0 .25/5. .3/6.0	
1/15	86.6	5370	.1/1.5 .15/2.25 .2/3.0 .25/3.75 .3/4.5	
1/10	80	6270	.1/1.0 .15/1.5 .2/2.0 .25/2.5 .3/3.0	
1/8	75	6980	.15/1.2 .2/1.6 .25/2.0 .3/2.4	
3/20	70	7660	.2/1.33 .25/1.66 .3/2.0	
1/5	60	9000	.25/1.25 .3/1.50	
1/4	50	10410		
Solid	0	17170		

↑ Inefficient ↑  
 ↑ Fragile ↑  
 ↓ Absurd ↓  
 ↓ Manuf. Limited ↓

\* Baseline

The first column lists the ratio of the web plate thickness to the cell size on "pitch" as defined in Appendix B. The next column converts these figures to a percentage of web weight removed. Then the third column shows what the mirror, based on the other baseline parameters, will weigh. Finally a listing is made of the different cell size and wall thickness possibilities corresponding to each.

It is clear that a very thin cell wall will be expensive to manufacture, while the combination of thin wall and large cell will be very fragile. As the cell increases in size, the faceplate span increases and with it the probability that the polished mirror figure will express the lightweighting pattern. Thus a reasonable compromise must be found.

### 3.3 Parameter variations.

Table 3.4 summarizes the results of the various trade-off studies in a qualitative form. In the corner of each box is the number of the figure where the data is presented in graphical form.

In all cases for the transverse 1 g load, the results are plotted as well in terms of percentage change in performance versus design parameter change.

For all load cases, the peak-to-peak, RMS and maximum displacements are plotted against the design parameter change. These curves are proportional throughout their ranges, thus making it possible to scale relatively easily from one performance measure to the other.

Figure 3.11 has some additional interest since it records the effect of various tool pressures and cell deflections against the mirror optical surface substrate thickness, and compares these to the entire mirror deflections.

TABLE 3.4  
DEPENDENCIES OF TRADE VARIABLES AND DEFLECTIONS FOR LOADS  
SUMMARY OF TRADE-OFF STUDIES

Variable	Weight	lgΔ (3.2)	1° Soak (3.17)	1° T to B (3.17)	1° Rad (3.17)	Actuator (3.26)
Web Density	Very Strong	Less Strong	Weak	Weak	Moderate	Strong
Top Pl Thickness	Strong	Less Strong	Weak	Moderate	Moderate	Moderate
Bottom Pl Thickness	Less Strong	Less Strong	Weak	Moderate	Less Strong	Less Strong
Mirror Depth	Strong	Strong	Less Strong	Strong	Less Strong	Strong
Rim Pl Thickness	Weak	Weak	---	---	---	---

Range {  
 Very Strong  
 Strong  
 Less Strong  
 Moderate  
 Weak

In the case of the actuator tests, only the local deflection effect at the actuator location was studied. Doubtlessly other parametric studies could be made from this data.

### 3.4 Summary and Conclusions

Some preliminary speculations might be projected from these results. Suppose one were interested in the stiffest mirror with respect to 1 g transverse loads:

Suppose the mirror parameters: all at baseline except

top plate: 1" thick  
back plate: 2" thick  
cell wall: 0.32" thick  
rim plate: 0.9" thick

Deflection would decrease by 18% below baseline.

Weight would increase by 17%.

Suppose the lowest-weight mirror were desired:

The mirror parameters: all at baseline except

top plate: 1" thick  
back plate: 1.25" thick

Deflection would decrease by 12.5%.

Weight would decrease by 13%.

Suppose a "low-cost" mirror were desired:

The mirror parameters: all at baseline except

Web cored and orbitally tooled to remove  
only 77% of web.

Deflection would decrease by 1.5%.

Weight would increase by 41.5%.

It is evident that as the performance requirements become clearer, many such games can be played, hopefully to achieve a better mirror.

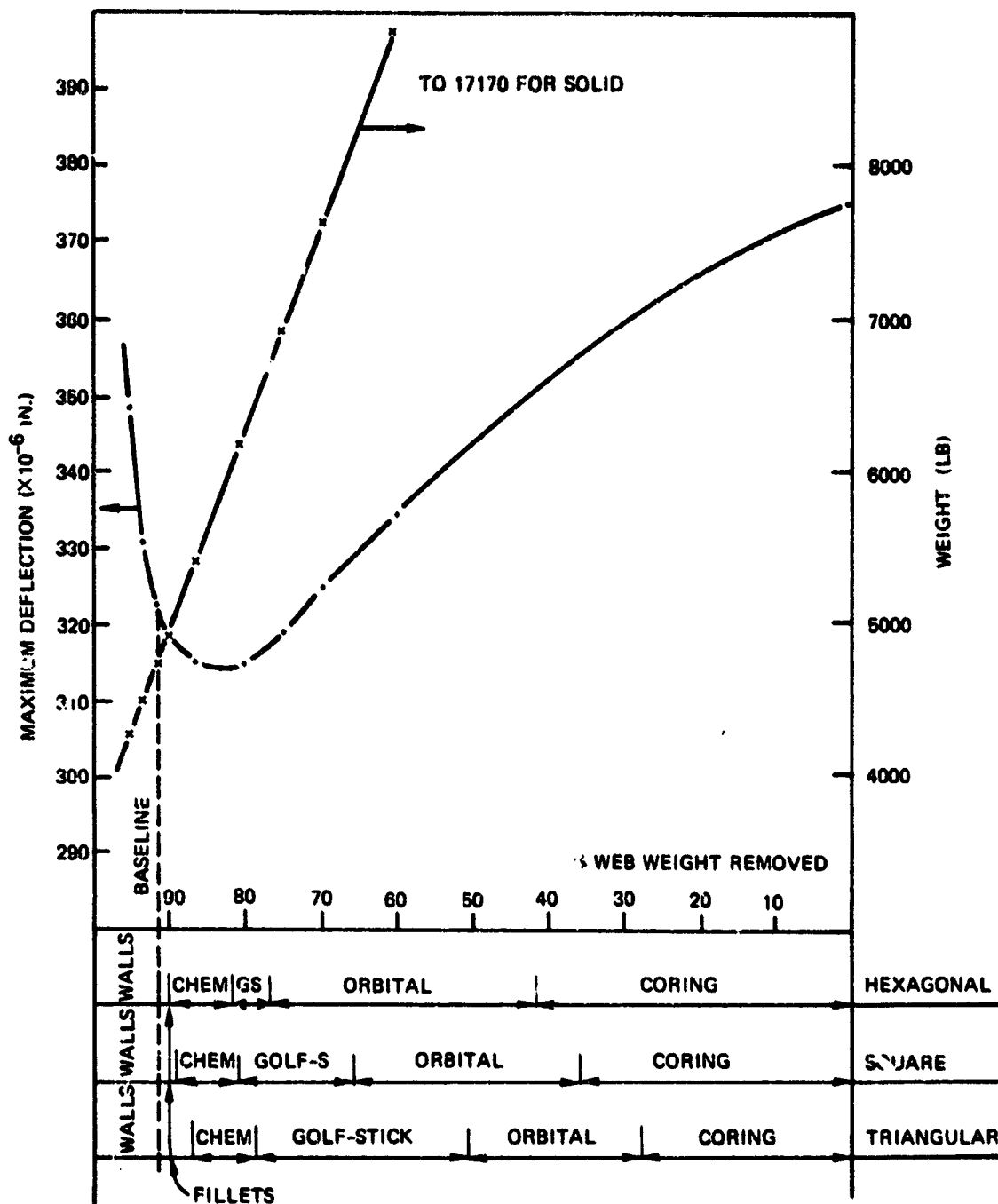


Figure 3.1 Limits on Cell Patterns (lg Transverse).

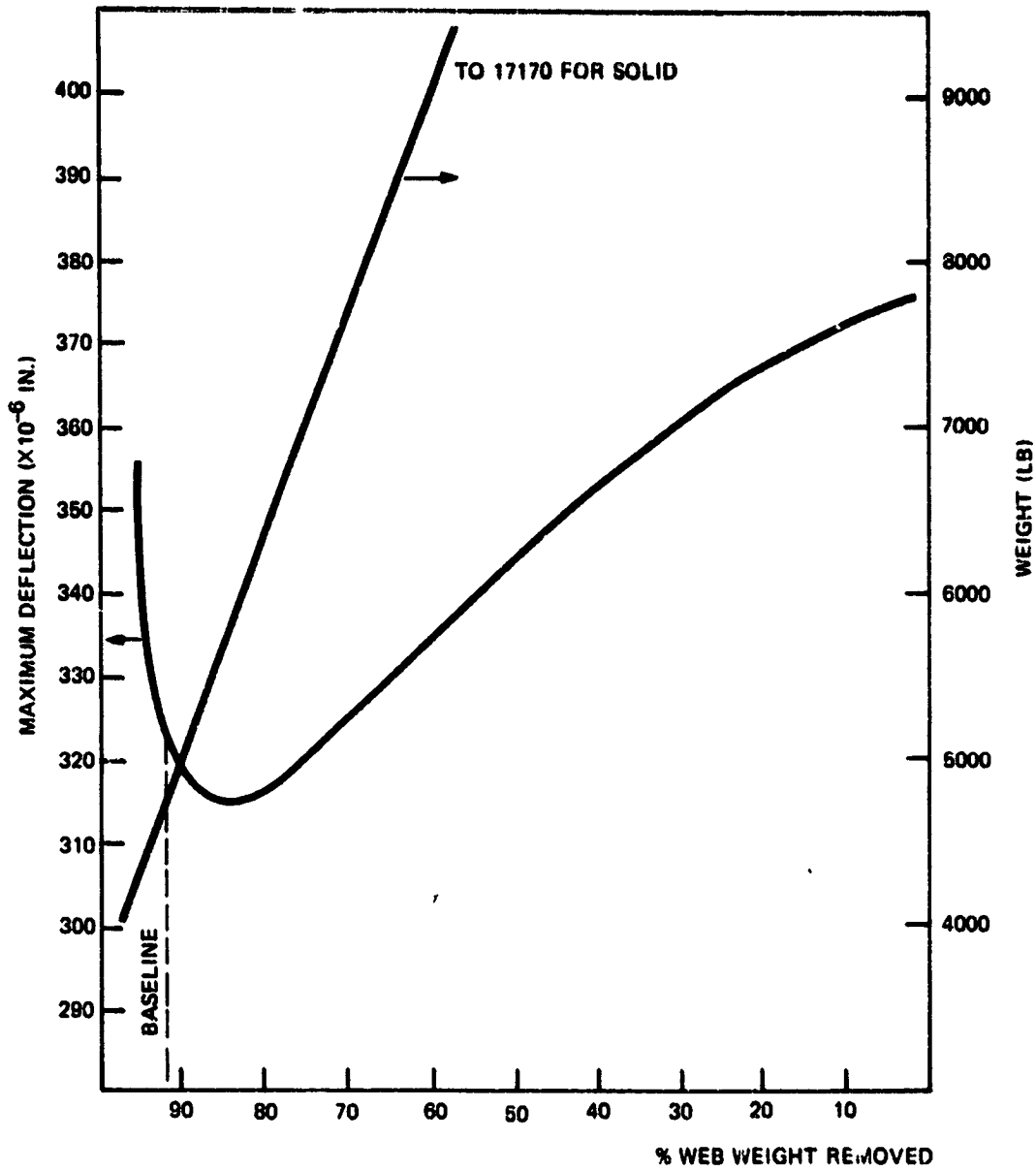


Figure 3.2 Variations on Web Density.  
 All Other Design Variables at Baseline.  
 1g Transverse Load.



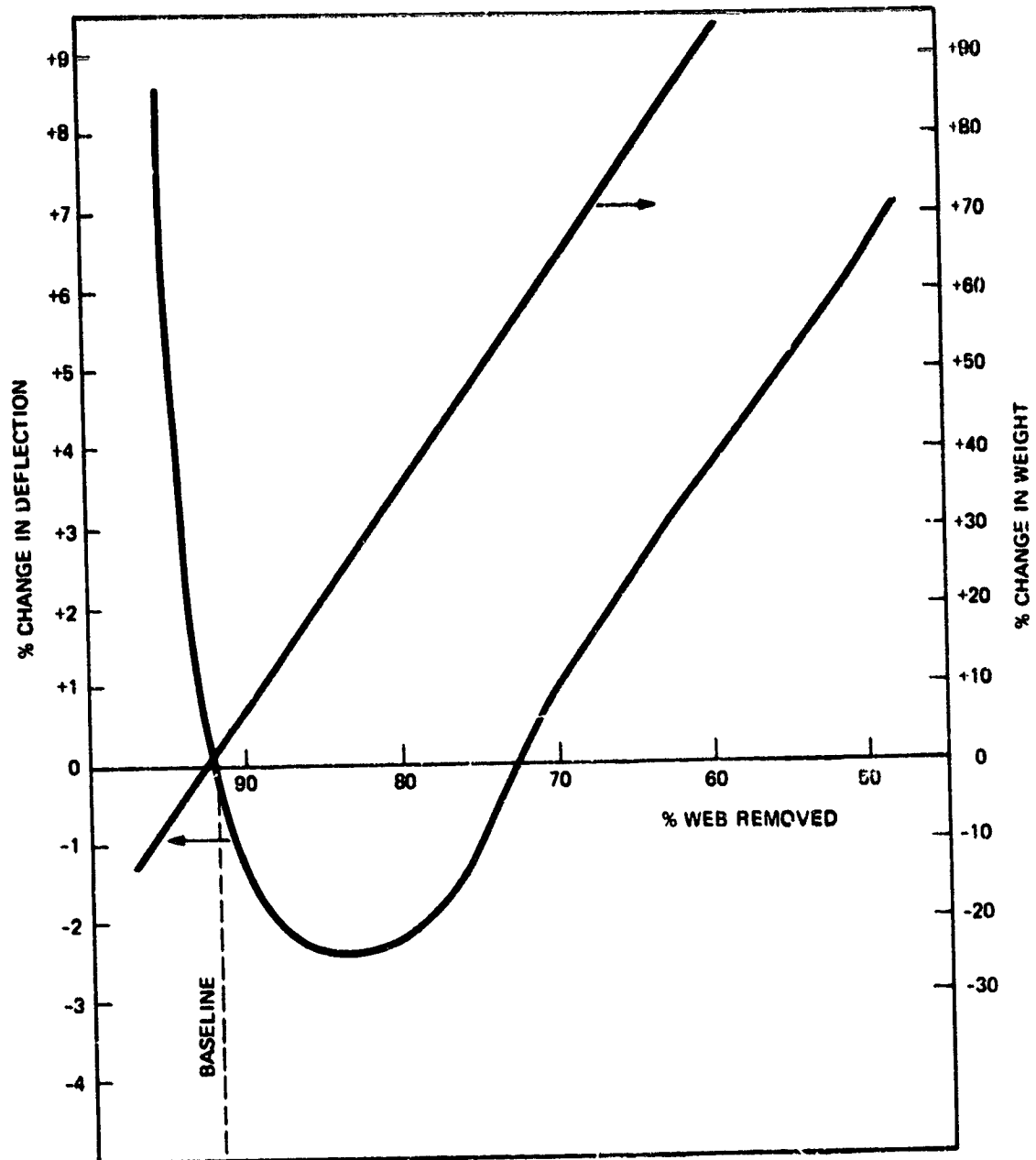


Figure 3.3 Variations in Web Density.  
 All Other Variables at Baseline,  
 1g Transverse Load.

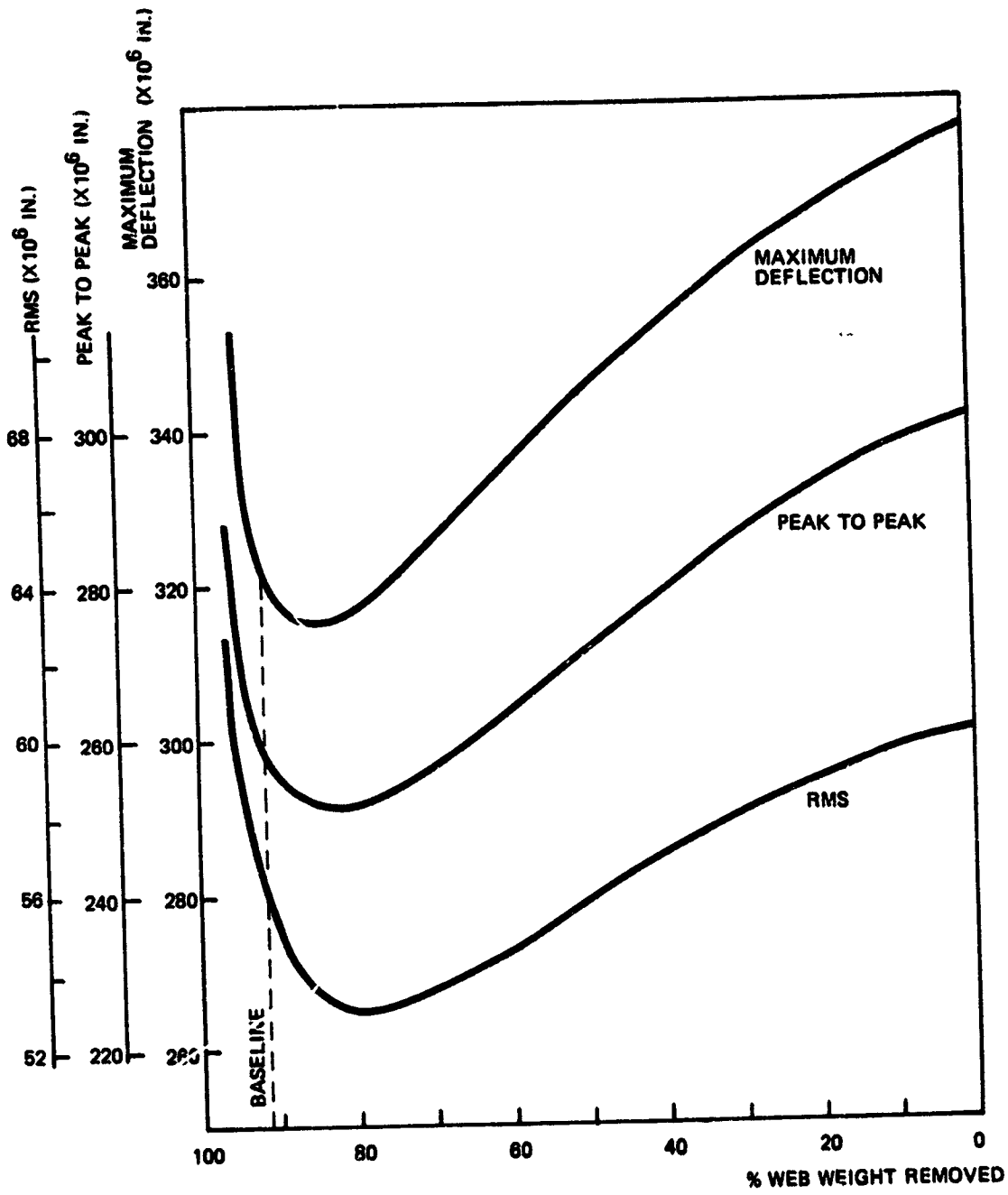


Figure 3.4 Variations on Web Weight - lg.

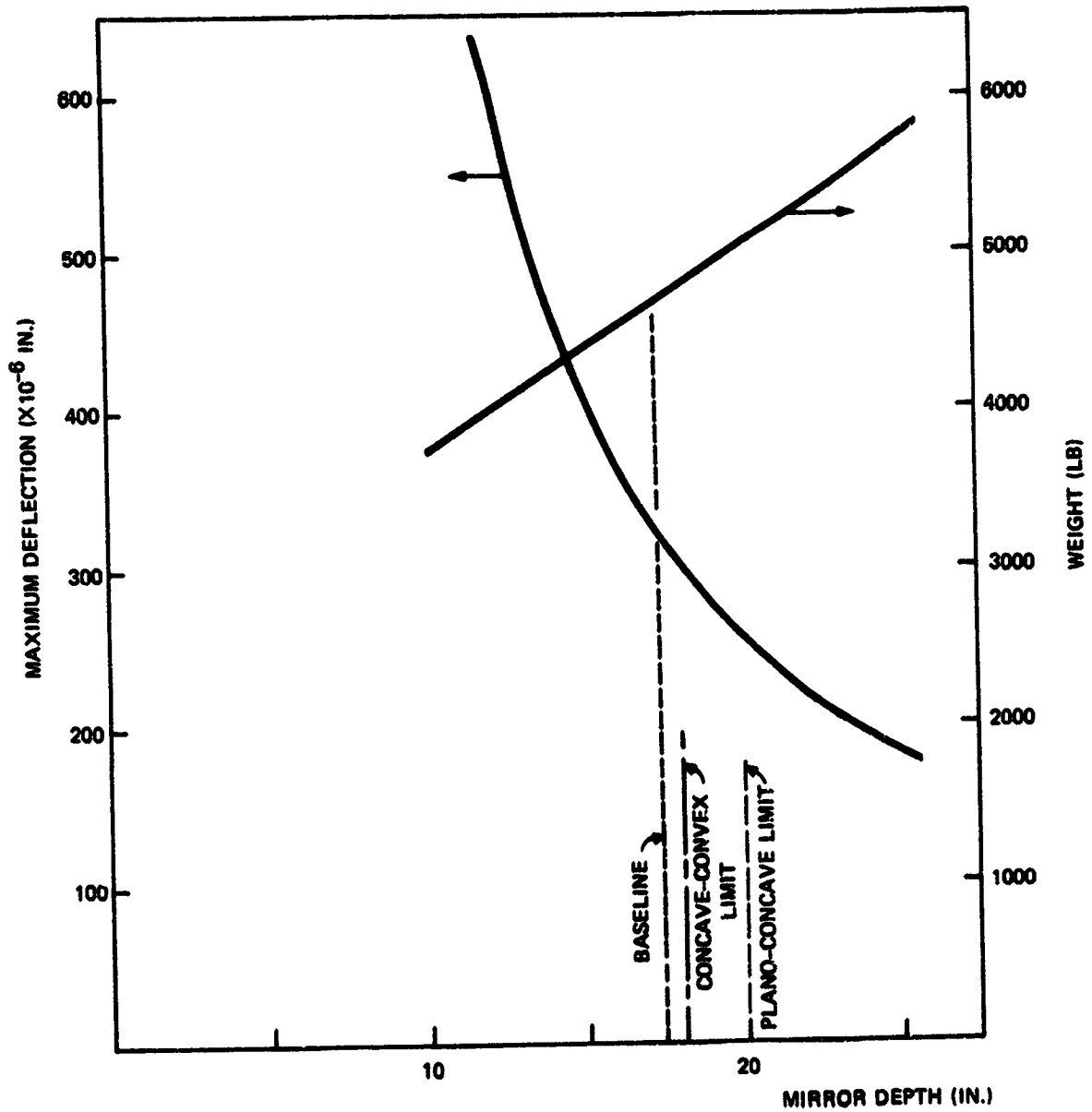


Figure 3.5 Variations on Mirror Depth - 1g.  
 All Other Design Parameters at Baseline.

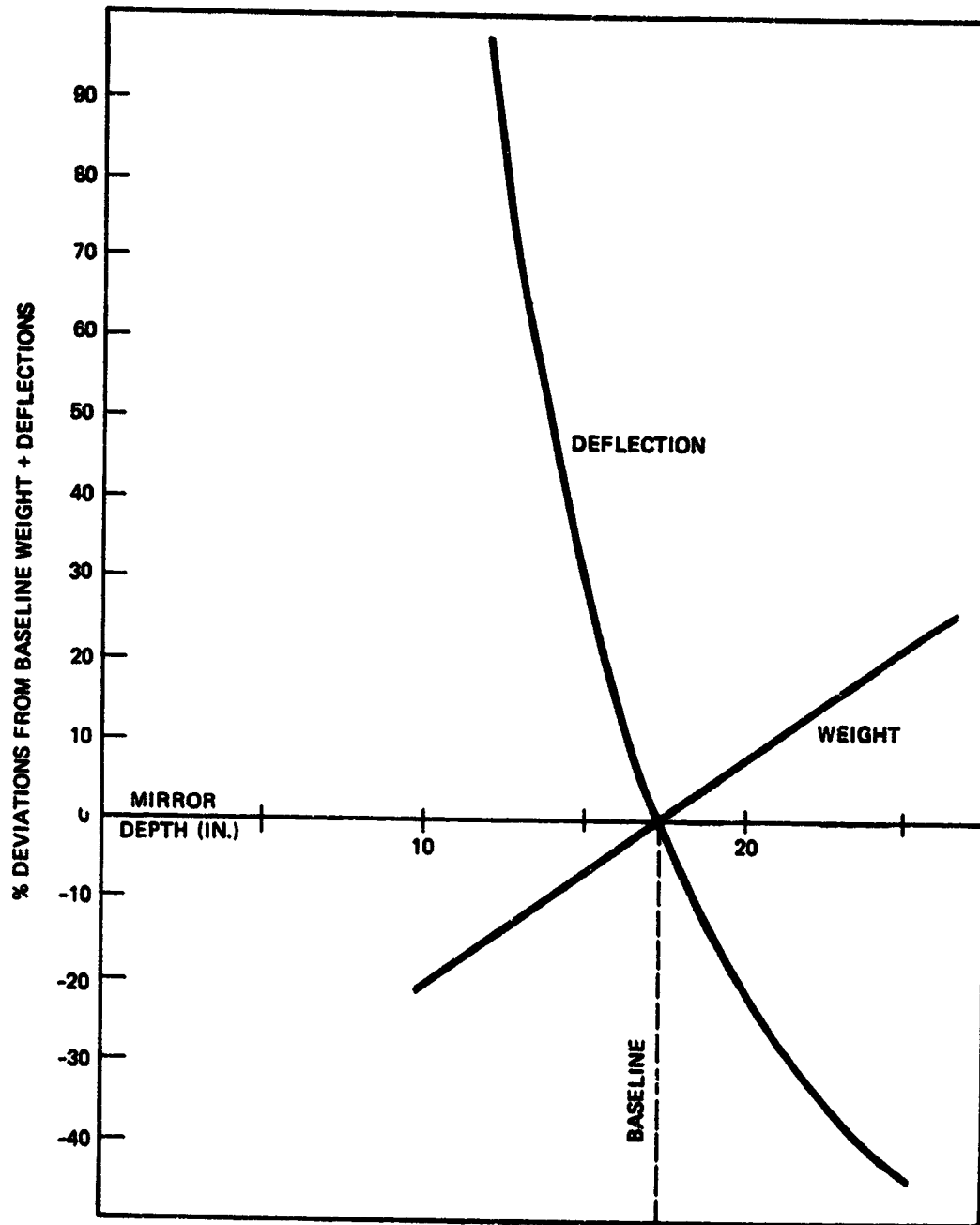


Figure 3.6 Variations on Mirror Depth - 1g.  
All Other Design Parameters at Baseline.

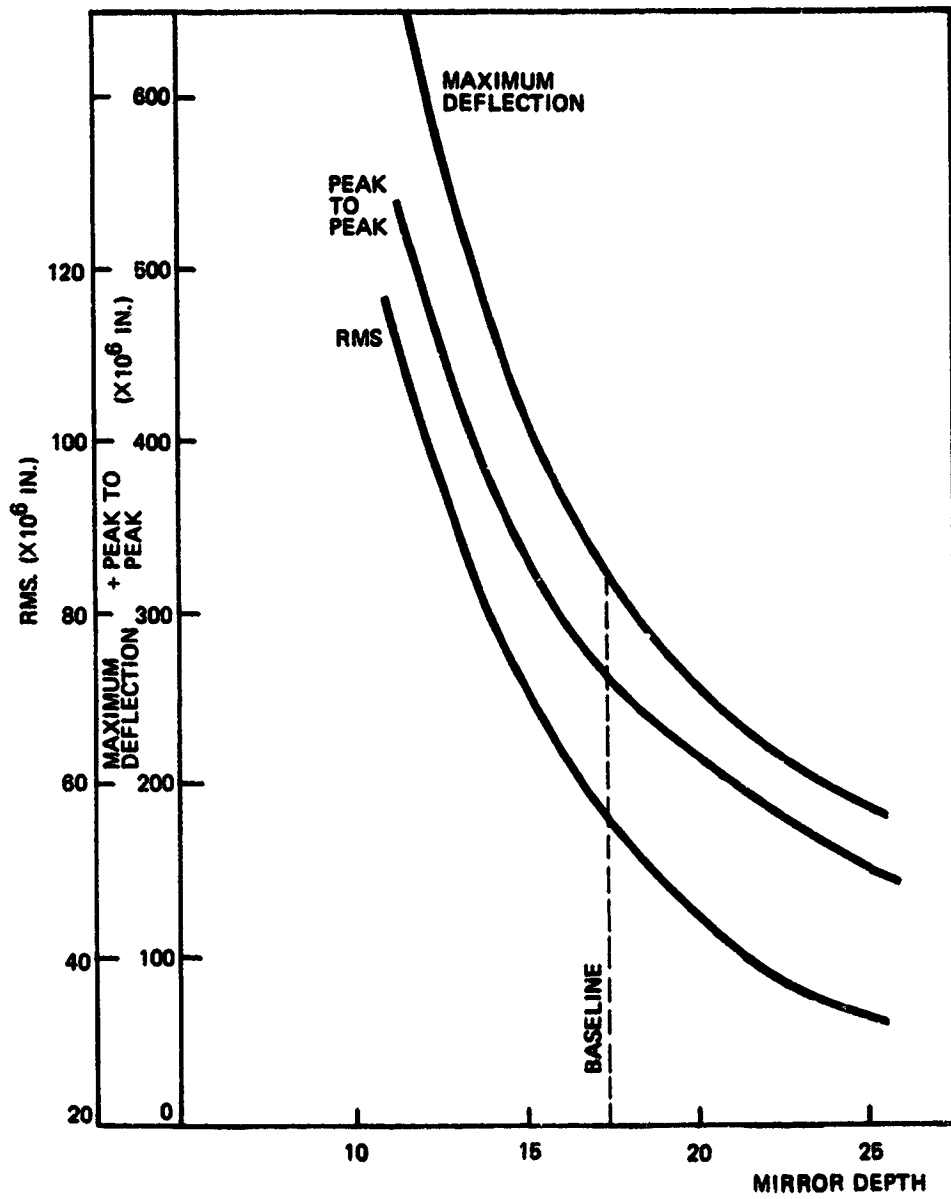


Figure 3.7 Variations on Mirror Depth - 1g.

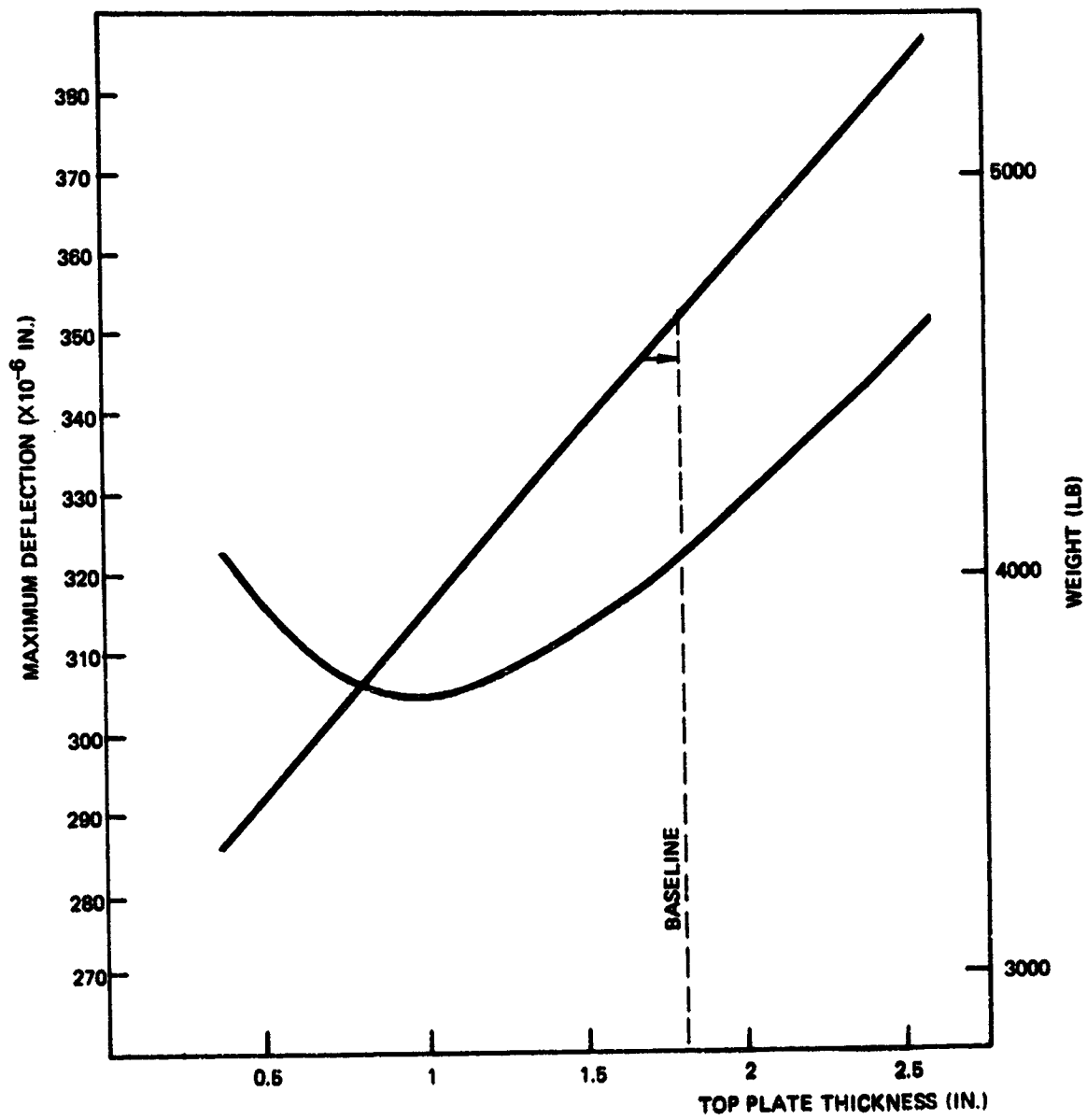


Figure 3.8 Variations on Top Plate Thickness - lg.  
All Other Design Parameters at Baseline.

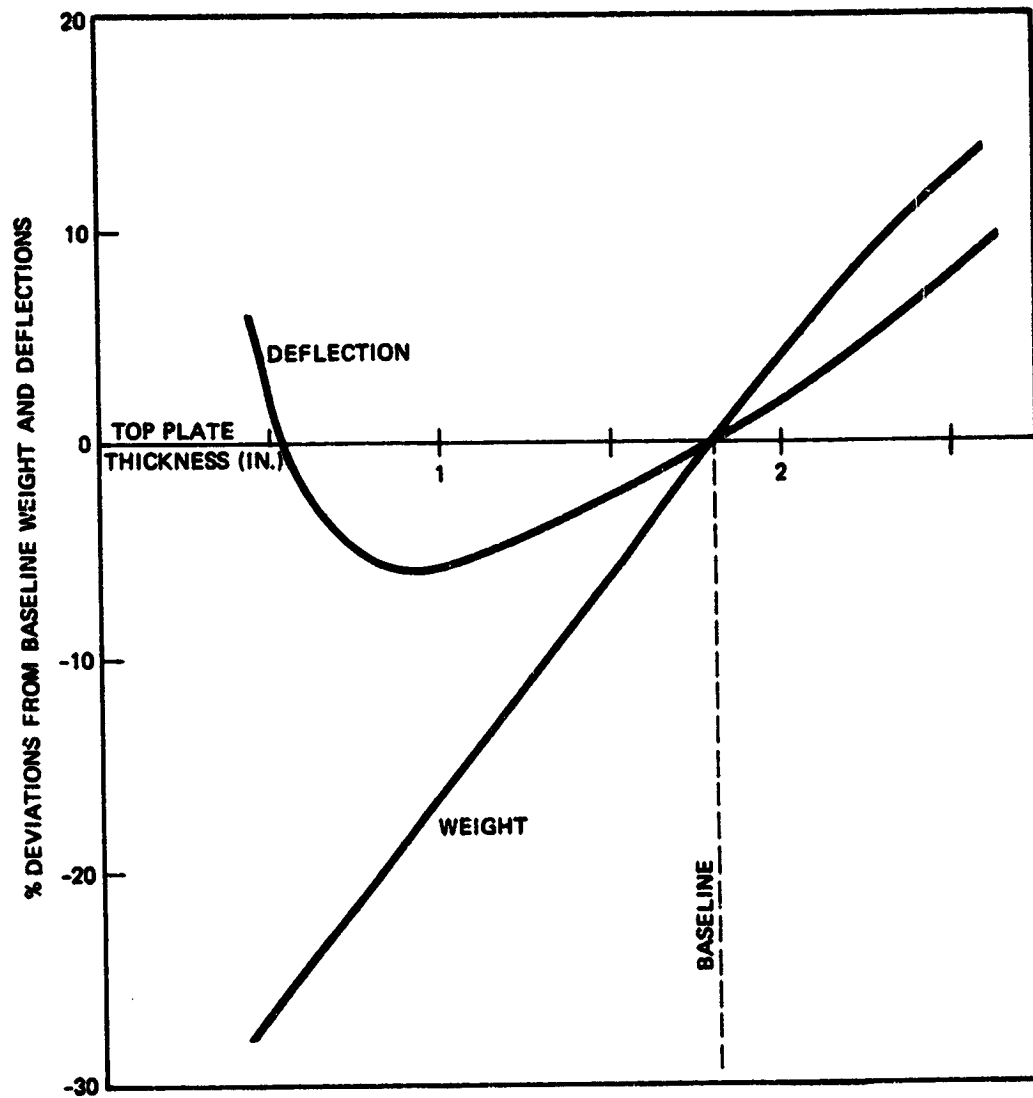


Figure 3.9 Variations on Top Plate Thickness - 1g.  
All Other Design Parameters at Baseline.

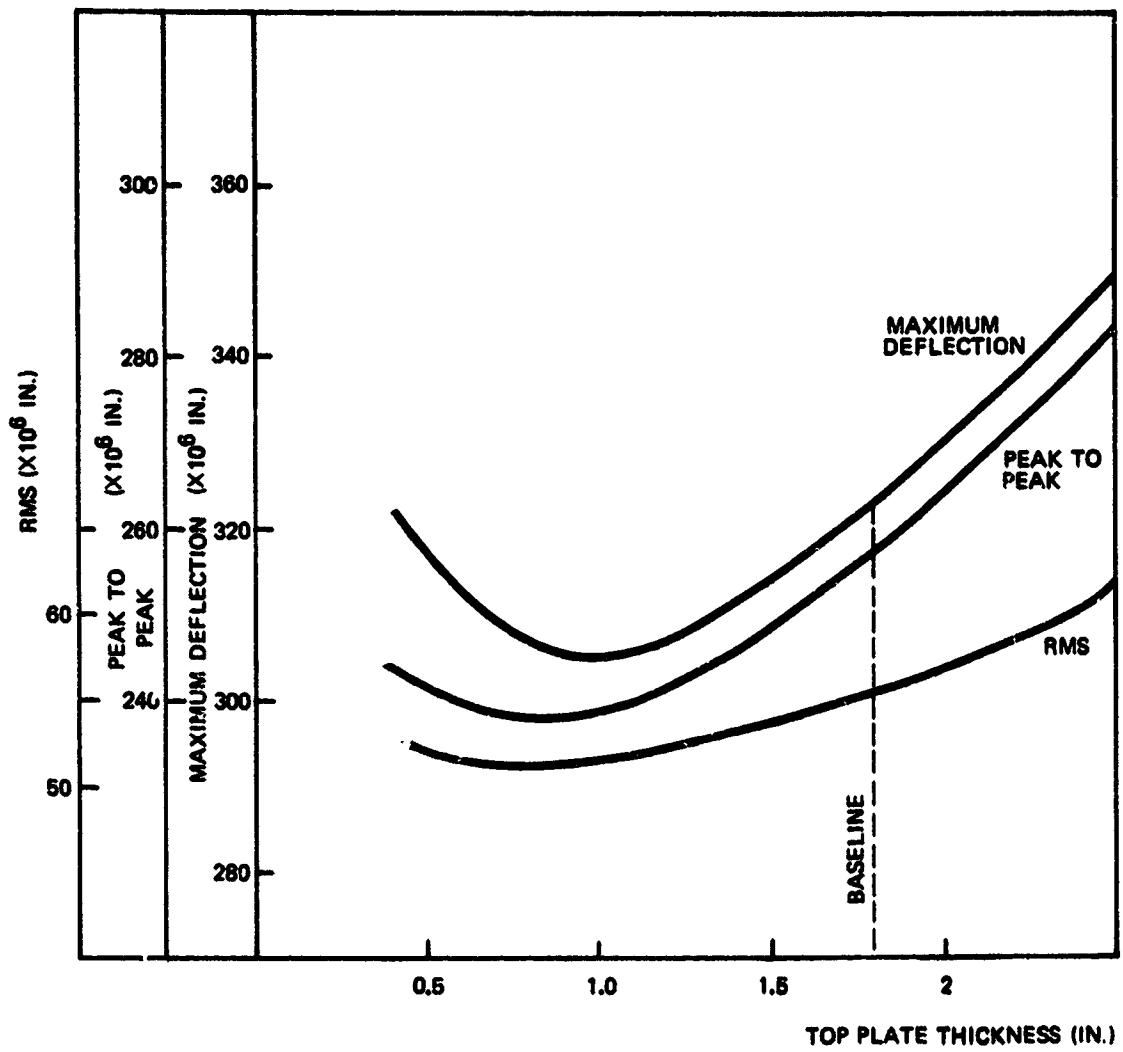


Figure 3.10 Variations on Top Plate Thickness - lg.  
All Other Variables at Baseline.



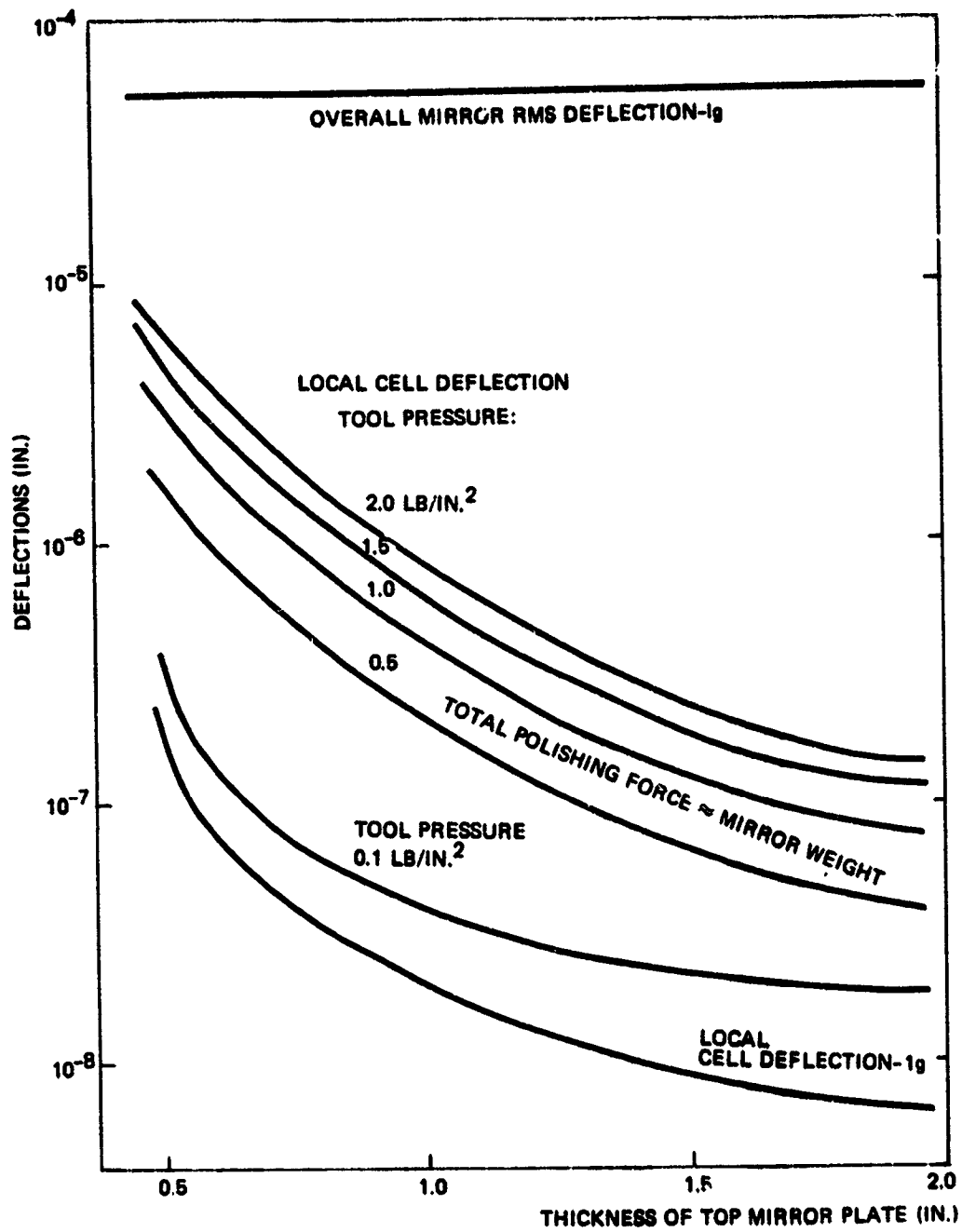


Figure 3.11 Local Cell Effects of Tool Pressure.  
Other Variables at Baseline.  
Perfectly Flexible Tool.

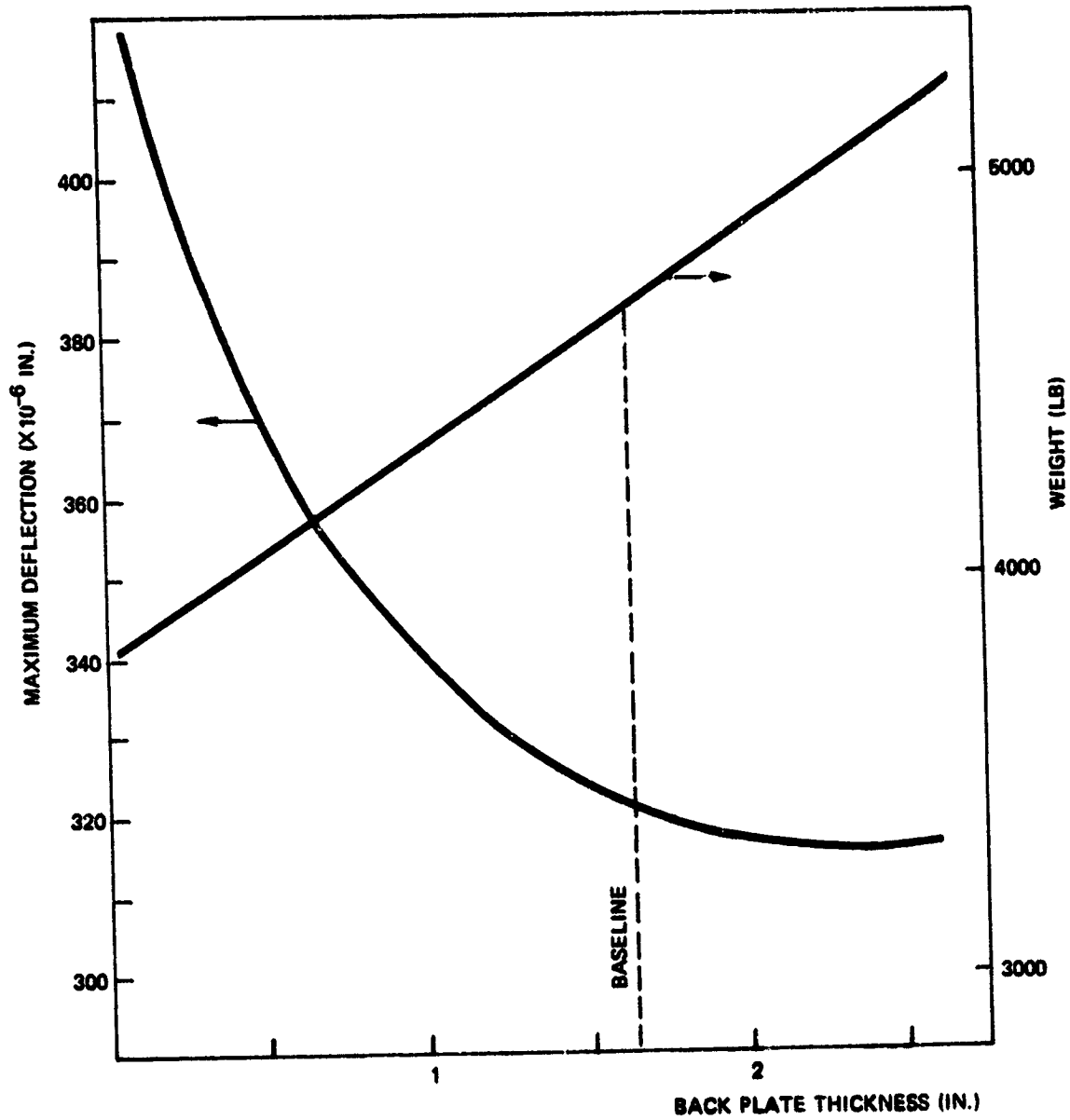


Figure 3.12 Variations on Back Plate Thickness - 1g.  
All Other Design Parameters at Baseline.

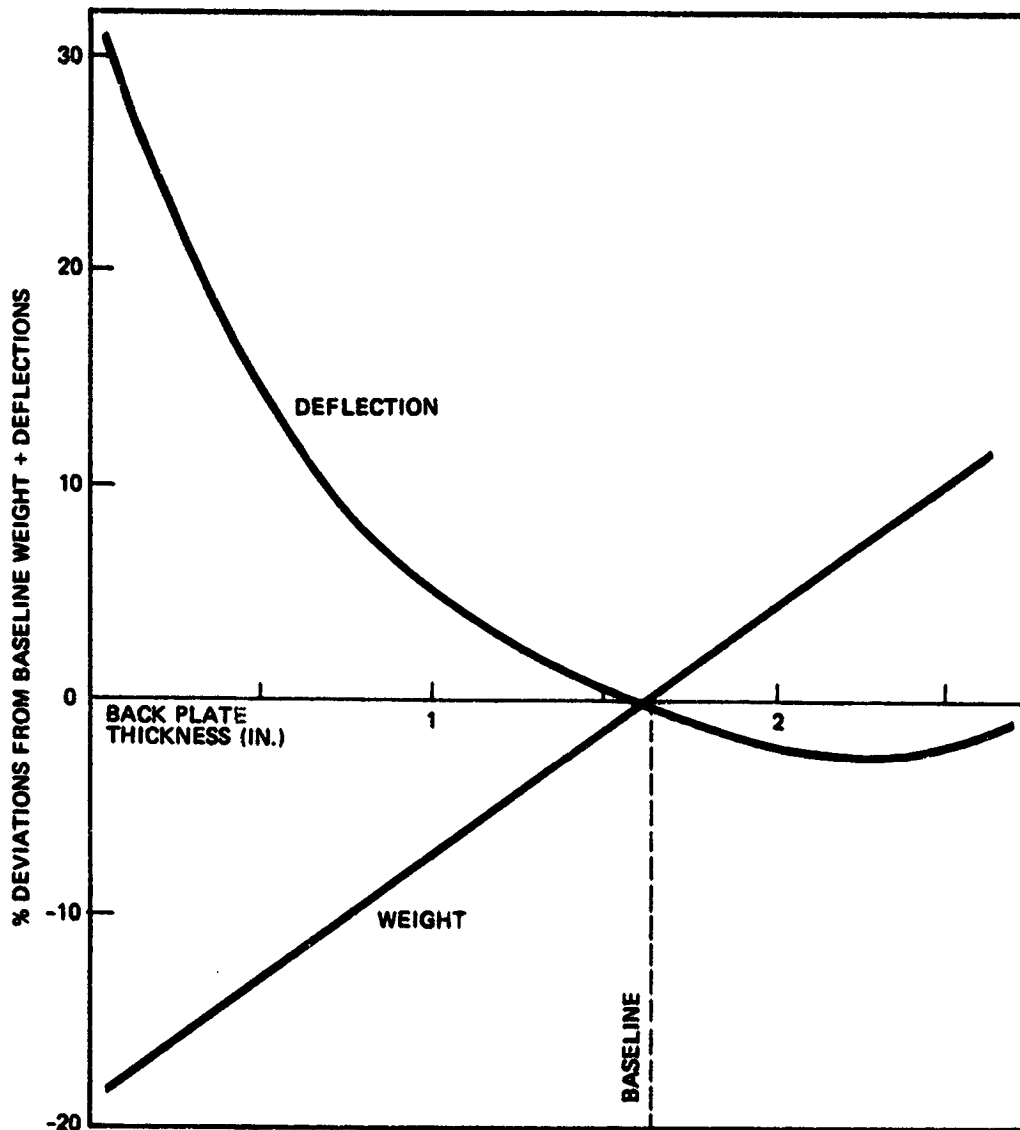


Figure 3.13 Variations on Back Plate Thickness - 1g.  
All Other Design Parameters at Baseline.

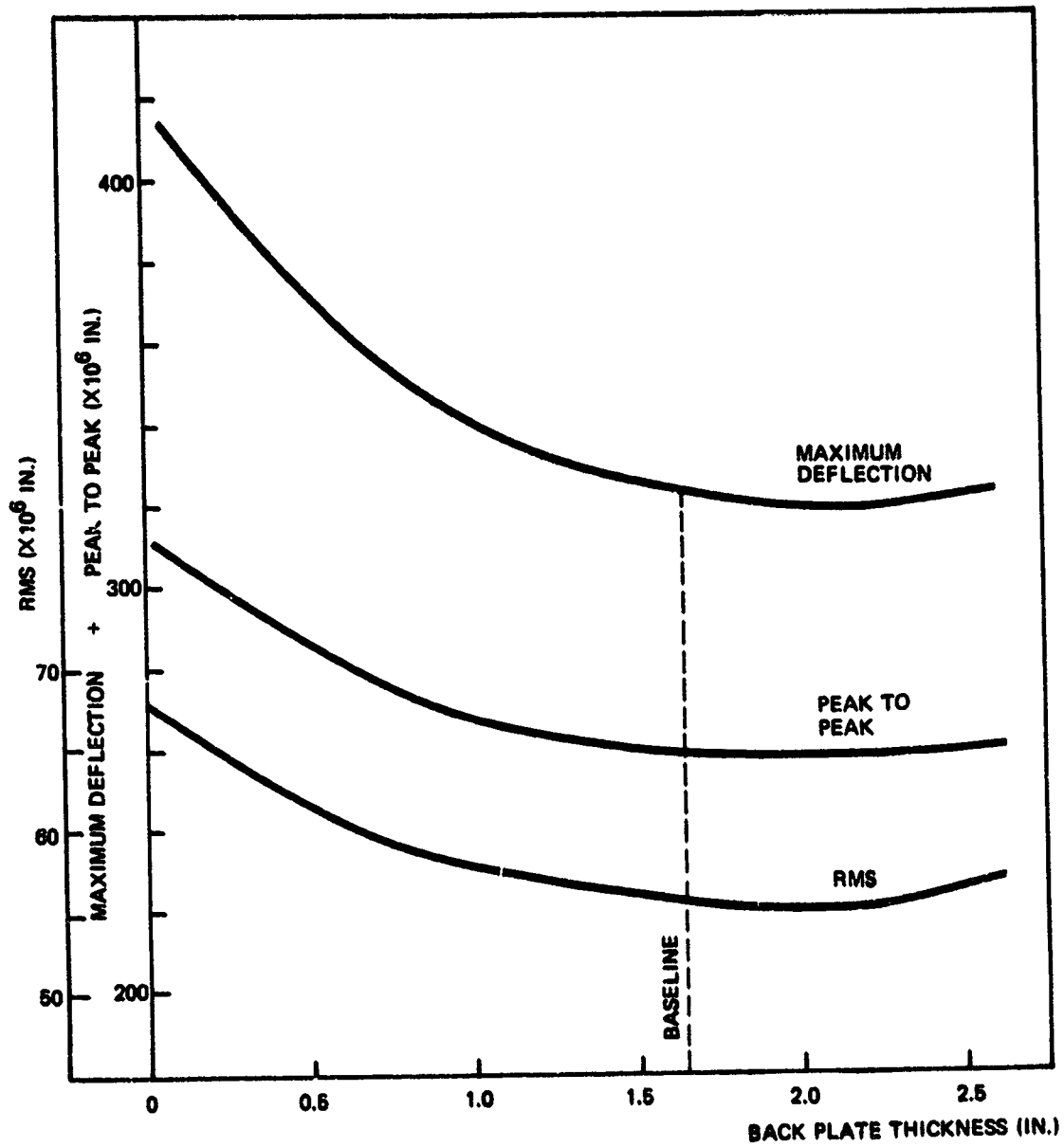


Figure 3.14 Variations on Back Plate Thickness - lg.  
Other Parameters at Baseline.

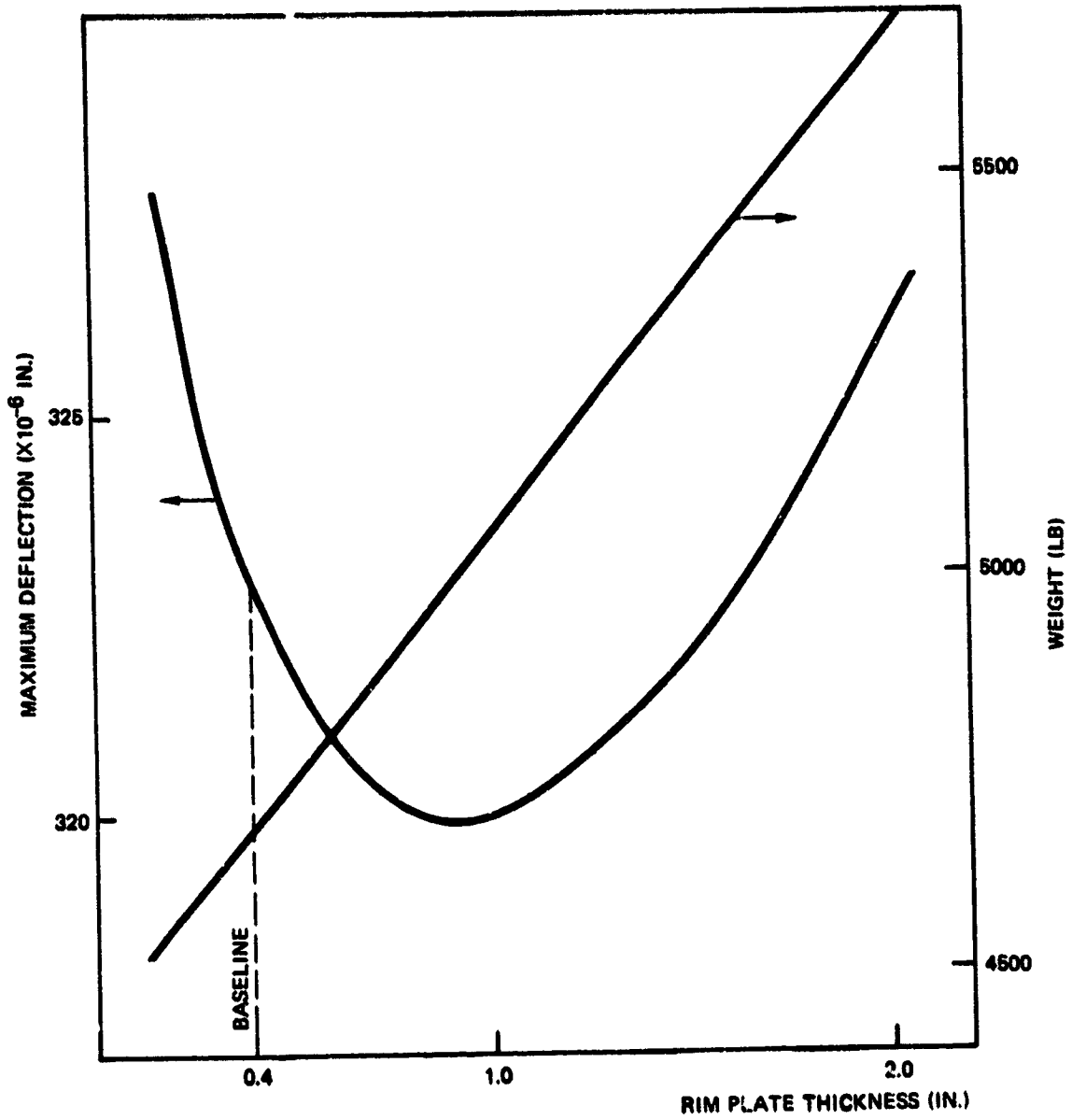


Figure 3.15 Variations on Rim Plate - lg.  
All Other Variable at Baseline.

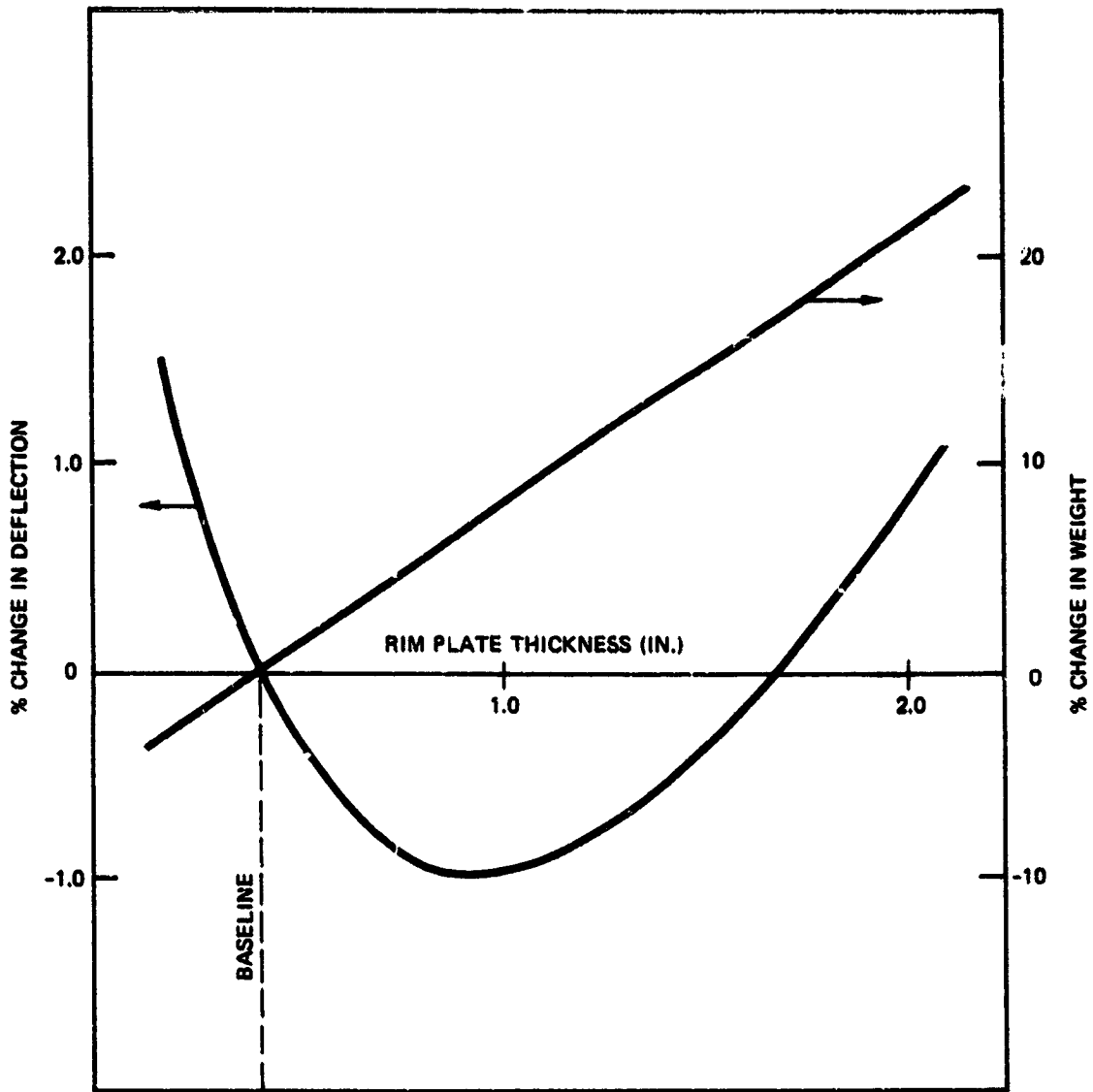


Figure 3.16 Variations on Rim Plate - lg.

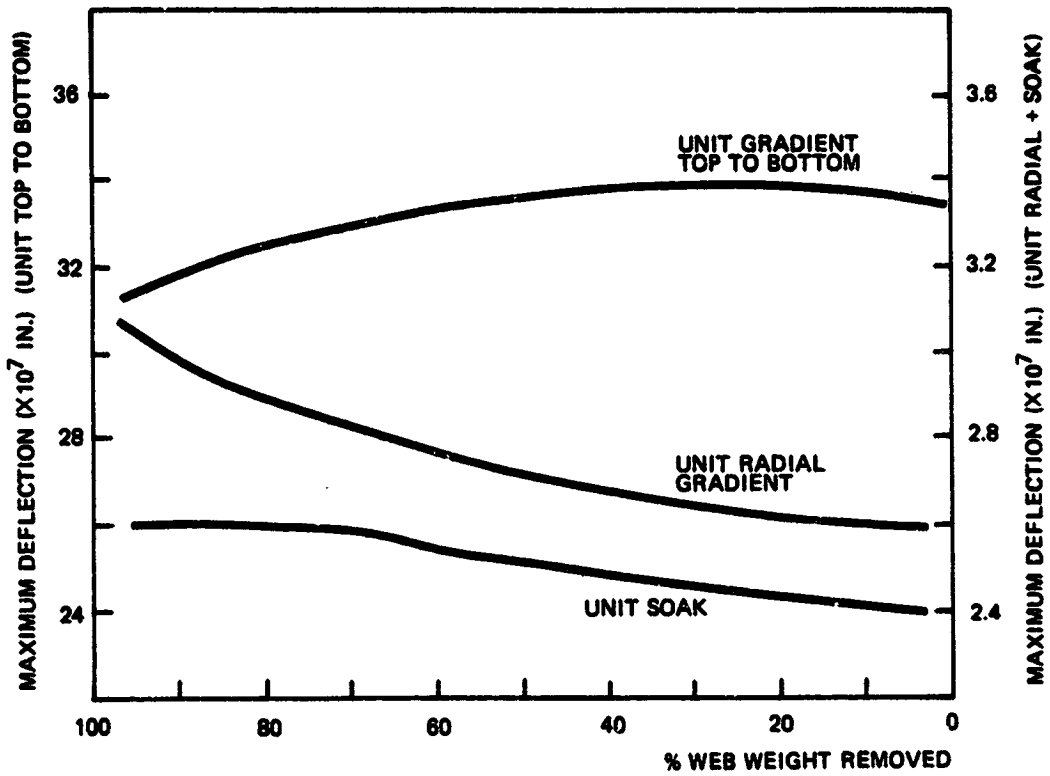


Figure 3.17 Variations on Web Density - Various Thermal Loads.

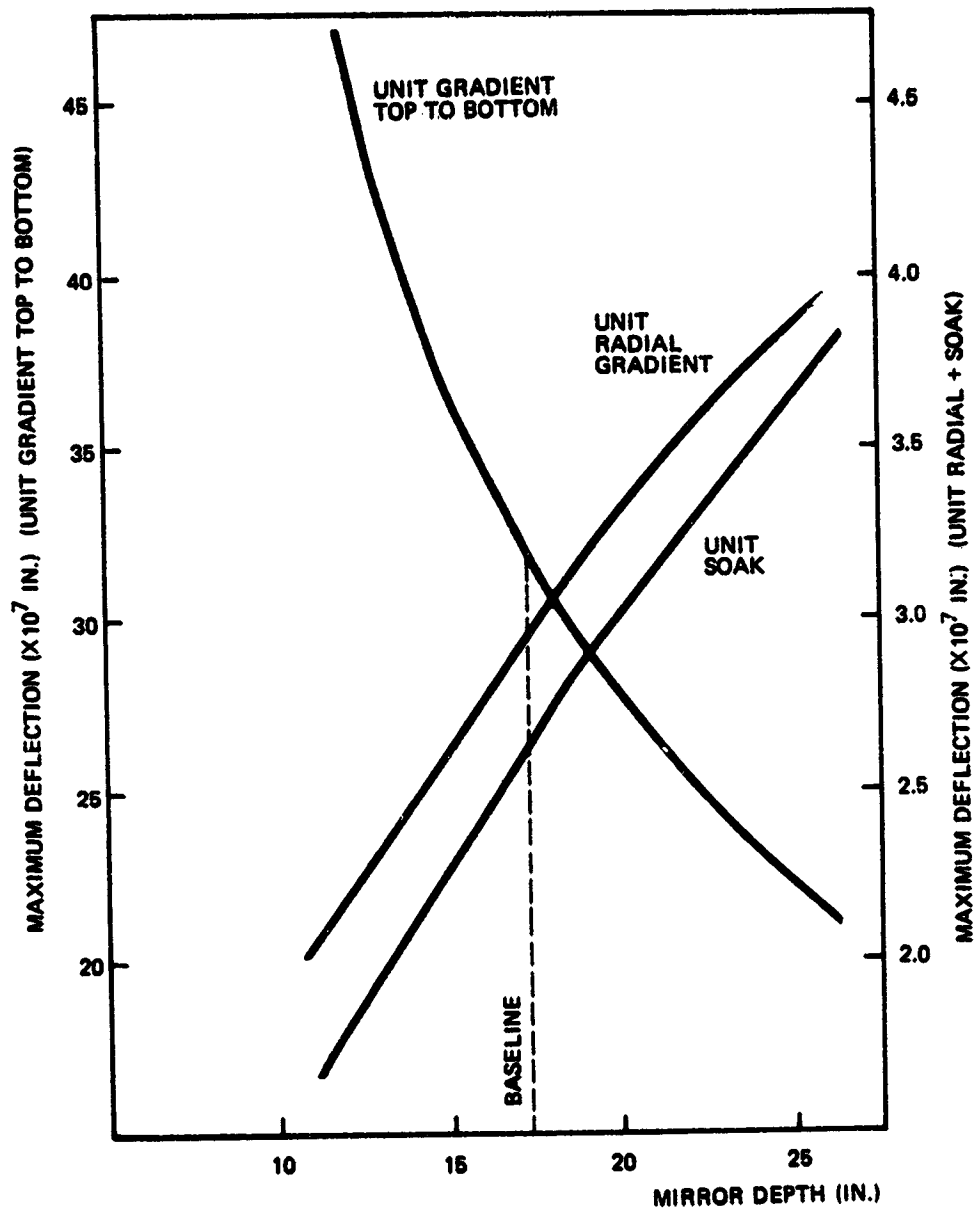


Figure 3.18 Variations on Mirror Depth - Thermal Loads.



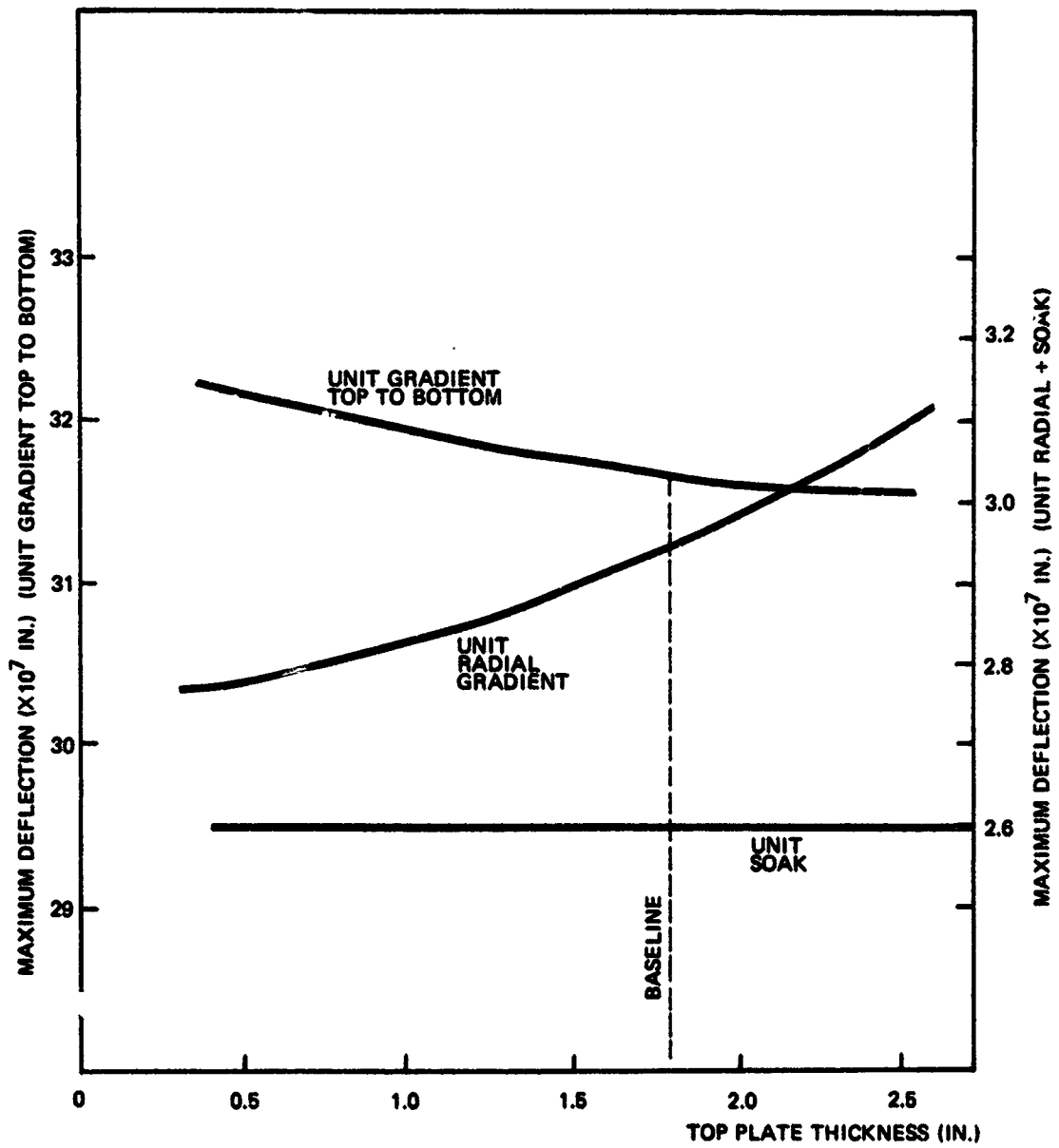


Figure 3.19 Variations on Top Plate Thickness - Thermal Loads.

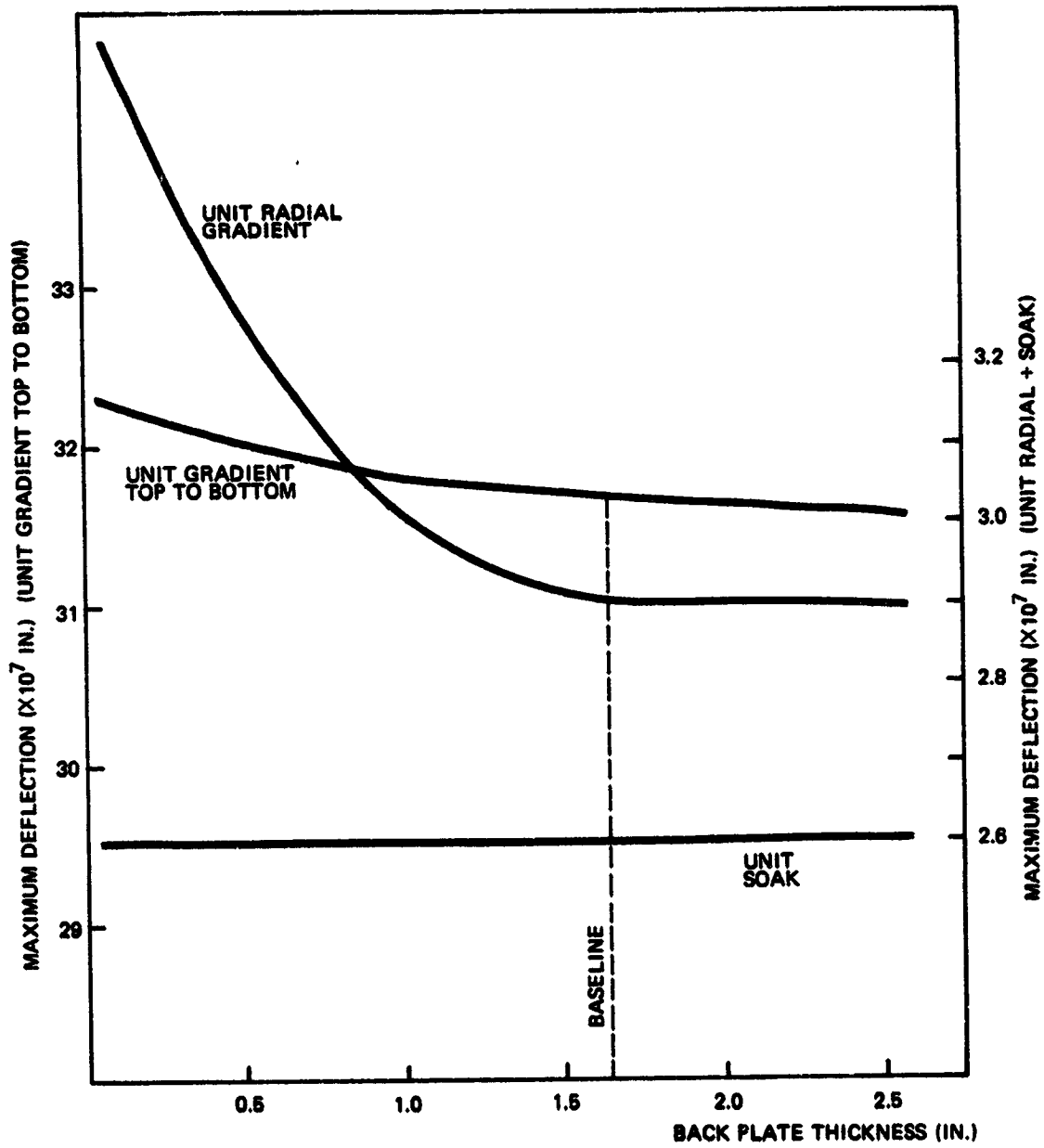


Figure 3.20 Variations on Back Plate Thickness - Thermal Loads.

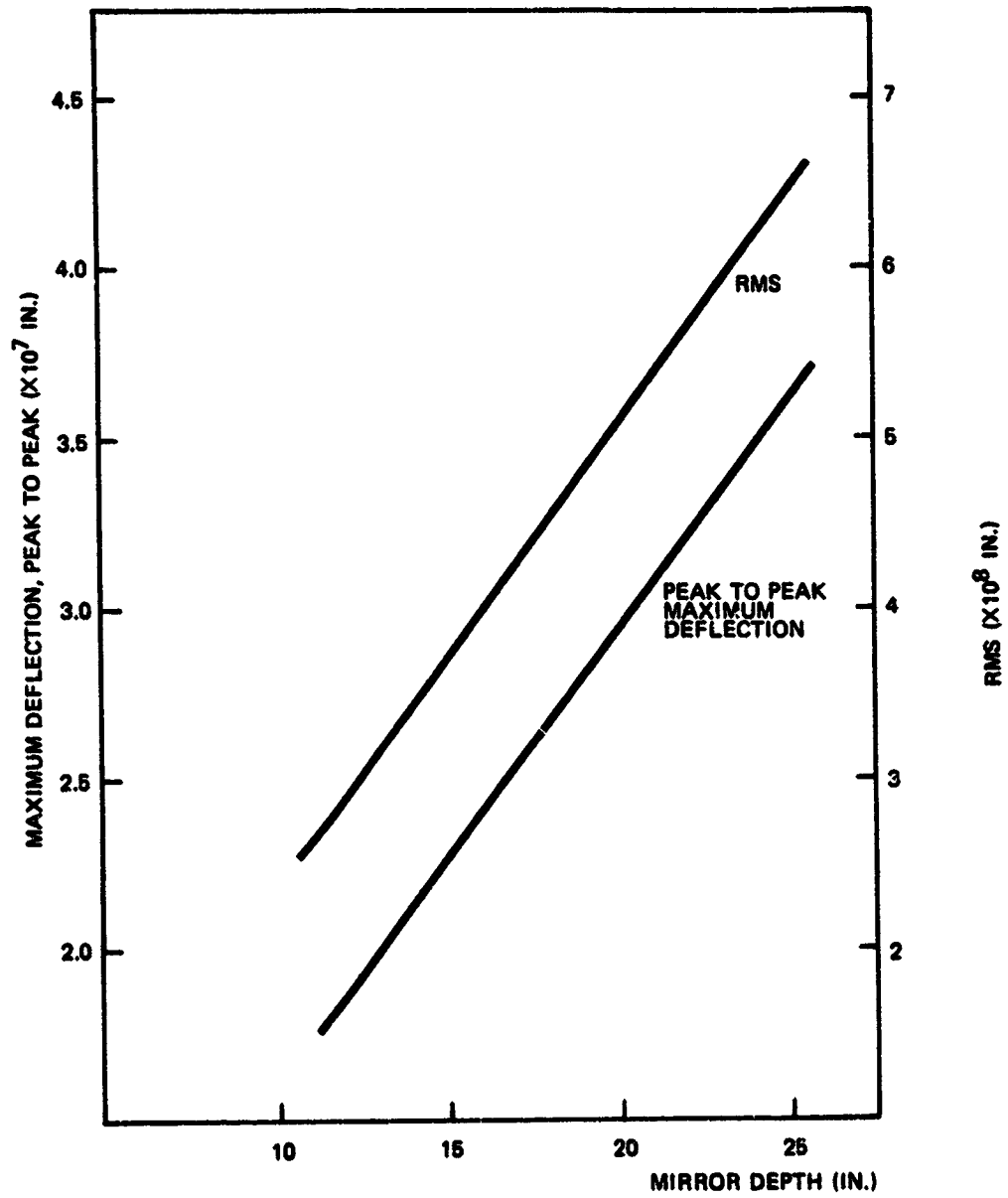


Figure 3.21 1° Soak.

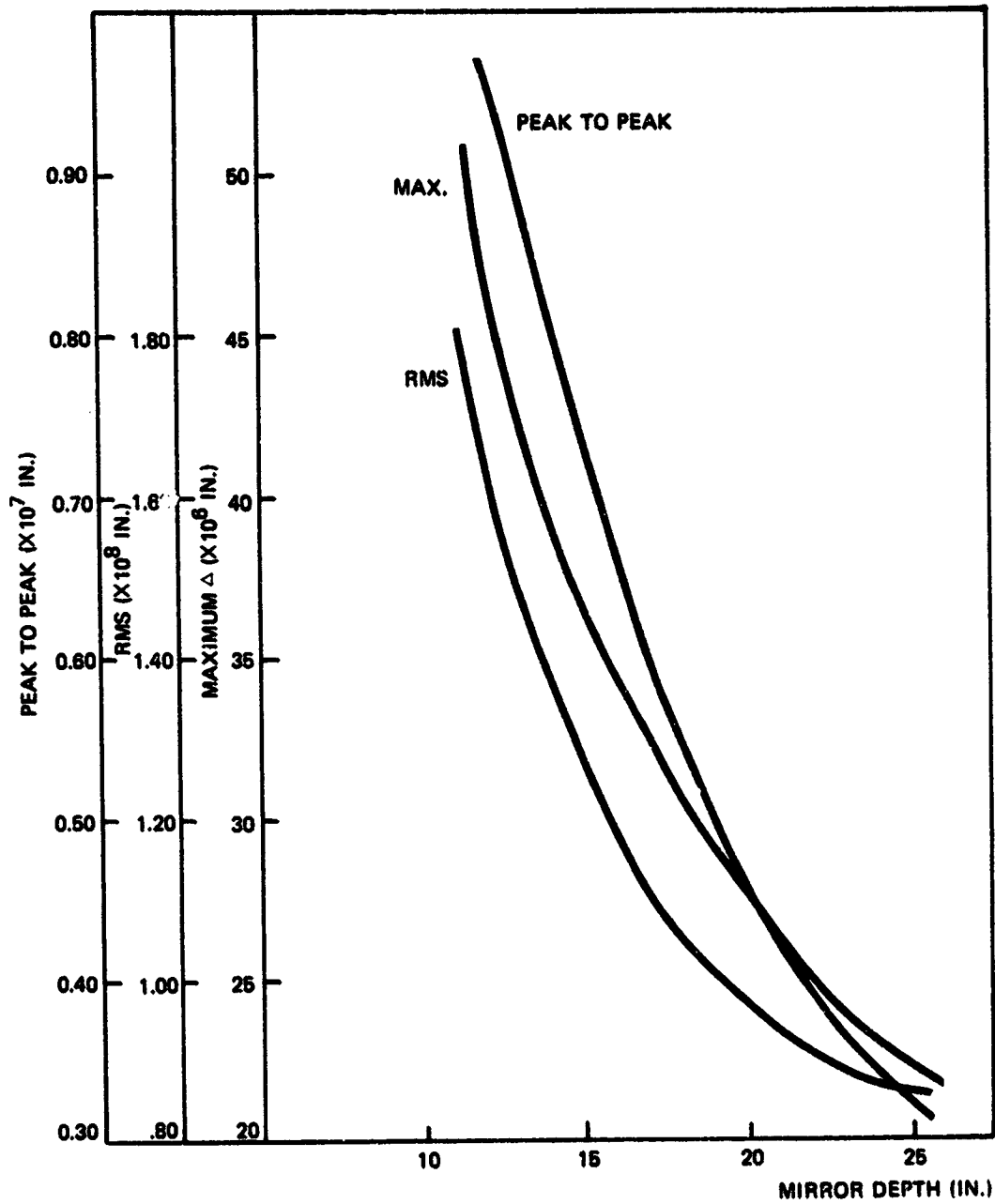


Figure 3.22 1° Transverse Gradient.

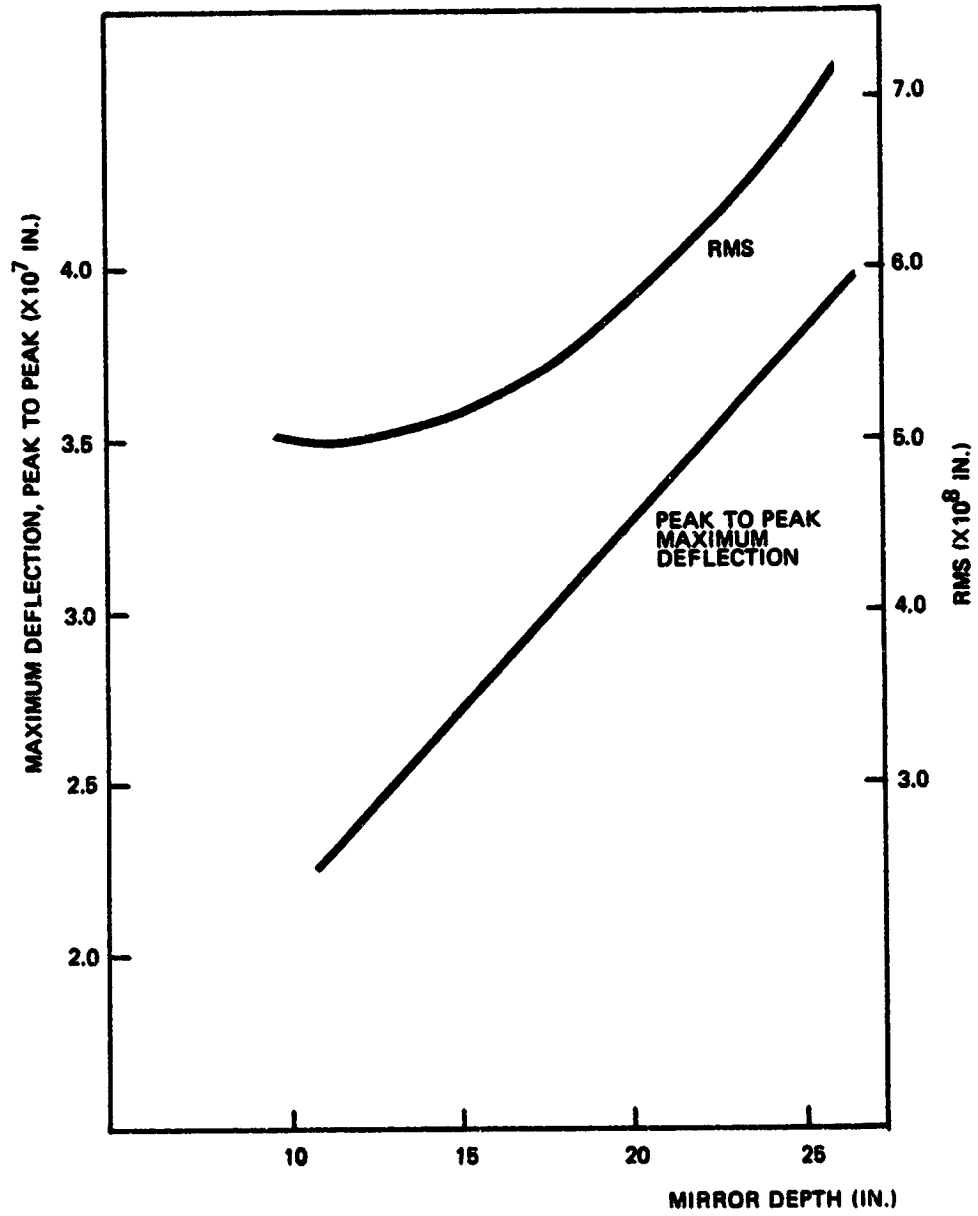
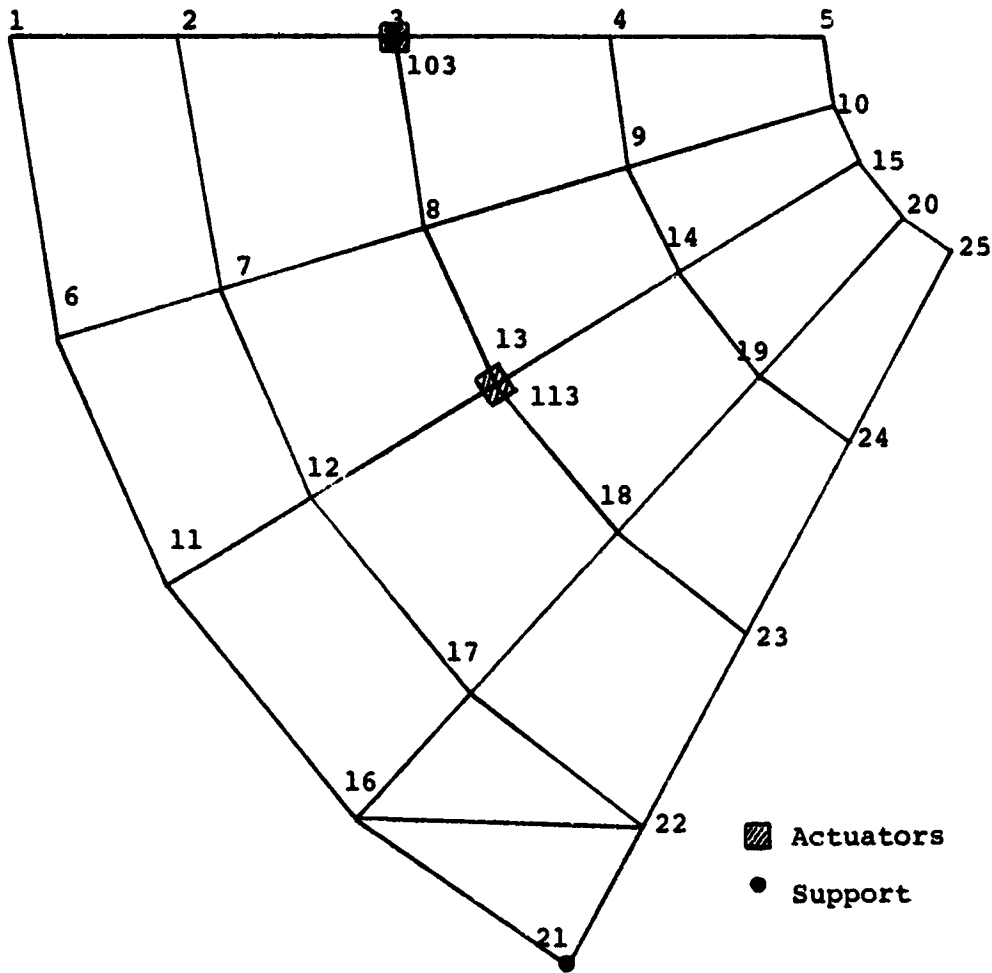


Figure 3.23 1° Radial Gradient.



**Figure 3.24 Actuator Locations - At Back of Mirror.**

**Note: At Node 103 - 3 actuators are used on Mirror.**

**At Node 113 - 6 actuators are used on Mirror.**

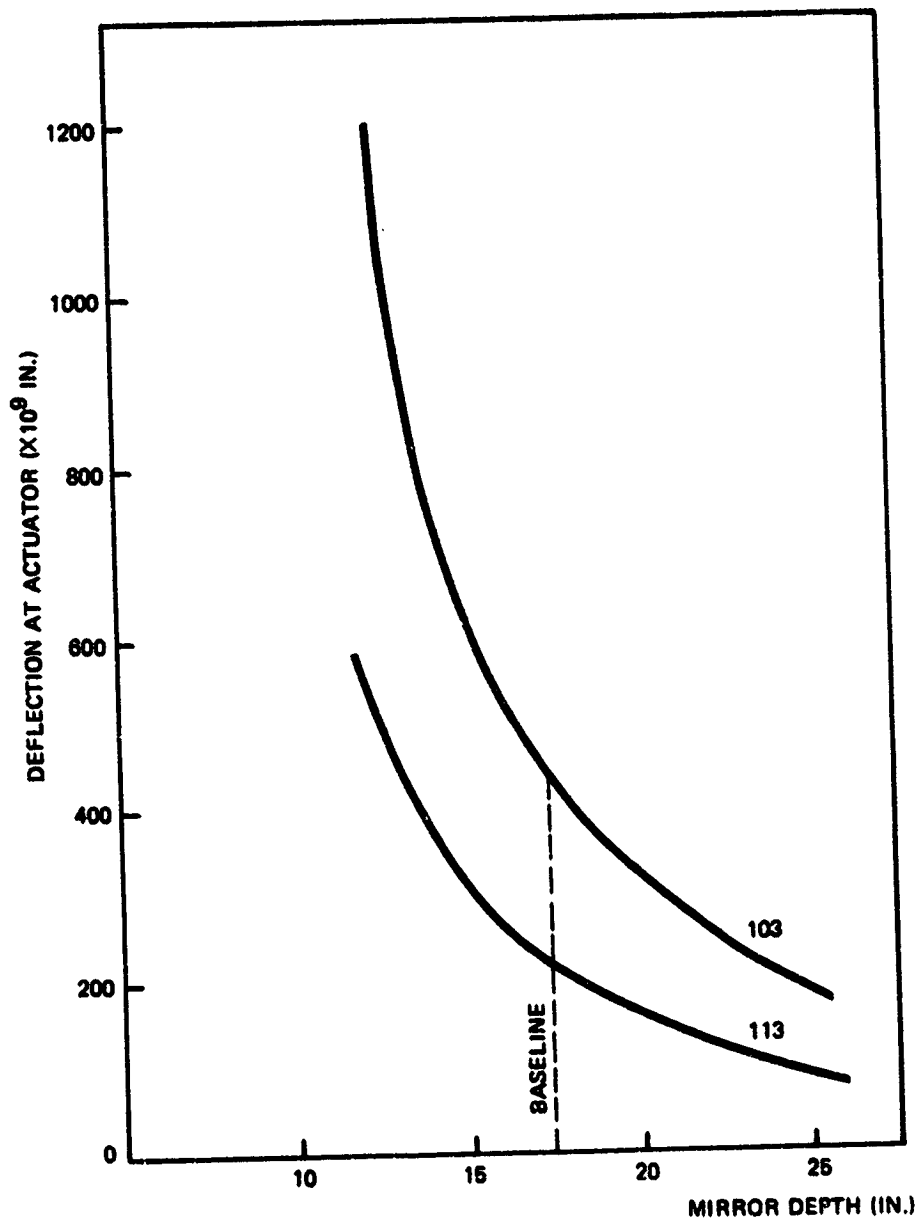


Figure 3.25 Variations on Mirror Depth - 1<sup>#</sup> Actuator Force.

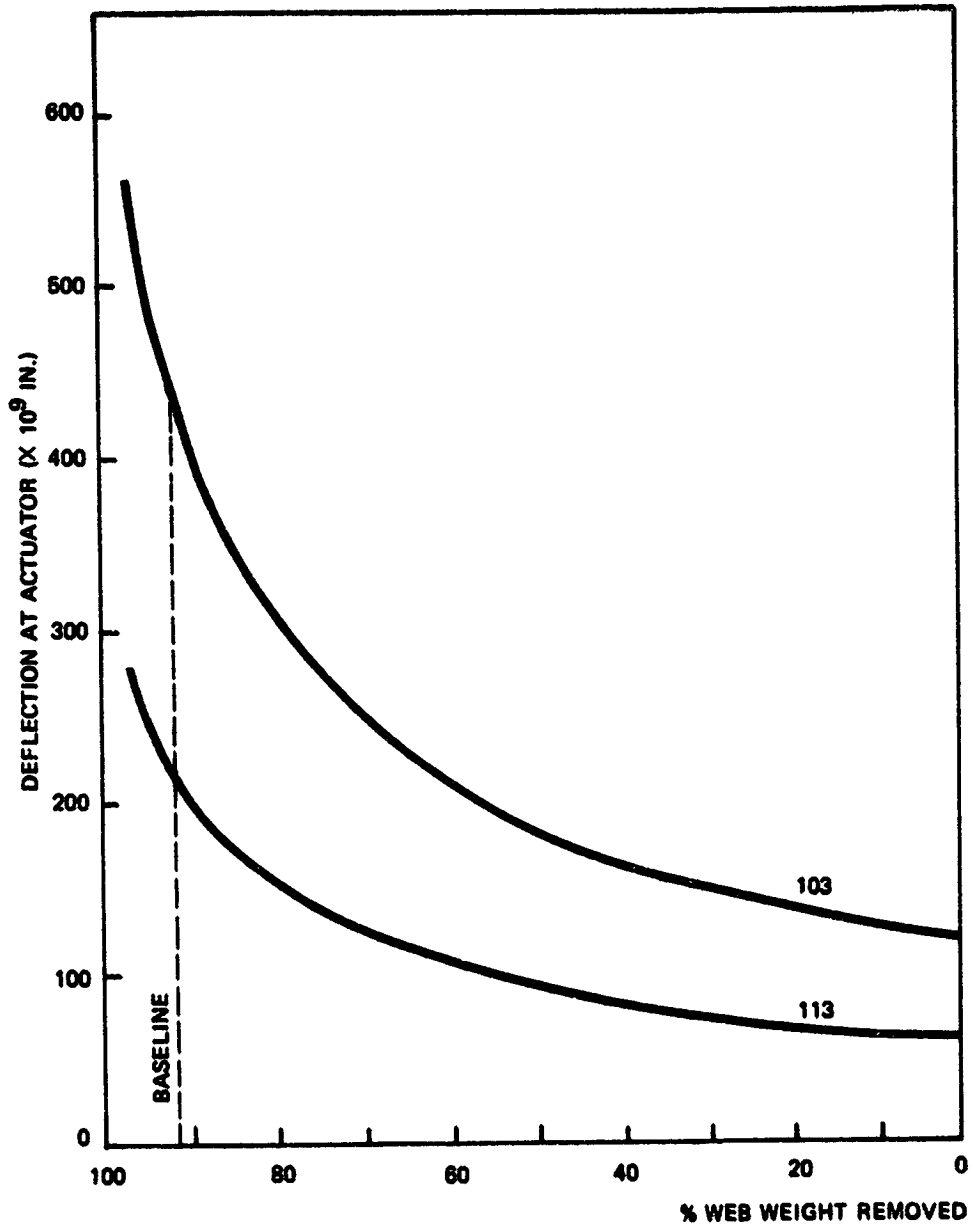


Figure 3.26 Variations on Web Density - 1<sup>#</sup> Actuator Load.



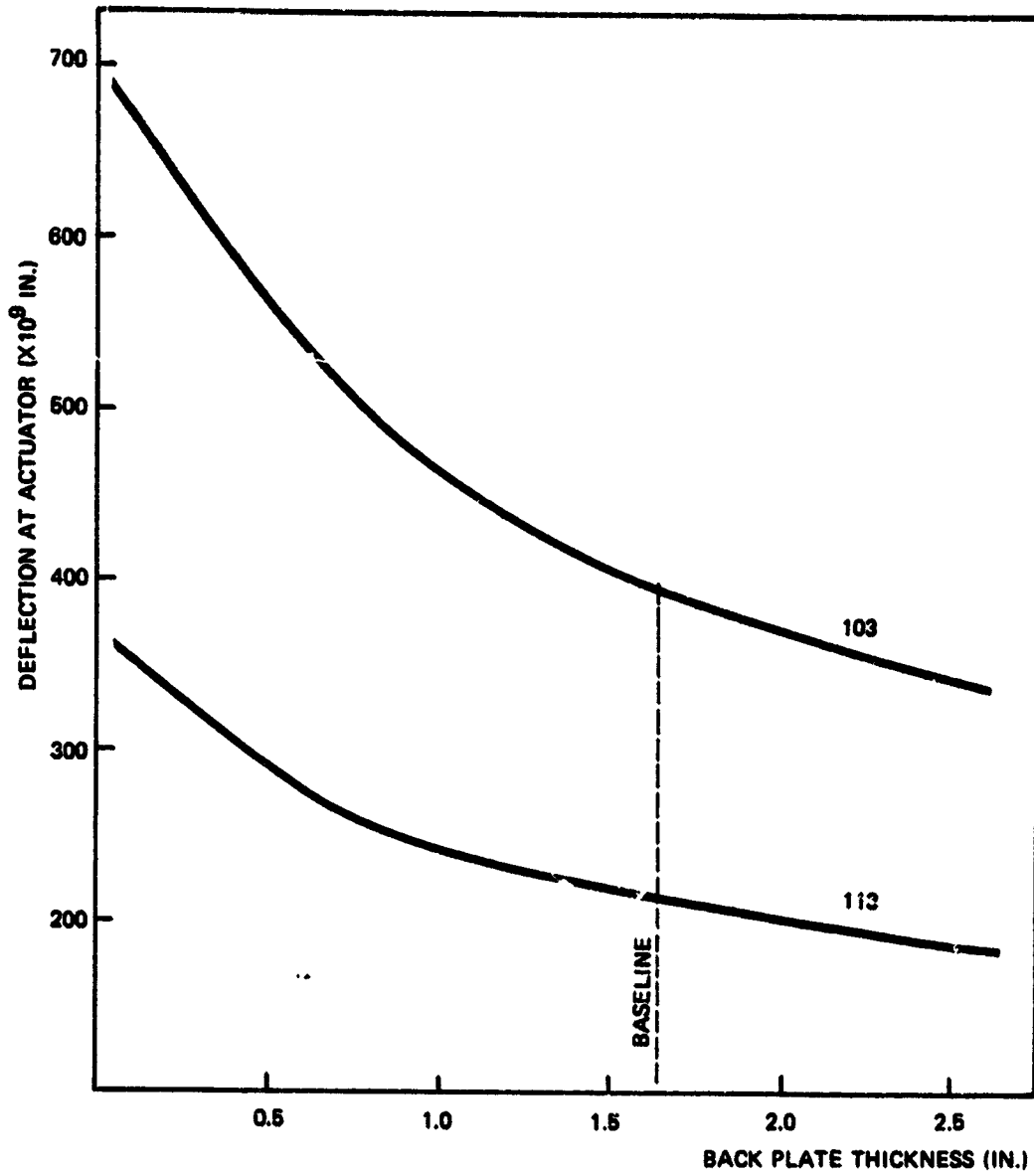


Figure 3.27 Variations on Back Plate Thickness - 1<sup>#</sup> Actuator Force.

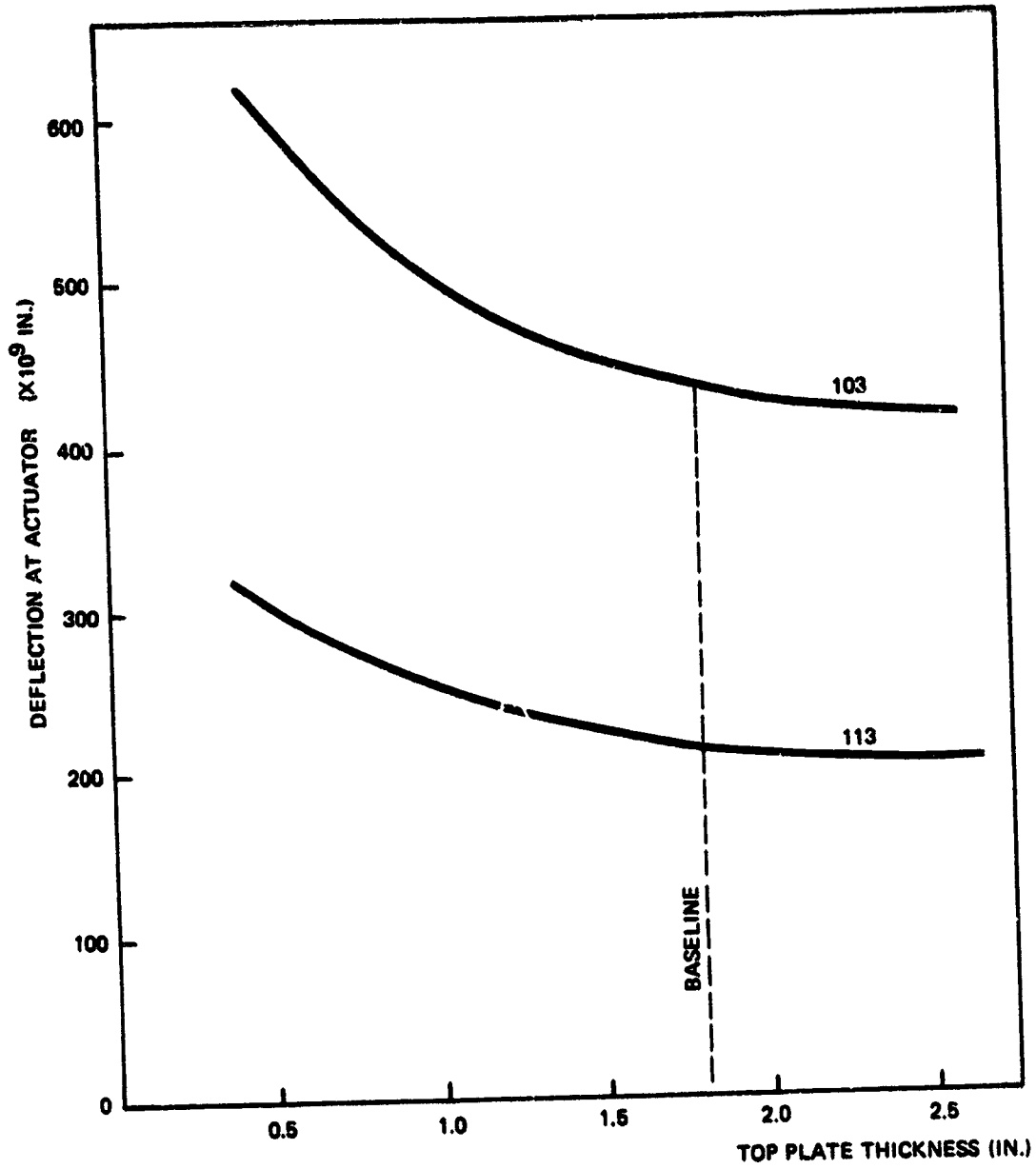


Figure 3.28 Variations on Top Plate Thickness - 1<sup>#</sup> Actuator Force.

## Chapter 4

### BREADBOARD MIRROR

#### 4.1 Necessity for Breadboard Mirror

As the lead time for the delivery of the polished Large Space Telescope primary mirror is at least several years from initial procurement, it is desirable to have some form of high quality reflector with which to develop and test the other optical subsystems necessary for the operation of the observatory. Such a mirror need not have the same aperture as LST, but it ought to exhibit as much of the same performance characteristics as possible. With such a reduced-size mirror, many other technology problems associated with the full system can be investigated as well.

Given the current Phase "A" CERVIT mirror configuration a number of manufacturing uncertainties remain which could be tested on a breadboard system. It is not clear, for instance, that the cell lightweighting procedure will be very successful in the immediate vicinity of the solid support area. Nor is it certain that the desired figure can be achieved if the mirror compliance differs by several orders of magnitude as one moves from the interior of the mirror to the supports.

Many unknowns associated with the structural performance prediction of lightweighted mirrors can be resolved here as well. It is usually not possible for computational reasons to model the fillets, although they probably contribute somewhat to stiffness. Similarly, the top plate of CERVIT lightweighted mirrors is rarely uniform in thickness since the cell holes are fabricated parallel to the optical axis,

while the top plate is curved. This effect is called "wedge" and it too is difficult to model without the use of solid three-dimensional elements. With a properly scaled "breadboard" mirror these details may be investigated experimentally.

The effects of the inhomogeneities in the material properties of the mirror may be included as well. Samples obtained during lightweighting can be tested, introduced into the mathematical model and the experimental results compared with the theory. This will result then in materials testing criteria for the full mirror blank.

Apart from acting as the prime reflector for the integration of the active optics, the breadboard mirror can be subjected to a number of interesting structural tests using the actuators. The figure control flexibility matrices can be determined experimentally, and the results compared to analytically derived values. With the use of the actuators, strength tests can be performed on the mirror to simulate the effect of an equivalent static "g" force that would be encountered during launch. With proper use of scaling laws this would be a simple and inexpensive proof test for fracture strength, and would minimize the risk on the full LST mirror.

The breadboard mirror can be extremely useful, in launch qualification testing for the evaluation of different support details in the transmission of the vibration.

#### 4.2 Breadboard Mirror Dimensions

For various, more or less arbitrary reasons, mainly involving availability of suitable CERVIT blanks, ease of handling, etc., the diameter of the breadboard mirror was fixed at 48". The configuration of this breadboard was

intended to resemble as much as possible the LST 120" Phase "A" CERVIT mirror. In this way all of the performance data obtained at the reduced scale could be related to the full size mirror by laws of similitude.

If a perfect geometrical reduction were to occur, the various dimensions of the breadboard would be as listed in Table 4.1. Such a mirror would have as many cells as the full size, and the time and cost of fabrication would not be significantly different. The cell wall thickness specified (0.08) would probably be extremely difficult, if not impossible, to achieve. The cell wall would need, therefore, to be thickened without, however, increasing the relative stiffnesses of the "flange" plate and the core, while preserving more or less the geometry of cells around the solid support. Since this latter characteristic was quite unique and a source of considerable uncertainty in terms of fabrication, it was felt essential to preserve it in the breadboard. Hence in Figure 4.1 it is seen that a number of other geometrical restrictions must be followed as well to preserve the symmetry. Table 4.2 considers a number of potential cell size/cell wall combinations. The configuration chosen is seen in Figure 4.2 with a cell size of 3.8 inches and a cell wall of 0.24. This appears to be readily manufacturable.

#### 4.3 Model Laws

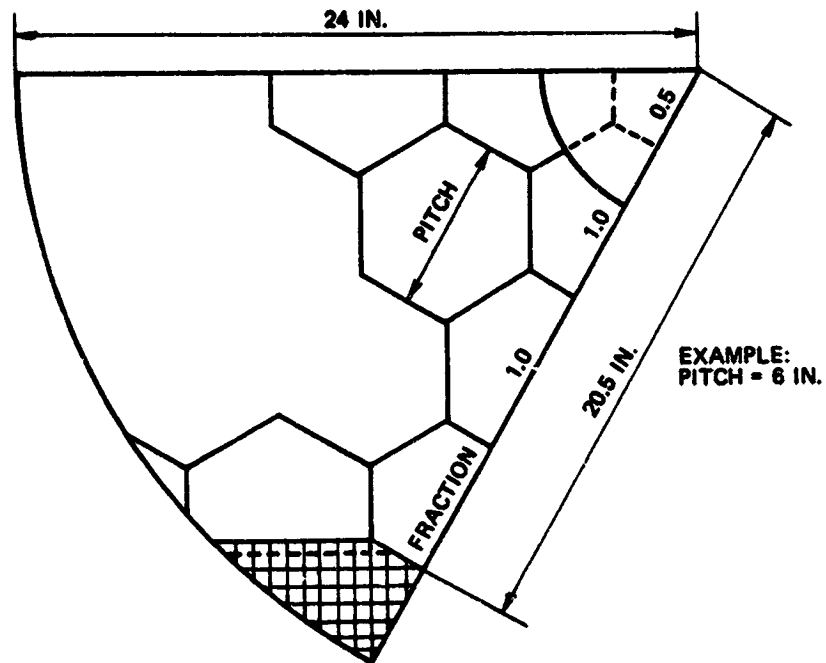
Since the model and prototype materials are the same, and the scale factor is fixed, no further variables can be postulated for the model laws. Table 4.3 lists the various dimensional relationships between the model and prototype structures. Note that "f" represents the scaling factor.

Table 4.4 details these relationships in an even more specific sense for the various structurally-important

TABLE 4.1

LST BREADBOARD - FULLY SCALED

Dimension	Full Scale	Breadboard
Diameter	120	48
Depth	17.37	7
Center Hole $\phi$	24	9.6
Front Plate	1.83	0.73
Back Plate	1.62	0.65
Rim Wall	0.4(0.8)	0.16(0.32)
Cell Pitch (size)	4.8	1.9
Cell Wall Plate	0.2(0.3)	0.08(0.12)
Back Plate Hole $\phi$	3.25	1.3
Elastic Modulus	$13.4 \times 10^6 \text{ #/in}^2$	Same
Poisson	0.252	Same
Density	$0.09 \text{ #/in}^3$	Same
Coeff. of Thermal	$0.277 \times 10^{-7} / ^\circ\text{F}$	Same



**Figure 4.1 Basic Requirements for Breadboard Cell Layout.**

1. Preserve Present  $60^\circ$  Symmetry.
2. Model Solid Area as Faithfully as Possible.

TABLE 4.2

INTEGRAL NUMBER OF CELLS IN 20.5" LENGTH

$$\therefore (n+0.5) \times \text{PITCH} = 20.5$$

n	PITCH	CELL WALL
1	13.65	0.87
2	8.70	0.52
3	5.86	0.37
4	4.57	0.29 (original size)
5	3.73	0.24 (cells 2x scaled)
6	3.15	0.20
7	2.74	0.175
8	2.41	0.153
9	2.15	0.136
10	1.95	0.12 (fully scaled)



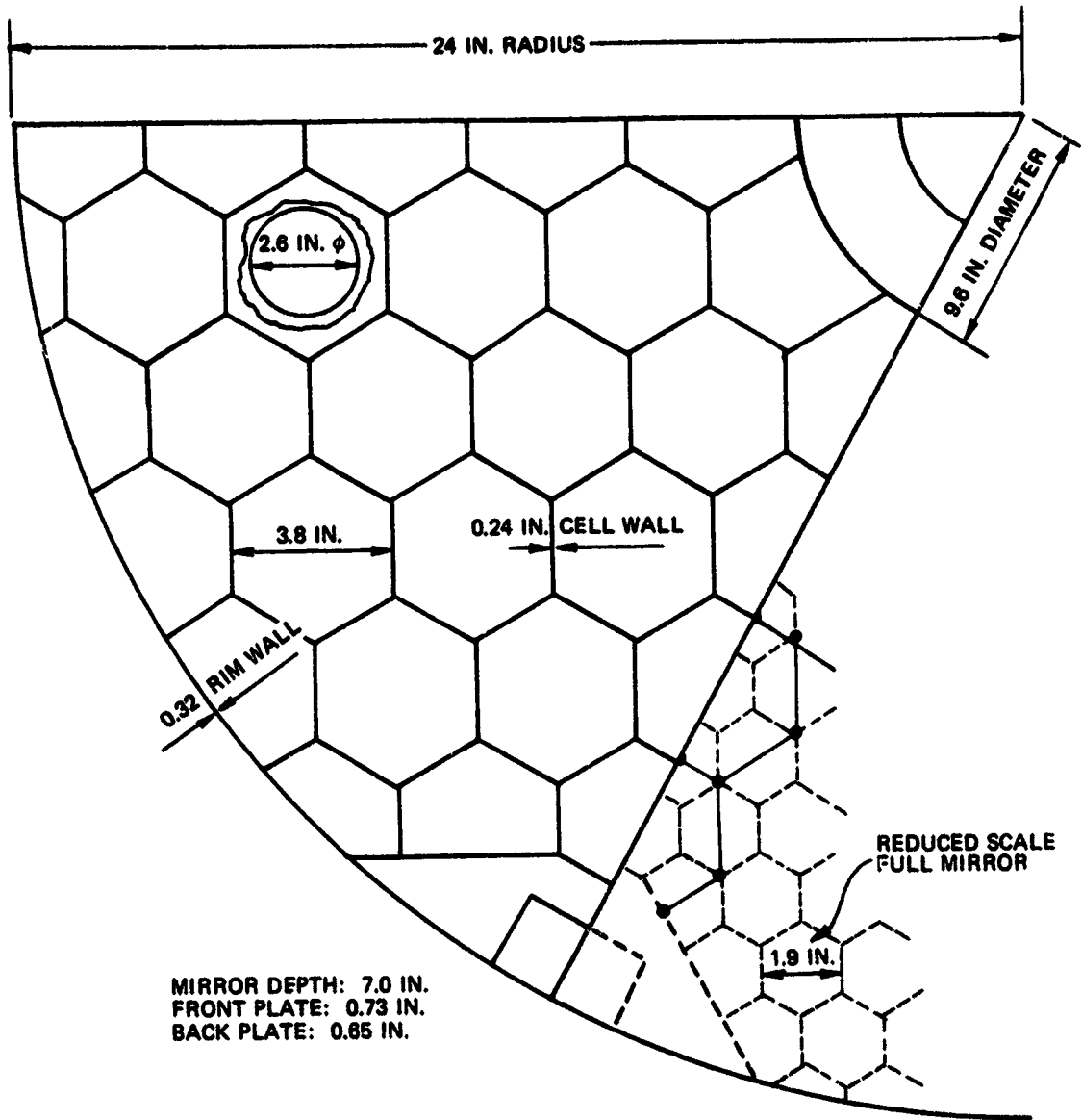


Figure 4.2 48" Breadboard Mirror.

TABLE 4.3

MODEL LAWS

Dimensional Variable	Scaling Law	Case at Hand
Length:	$l_m = f_l l_p$	$f_l = 0.4$
Displacements:	$\Delta_m = f_\Delta \Delta_p = f_l \Delta_p$	
Modulus:	$E_m = f_E E_p$	$f_E = 1.0$
Stresses:	$\sigma_m = f_\sigma \sigma_p = f_E \sigma_p$	
Pressures:	$P_m = f_p P_p = f_E P_p$	
Lumped Forces:	$F_m = f_F F_p$	
Thermal:	$\alpha_m = f_\alpha \alpha_p$	$f_\alpha = 1.0$
Density:	$\delta_m = f_\delta \delta_p$	$f_\delta = 1.0$

where  $f_l$ ,  $f_\Delta$  etc. are dimensionless scaling numbers relating full mirror "prototype" performance to reduced "model" performance.

TABLE 4.4

RELATIONS BETWEEN FULLSCALE AND BREADBOARD

Basic Laws:  $f_L = 0.4$      $f_a = 1.0$   
 $f_E = 1.0$      $f_\delta = 1.0$

Loading Variable	Full Scale	Breadboard	If $\sigma_B = \sigma_F$	If $\Delta_B = \Delta_F$
g Load	1g	1g	2.5g	6.25g
Stress	$\sigma$	$0.4\sigma$	$\sigma$	$2.5\sigma$
Deflection	$\Delta$	$0.16\Delta$	$0.4\Delta$	$\Delta$
Manufacturing Load	1psi	1psi	1psi	2.5psi
Stress	$\sigma$	$\sigma$	$\sigma$	$2.5\sigma$
Deflection	$\Delta$	$0.4\Delta$	$0.4\Delta$	$\Delta$
Actuator Force	1#	1#	0.16#	0.4#
Stress	$\sigma$	$6.25\sigma$	$\sigma$	$2.5\sigma$
Deflection	$\Delta$	$2.5\Delta$	$0.4\Delta$	$\Delta$
Eigenvalue	1xHz	2.5xHz	----	----
Thermal Load	1°	1°	1°	2.5°
Stress	$\sigma$	$\sigma$	$\sigma$	$2.5\sigma$
Deflection	$\Delta$	$0.4\Delta$	$0.4\Delta$	$\Delta$

environments that the mirror will see. It should be observed that these are considered under two separate performance categories. In the first case, the stress in the breadboard ( $\sigma_B$ ) is made equal to the stress in the full scale ( $\sigma_F$ ). This case represents the strength performance of the mirror under various load environments, and it is seen which scale factors must be applied to the loading conditions to get stress-equivalent performance. In the second case, there is an attempt to obtain the same deflections in the model and prototype mirrors. This relates primarily to the optical performance.

#### 4.4 Conclusions

It is very strongly felt that under the circumstances of uncertainty in the mirror manufacture and in the optical performance under various thermal and mechanical loads, that a properly designed and scaled breadboard mirror be constructed and tested.

## Chapter 5

### SUMMARY, CONCLUSIONS, AND RECOMMENDATIONS

The Phase A CERVIT 101 Large Space Telescope primary mirror was analyzed, using a highly complex finite element model, for a number of loading conditions. From these results it can be concluded that a rather well-designed fabrication mount is necessary. Stress levels are not unreasonable, about 30 psi tension per unit transverse "g" load, although the actual "g" levels are yet to be determined, and the tolerable tensile stress is not known. In a thermal environment close to the real, acceptable thermal distortions were observed, although based on idealized thermal expansion coefficients. Extensive materials tests are therefore recommended.

Two less complex mirror structural models were developed and found to give useful results at much lower costs. Trade off studies were performed which indicated that some optimization of cost, weight or stiffness (whichever criterion may be chosen) was possible from the baseline structure.

A design was made for the "Breadboard Mirror", and the model laws relating this to the fullscale LST mirror were developed.

It is worthwhile mentioning again that there still do not exist results comparing mathematical results to a laboratory test on a mirror of the type modelled here. It is very strongly urged that this major gap in analytical technology verification be closed.

## APPENDIX A

### EQUIVALENT PLATE REPRESENTATION OF HEXAGONAL PLATE WITH HOLE

#### A.1 Introduction

While it is possible to model the backplate of light-weighted CERVIT mirrors allowing for full representation of the circular hole within each hexagonal cell, it becomes extremely costly in computational terms, and results in small benefits of improved accuracy. In earlier studies the approach was taken, therefore, to use an equivalent continuous solid backplate. This process was, however, limited to the assumption of equal biaxial in-plane stress resultants and to cells where the size of the backplate hole was sufficiently small as to maintain an analytically acceptable value for the equivalent Poisson ratio ( $\nu_e$ ). In this appendix, these assumptions will be questioned, and wherever necessary, improved modelling methods will be developed. To maintain continuity with the earlier studies, the dimensional parameters used such as 5.2 inch cell size and 2.75 inch diameter holes are maintained.

#### A.2 Unequal In-Plane Stress Resultants

In the previous study,<sup>(5)</sup> it was assumed that the in-plane stress resultants  $N_x$  and  $N_y$  were equal. This assumption is somewhat restrictive, and it is desirable to test its limits of applicability.

If instead, the following assumption is made that the stress resultants are,

$$N_x \text{ and } N_y = aN_x \quad (A.1)$$

where  $a$  is an arbitrary constant, and

$$N^* = N_x = \frac{1}{3} \text{ lb./in.} \quad (\text{A.2})$$

then the strain energy of the plate with the hole can be stated as,

$$(\text{S.E.})_H = \frac{(0.1)(0.034)}{N^{*2} t} \left[ N_x^2 + a^2 N_x^2 - (0.915) a N_x^2 \right] \quad (\text{A.3})$$

and for the equivalent uniform plate the strain energy becomes

$$(\text{S.E.})_U = \frac{(23.4)}{2E_e t_e} \left[ N_x^2 + a^2 N_x^2 - 2v_e a N_x^2 \right] \quad (\text{A.4})$$

Equating (A.3) and (A.4) and cancelling  $N_x^2$  terms, the following expression may be derived,

$$\frac{E_e t_e}{t} = (383) \frac{1 - 2v_e a + a^2}{1 - (0.915)a + a^2} \quad (\text{A.5})$$

Expression (A.5) can be shown independent of "a" under the following conditions:

$$\frac{E_e t_e}{t} = 383 \quad (\text{A.6})$$

$$v_e = 0.457 \quad (\text{A.7})$$

The same values may be used for  $E_e$  and  $E$ . In the element study, an arbitrary value of 1000 psi was picked for  $E$ , thus

$$t_e = (0.383)t \quad (\text{A.8})$$

These results were obtained as well when  $N_x = N_y$ , thus the computation of the equivalent plate thickness ( $t_e$ ) and the equivalent Poisson ratio ( $\nu_e$ ) is not restricted to that earlier assumption.

### A.3 Backplate Hole Relatively Large

With a cell size of 5.2 inch across the flats and a backplate hole of 2.75 inch in diameter, the equivalent Poisson ratio is already 0.457. With increasing hole diameter, this value, based on the method of computation outlined earlier, can easily exceed 0.5. This brings us into potential conflict with a number of basic considerations in the energy theorems used to derive the finite element method. It is important, therefore, for most element formulations, to establish some alternate means of backplate representation.

It is proposed to augment the continuous backplate by truss members connecting between the nodes, directly underneath the web members. This approach does not require additional degrees of freedom in the backplate.

Consider first such a truss acting alone (Fig. A.3.1). Assume the 'mechanism' mode is inhibited by other forms of stiffening, and that the hexagonal truss is uniformly loaded with  $N_x = N_y = N^* = \frac{1}{3}$  lb./in.

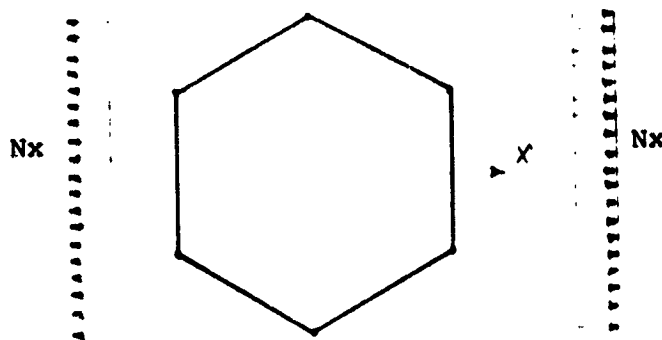


Figure A.3.1  
Hexagonal Truss Model



The strain energy equation that results is,

$$(S.E.)_T = \frac{(.0977)(.125)}{AN^{*2}} [ N_x^2 + N_y^2 - 1.35N_xN_y ] \quad (A.9)$$

Only one variable, "A" the cross-sectional area, is free in this equation, so that it cannot be equated with the initial strain energy relation as expressed in (A.3). The transverse contraction of this truss does not depend on some equivalent Poisson ratio but is determined from the member area and the geometry of the assembly. The fact remains, however, that the absolute value of the  $N_xN_y$  coefficient in (A.9) is greater than the value (0.915) encountered in (A.3). This gives great encouragement that a combination of edge-truss and solid plate can properly represent a plate with a hole. Let us assume that the strain energy for such a stiffened plate is expressible in the following form.

$$(S.E.)_C = C_1(A/L,t) [ N_x^2 + N_y^2 - C_3(\nu_e)N_xN_y ] \quad (A.10)$$

where  $C_1$  and  $C_3$  are functionals.

A is the truss member area  
 L is the length of the truss element  
 t is the thickness of the plate elements  
 $\nu$  is Poisson ratio of the plate

The plate edge beam model was run on STRUDL II with the following characteristics

E = 1000 psi  
 $\nu$  = .252

$$\begin{aligned}
 A &= .0489 \text{ in}^2 \\
 L &= 3 \text{ inch} \\
 t &= .0376 \text{ inch}
 \end{aligned}$$

From eq. (A.10)  $C_1$  resulted as .027.

It is desirable however, that  $C_1$  be set up independent of the area  $A$  and the thickness  $t$  and can be represented as of the form

$$C_1 = \frac{R_1 \left( \frac{.0489}{3} \right) + .0376}{R_2 (A/L) + t}$$

Values for  $R_1$  and  $R_2$  were obtained by several STRUDL runs with different  $A/L$  and  $t$  values and by equating the resulting  $C_1$  values. For  $\frac{A/L}{t}$  ratios close to  $\frac{.0489/3}{.0376} \approx .434$ ,  $R_1 = R_2 = .5$  was found to give a good agreement with the results.

The strain energy expression (A.10) then becomes

$$(\text{S.E.})_C = \frac{(.0163 \times .5 + .0376) (.027)}{\left( \frac{A}{2L} + t \right) N^2} \left[ N_x^2 + N_y^2 - C_3 N_x N_y \right] \quad (\text{A.11})$$

$$\text{If } \frac{A/L}{t} = .434$$

Equating eq. (A.11) with eq. (A.3) we find as a first requirement that

$$t_e = .298t$$

$$\text{for } t = .625 \text{ we obtain } \begin{cases} t_e = .186 \\ A_e = 3 \times .434 \times .186 = .242 \end{cases}$$

In order to check the results, another STRUDL II run with different values of Poisson ratio  $\nu$  and found good agreement for the  $N_x^2$  and  $N_y^2$  coefficients.

For the second equivalence requirement, that is,  $C_3 = .915$   
we assume

$$C_3 = Av^2 + Bv + C$$

With STRUDL runs for different values of  $v$  it is found that  
the coefficient  $C_3$  is of the form

$$C_3 = 3v + .6 \quad (\text{straight line}) \quad (\text{A.12})$$

From eq. (A.3)

$$C_3 = .915 = 3v_e + .6$$

Solving for  $v_e$  we find that

$$v_e = .105$$

#### A.4 Bending in Backplate

In most instances of lightweighted mirror loadings, the front and back plates experience almost pure in-plane behavior. Thus plane stress elements are entirely adequate for proper finite element modelling. In some circumstances, however, local bending will occur. This can arise from actuators, local supports, launch snubbers, etc. While the result of this bending is a many fold complication of the modelling problem, with a doubling of the degrees of freedom, and an increase in run times, it is not to be neglected by the conservative analyst. Fortunately, the bending and stretching problems are uncoupled, so that the equivalent studies can too be uncoupled. This involves then the super-imposition of separate bending and stretching elements whose stiffness properties will not be derivable from each other. With a well-designed finite element analyzer, this 'trick' should present no problems.

The procedure used in deriving the equivalent solid plate bending model is very similar to the stretching model. The strain energy of the actual plate, subject to arbitrary edge moments, is equated to the strain energy of the equivalent continuous plate under the same moments.

A finite element model is used to obtain the strain energy of the plates. The grid is shown in Figure (A.4.1). The 'CPT' plate bending element in STRUDL II was used. Figure (A.4.2) shows the loadings that were applied, uniform moments in the x and y directions, and the corresponding consistent nodal loads. In order to obtain the strain energy for arbitrary moment distributions  $M_x$  and  $M_y$ , a known distribution  $M^*$  was applied in both directions. The resulting rotations for each case are multiplied by  $M_y/M^*$  respectively and then superimposed. (Figure A.4.3)

The resulting strain energy is:

$$SE_{Fe} = \frac{(0.1)(.0223)}{M^*2_t} [ M_x^2 + M_y^2 - .600M_xM_y ] \quad (A.13)$$

From Timoshenko's "Theory of Plates and Shells" the strain energy of a continuous plate subject to  $M_x$  and  $M_y$  is:

$$SE = \frac{1}{2} \frac{A}{D(1-\nu_e^2)} [ M_x^2 + M_y^2 - 2\nu_e M_xM_y ]$$

or

$$SE = \frac{6A}{E_e t_e^3} [ M_x^2 + M_y^2 - 2\nu_e M_xM_y ] \quad (A.14)$$

The area A of the continuous plate of Figure 1 is 23.4 in<sup>2</sup> and the subscript "e" denotes the equivalent properties of

the continuous plate. Equating (A.13) and (A.14) gives

$$2v_e = .600$$

$$\frac{140.4}{E_e t_e^3} = \frac{0.1 \times .0223}{(.01)^2 t}$$

or  $v_e = .300$

$$E_e t_e^3 = \frac{.01404}{.00223} t = 6.3t$$

The finite element program used  $\nu = .252$  and  $E = 1000$  psi.  
If  $E_e$  was arbitrarily set to  $E$  the equivalent thickness becomes

$$t_e = \sqrt[3]{\frac{6.3}{t}} 10^{-1}$$

$$t_e = .185 \sqrt[3]{t}$$

The continuous plate must have a higher Poisson ratio and a smaller thickness to be equivalent to the hexagonal plate with 1.375 in. radius hole. This result could be intuitively expected.

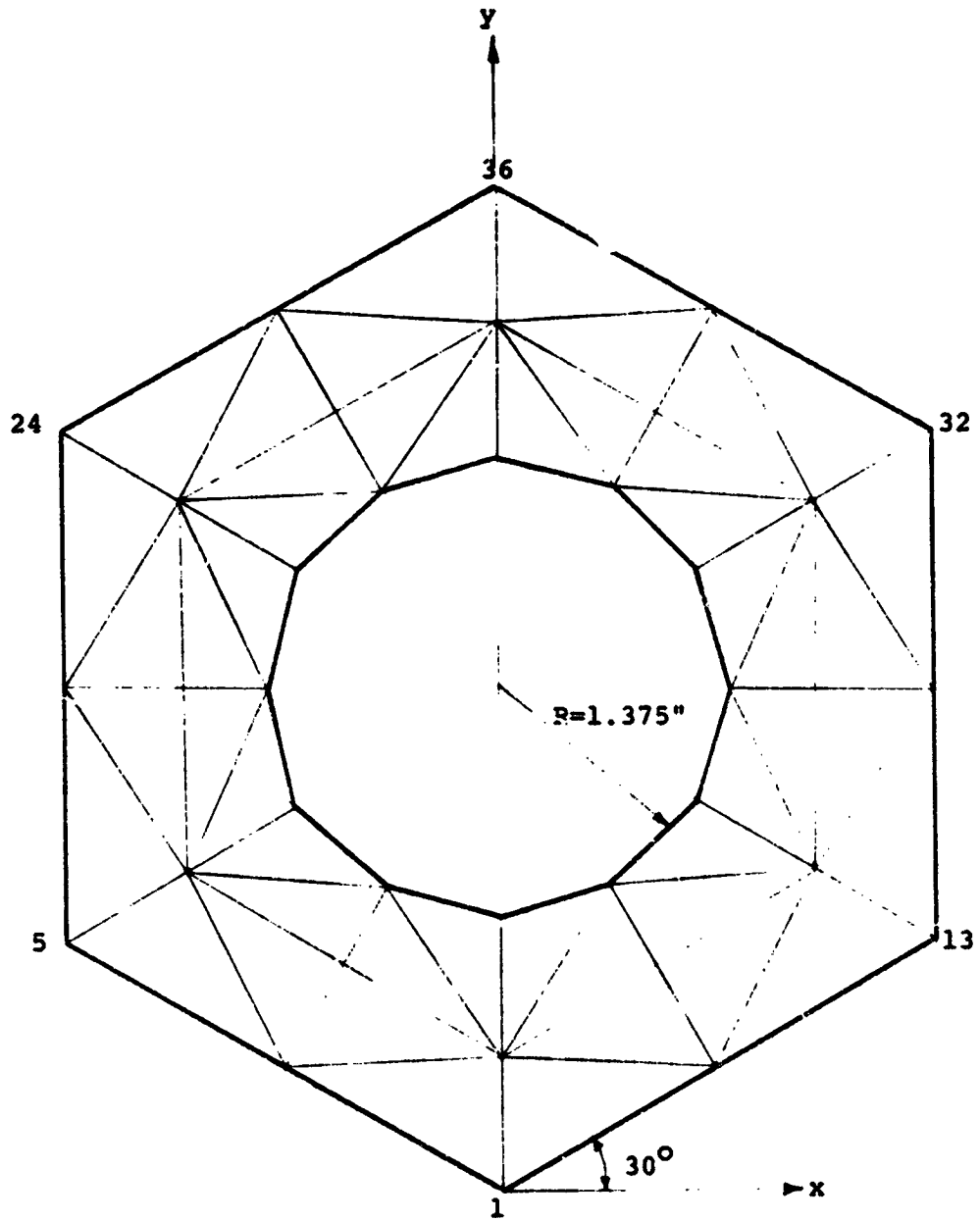


Figure A.4.1

FINITE ELEMENT GRID OF BACKPLATE-CPT ELEMENTS

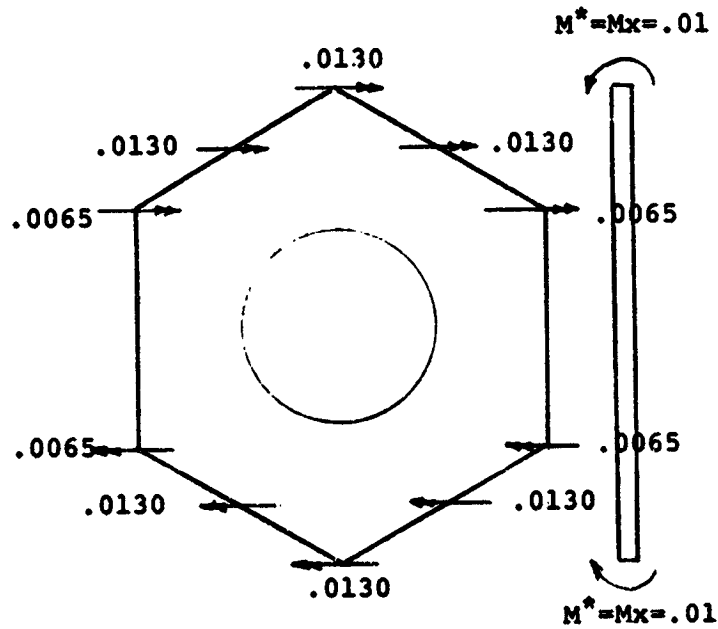
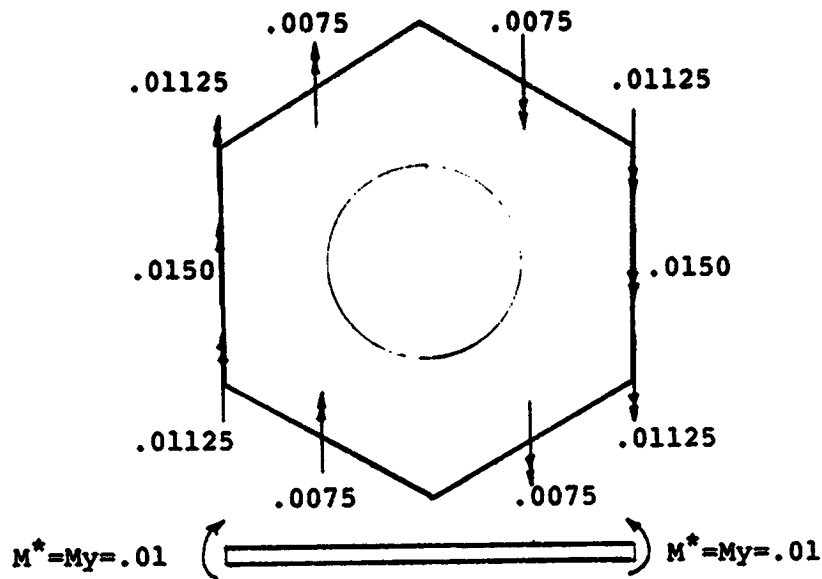


Figure A.4.2

LOADINGS CONSIDERED FOR STRAIN ENERGY COMPUTATION

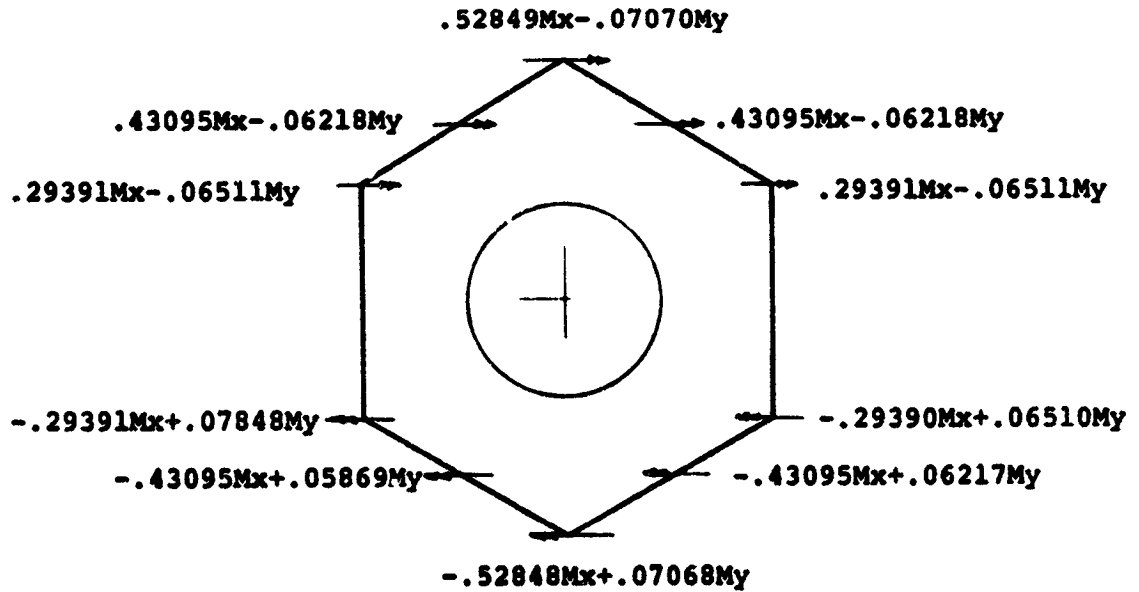
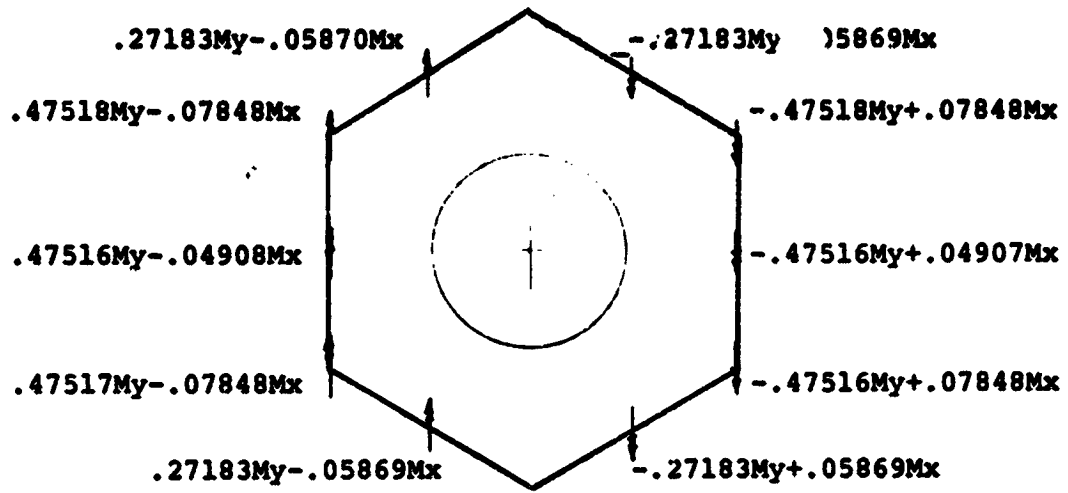


Figure A.4.3  
 NODAL ROTATIONS ( $\times 1/M^2t$ )



APPENDIX B  
FORMULATION OF HONEYCOMBED MIRROR WEB PLATE  
STRUCTURES AS AN EQUIVALENT CONTINUUM

**B.1 Introduction**

The detailed finite element analysis of a honeycombed mirror is a costly and time consuming procedure if every web-plate is included in the model. When trade-off studies on the mirror configuration are desired, a low cost but nonetheless realistic structural model is mandatory. Approximate analytical results can be obtained by modeling the honeycombed structure as an equivalent continuous thick plate, and then referring to the theory of thick plates for analytical results. This appendix shall show a simple procedure for determining the properties of the equivalent plate.

In continuum theory, one develops constitutive relations by considering an infinitesimal element of material. In order to treat a honeycombed plate as a two-dimensional continuum, one must consider finite-sized rectangles which represent a basic repeating pattern. This fact, along with the strain distributions assumed for this finite-sized element, defines the approximate nature of this approach. The smaller the rectangle required to represent the repeating pattern, the more accurate is the approach. The equivalent plate is defined by equating the strain energy of a plate of continuous material.

Figure B.1 shows the rectangles used for triangular, hexagonal, and square honeycombed mirror lightweighting patterns. The geometric variables are defined as follows:

c	cell dimension
t	web plate thickness
h	distance from middle plane of top plate to middle plane of bottom plate

The parameters which define the equivalent plate are the equivalent bending rigidity,  $D_{B_e}$  and the equivalent shear modulus,  $G_e$ . The bending rigidity  $D_{B_e}$  of the flanges is fully retained as the flanges are kept in the simpler "trade-off" model. For the purpose of this analysis the bending component of the web can be reasonably disregarded. The determination of the equivalent shear modulus  $G_e$  is described below.

## B.2 Equivalent Shear Modulus

The equivalent shear modulus is found by assuming that the material between the top and bottom plate is in a state of pure shear, defined by the cartesian shear components  $\gamma_{xz}$  and  $\gamma_{yz}$ . The strain energy carried by the webs in this state is equated to that which would be carried by a fictitious uniform material between the top and bottom plates, of equivalent shear modulus  $G_e$ . A unified definition of pitch,  $P$ , leads to the following relations with the cell dimension  $c$ .

Traingular pattern	$c_t = P\sqrt{3}$
Hexagonal pattern	$c_h = P/\sqrt{3}$
Square pattern	$c_s = P$

### Triangular Pattern

The components of the transverse shear strains  $\gamma_{xz}$  and  $\gamma_{yz}$  resolved onto the web plates are:

$$\gamma_1 = \gamma_{xz}; \gamma_2 = \frac{1}{2}\gamma_{xz} + \frac{\sqrt{3}}{2}\gamma_{yz}; \gamma_3 = -\frac{1}{2}\gamma_{xz} + \frac{\sqrt{3}}{2}\gamma_{yz} \quad (B.1)$$

$\gamma_1$ ,  $\gamma_2$ , and  $\gamma_3$  are the shear strains in plates 1, 2, and 3, as numbered in Fig. B.1. The total strain energy in the

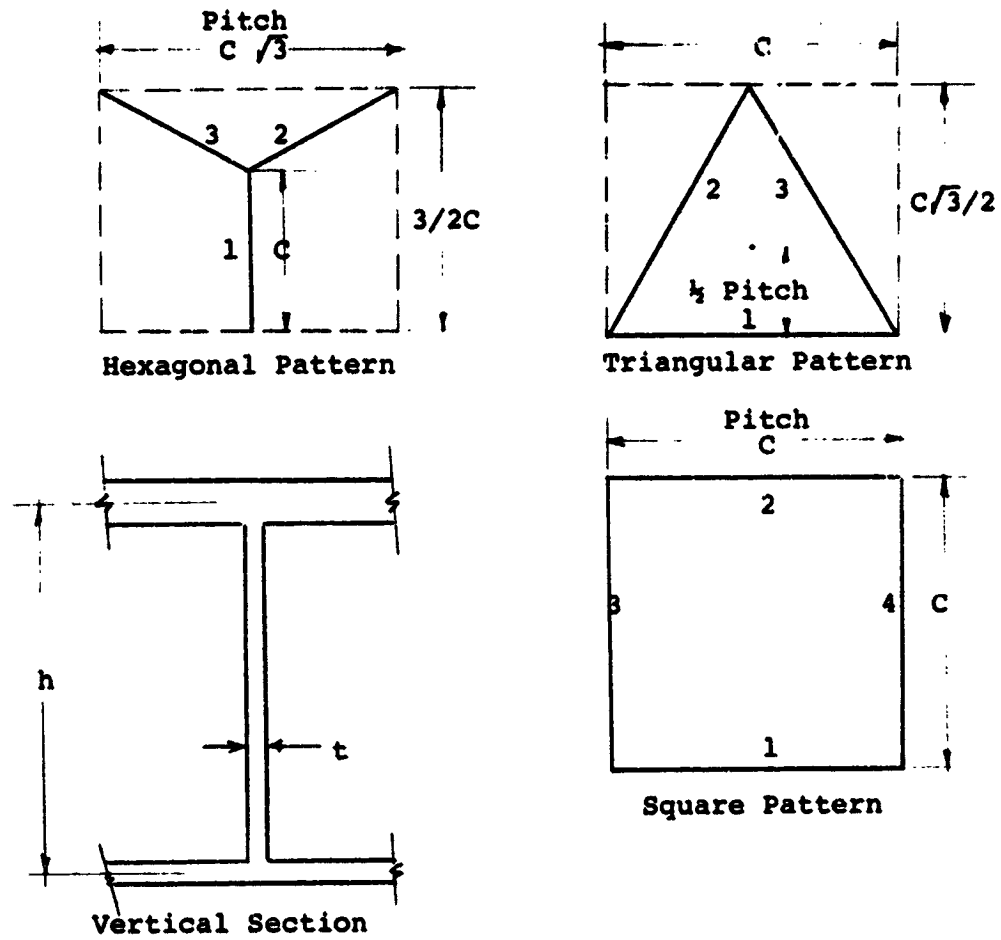


Figure B.1  
 BASIC REPEATING UNITS FOR LIGHTWEIGHT MIRRORS  
 AND TYPICAL VERTICAL SECTION

rectangular unit is:

$$U_{TS} = 3/4Gc_t h(\gamma_{xz}^2 + \gamma_{yz}^2) \quad (B.2)$$

$U_{TS}$  = strain energy due to transverse shear

$G$  = shear modulus of mirror material

The strain energy for an equivalent uniform core is equal to:

$$U_{TS_e} = \sqrt{3}/4G_e c_t^2 h(\gamma_{xz}^2 + \gamma_{yz}^2) \quad (B.3)$$

Equating B.2 and B.3, one obtains:

$$G_e = \frac{\sqrt{3}tG}{c_t} = \frac{tG}{P} \quad (B.4)$$

### Hexagonal Pattern

Shear strain components:

$$\gamma_1 = \gamma_{yz}; \gamma_2 = \sqrt{3}/2\gamma_{xz} + 1/2\gamma_{yz}; \gamma_3 = -\sqrt{3}/2\gamma_{xz} + 1/2\gamma_{yz} \quad (B.5)$$

Strain energy:

$$U_{TS} = 3/4Gtc_h h(\gamma_{xz}^2 + \gamma_{yz}^2) \quad (B.6)$$

Strain energy of equivalent material:

$$U_{TS_e} = 3 \sqrt{3}/4 G_e c_h^2 h (\gamma_{xz}^2 + \gamma_{yz}^2) \quad (B.7)$$

Equivalent shear modulus:

$$G_e = \frac{\sqrt{3}}{3} \frac{Gt}{c_h} = \frac{tG}{P} \quad (B.8)$$

### Square Pattern

Shear strain components:

$$\gamma_1 = \gamma_2 = \gamma_{xz}; \gamma_3 = \gamma_4 = \gamma_{yz} \quad (B.9)$$

Strain energy:

$$U_{TS} = \frac{1}{2} G t c_s h (\gamma_{xz}^2 + \gamma_{yz}^2) \quad (B.10)$$

Strain energy of equivalent material:

$$U_{TS_e} = \frac{1}{2} G_e c_s^2 h (\gamma_{xz}^2 + \gamma_{yz}^2) \quad (B.11)$$

Equivalent shear modulus:

$$G_e = \frac{Gt}{c_s} = \frac{tG}{P} \quad (\text{B.12})$$

### Conclusion

It can be seen that a unified definition of  $G_e$  and  $\gamma_e$  can be used for the various patterns with use of the pitch  $P$ .

$$\text{For all cases } G_e = \frac{tG}{P}$$

$$\text{Density of core } \gamma_e = \frac{t}{P} \gamma_{\text{solid}}$$

## BIBLIOGRAPHY

1. Couder, A., "Bulletin Astronomique", 7:201, 1931, Translation by E. T. Pearson, KPNO.
2. Reissner, E., "The Effect of Transverse Shear Deformation on the Bending of Elastic Plates", ASME Journal of Applied Mechanics, Volume 2, A-69, 1945.
3. Selke, L. A., "Theoretical Elastic Deflections of a Thick Horizontal Circular Mirror on a Ring Support", Applied Optics, Volume 9, No. 1, January 1970.
4. Soosaar, K., "Design of Optical Mirror Structures", MIT/CSDL Report R-673, January 1971.
5. Maser, K., Soosaar, K., "Structural Analysis of Large Telescope Mirrors and Supports", MIT/CSDL Report R-716, March 1972.